Master's thesis

NTNU
Norwegian University of Science and Technology
Faculty of Natural Sciences
Department of Biotechnology and Food Science

Tobias Ludviksen

Shape Dependency of Gold Nanoparticles Performance as Oligonucleotide Based Biosensors

Master's thesis in Sustainable Chemical and BIochemical Engineering
Supervisor: Berit Løkensgard Strand
Co-supervisor: Sulalit Bandyopadhyay
June 2023

NTNU
Norwegian University of Science and Technology

Tobias Ludviksen

Shape Dependency of Gold Nanoparticles Performance as Oligonucleotide Based Biosensors

Master's thesis in Sustainable Chemical and BIochemical Engineering
Supervisor: Berit Løkensgard Strand
Co-supervisor: Sulalit Bandyopadhyay
June 2023

Norwegian University of Science and Technology
Faculty of Natural Sciences
Department of Biotechnology and Food Science

NTNU
Norwegian University of
Science and Technology

Preface

This thesis is the final part of my two-year degree in 'Sustainable Chemical and Biochemical Engineering' at NTNU. This thesis was written in collaboration with the Particle Engineering Centre, and I have been lucky enough to be a part of their research group for the last 12 months. All of the experimental work was performed at the Department of Chemical Engineering, the NanoLab at NTNU and Laboratoriesenteret at St. Olavs Hospital.

During my work, I received advice and had helpful discussion with the members of the Particle Engineering group research group. Their input and support helped me overcome the obstacles I faced and gave me motivation to get through the semester. First and foremost, my supervisor Sulalit Bandyopadhyay has been of enormous help, by guiding me in a direction which I have found extremely interesting and offered his inputs on how to make the thesis better throughout the entire process. Though many people in the team offered their help during this time, I want to direct a special thanks to Katharina Zürbes and Muhammad Bilal for always being there when I had questions and needed guidance in the laboratory. I am grateful for all the help they gave me, and their input helped me more than they are probably aware of. I would also like to thank Magnar Bjørås and Erlend Ravlo for giving their input and preparing the final part of the project for me. I would also like to thank my fellow Master's students in the research team for being a great support group and always being a delight to work with in and outside the laboratory.

I would also like to thank Berit Løkensgard Strand for being my internal supervisor at the Department of Biotechnology and Food Science and finally my girlfriend, family and friends for supporting me all throughout my time as a student.

Tobias Ludviksen
Trondheim, June 16, 2023

Abstract

Gold nanoparticles are rapidly emerging as an alternative to traditional biosensors and have the potential of being tailored to specific targets such as antigens, proteins and viral RNA. They can also be synthesized in numerous shapes and sizes, all with their own optical properties. The shape and size of the particles gives them different sensitivity and performance for specific uses, and they have to be functionalized often in multi-step processes to be usable as biosensors. The aim of this thesis was to synthesize, functionalize and compare the biosensing performance of three common gold nanoparticles, while optimizing each step to create a repeatable pathway for the preparation of each of the particle. The three shapes were spherical, rod-shaped and sea-urchin like, and they were all functionalized with a single stranded DNA sequence which was complementary to a specific sequence of the initial SARS-CoV-2 virus RNA.

Firstly, three different synthesis methods were tested to get the three particle shapes, all building on first synthesizing a seed solution before using those to create larger sized particles or specific shapes. These resulting particles were characterized to find their size, shape, aspect ratios and zeta potentials. The synthesis of nanospheres had to be optimized to get the same sized particles each time and the nanourchins were studied both in terms of repeatability of the synthesis and stability. It was found that the synthesis was less repeatable and the particles were less stable compared to the other two shapes. There were observed morphological changes over longer periods of time and the particles were only stable in solution for just over ten minutes after sonication and vortex.

The functionalization was done differently for each type of particle. The simplest to functionalize were the nanospheres, which could be functionalized directly with thiol-modified oligonucleotides. The nanorods were first functionalized with thiolated PEG, before performing a ligand exchange to achieve a MUA-capping. This ligand exchange required changes to be made to an existing protocol, which were implemented with great success. The nanourchins were functionalized directly with MUA, and both the nanourchins and nanorods were functionalized with amine-modified oligonucleotides through EDC/NHS coupling. The PEG- and MUA-functionalizations were verified through FTIR analyses, changes in zeta potential and looking at dispersbility changes in water and ethanol before and after the functionalization. Due to lack of available methods and time, the success of the oligonucleotide functionalization could not be confirmed, but the particles were still tested as biosensors.

These tests found that the nanorods had the highest potential for use as oligonucleotide based biosensors as they portrayed both changes in absorbance intensity and peak wavelength shifts. The nanourchins also showed some potential, but there were also many limitations and drawbacks with their use, making them the least viable option. The nanospheres showed perhaps the least clear changes when incubated with the target RNA, but did in some experiments show some potential which makes them interesting to look further into.

Sammendrag

Gullnanopartikler vokser raskt frem som et alternativ til tradisjonelle biosensorer og kan bli skreddersydd til spesifikke mål som antigen, proteiner og viralt RNA. De kan også syntetiseres i en rekke former og størrelser, som alle har sine egne optiske egenskaper. Formen og størrelsen på disse partiklene gir dem ulik sensitiviet og prestasjon til spesifikke formål, og for å kunne brukes som biosensorer må de funksjonaliseres gjennom prosesser ofte bestående av flere steg. Målet med denne oppgaven var å syntetisere, funksjonalisere og sammenligne prestasjonen av tre vanlige gullnanopartikler når brukt som biosensorer, og samtidig optimalisere hvert steg for å ende opp med en repeterbar prosess for hver av disse partiklene. De tre partikkelformene som ble syntetisert var runde, stavformede og kråkebolle-lignende, og de ble alle funksjonalisert med en enkelttrådet DNA-sekvens som var komplementær med en spesifikk sekvens i den første utgaven av SARS-CoV-2 virusets RNA.

Innledningsvis ble tre ulike syntetiseringsmetoder testet ut for å oppnå de tre ulike partikkelformene, og alle disse metodene var synteser der et "nanopartikkel-frø" ble laget først for å så bygges på for å få større partikler eller ulike former. De ferdige nanopartiklene ble karakterisert med hensyn på størrelse, form, størrelsesforhold og zetapotensial. Syntesen av nanosfærer måtte optimaliseres for å produsere nanopartikler med lik størrelse hver gang, og de kråkebolleformede nanopartklene ble undersøkt for å finne ut hvor stabile de var og om syntesen kunne reproduseres. Gjennom disse undersøkelsene ble det funnet ut at disse nanopartiklene var mindre stabile enn de to andre og at syntesen var mindre repeterbar. Det ble observert morfologiske endringer over tid og partiklene var bare stabil i løsning i litt over ti minutter.

Funksjonaliseringen ble gjort ulikt for hver type nanopartikkel. De enkleste å funksjonalisere var nanosfærene, som kunne bli funksjonalisert direkte med tiol-modifiserte oligonukleotider. Nanostavene ble først funksjonalisert med PEG-tiol, før det ble gjort et ligand-bytte for å oppnå MUA-funksjonaliserte nanostaver. Dette ligand-byttet krevde at det ble gjort endringer i prosessen, og både nanokråkebollene og nanostavene ble funksjonalisert med amin-modifiserte oligonukleotider gjennom en EDC/NHS kobling. PEG- og MUA-funksjonaliseringen ble verifisert basert på FTIR-analyser, endringer i zetapotensialer og endringer i dispergerbarhet i vann og etanol. På grunn av mangel på tid og tilgjengelige metoder kunne ikke funksjonaliseringen med oligonukleotider bli verifisert, men nanopartiklene ble fremdles testet ut som biosensorer.

Disse testene viste at nanostavene hadde høyest potensial for brukt som oligonukleotid-baserte biosensorer ettersom det ble observert endringer i både absorbansintensitet og skift i topppunkt-bølgelengde. Nanokråkebollene viste noe potensial som biosensorer, men på grunn av mange begrensninger og ulemper, var disse ikke et godt alternativ som biosensor. Nanosfærene viste de minste endringene etter at de ble inkubert med viralt RNA, men viste antydninger til å kunne ha en god effekt i noen resultater. De er derfor også verdt å se nærmere på.

Acronyms

Au NPs gold nanoparticles

CTAB Hexadecyltrimethylammonium bromide

EDC N-(3-Dimethylaminopropyl)-N- ethylcarbodiimide hydrochloride

ELS Electrophoretic Light Scattering

FAM carboxyfluorscein

FTIR Fourier Transform Infrared

LSPR localized surface plasmon resonance

MUA 11-mercaptoundecanoic acid

NHS N-Hydroxysuccinimide

NRs nanorods

NSs nanospheres

NUs nanourchins

PEG-SH o−[2−(3−mercaptopropionylamino)ethyl]-o′−methylpolyethylene glycol

PTA Particle Tracking Analysis

PVP polyvinylpyrrolidone

RT-PCR reverse transcriptase polymerase chain reation

SN silver nitrate

ssDNA single stranded DNA

TEM Transmission Electron Microscopy

UV-Vis Ultraviolet visible

Contents

1 Introduction

1.1 Motivation

Detection of viral infections has since the outbreak of the COVID-19 pandemic in 2020 been a field of increased interest[1]. Several test methods were studied and developed during this period, some utilizing on antibody and antigen interactions, while others used methods in which specific sequences of the viral RNA are identified. Antigen tests and reverse transcriptase polymerase chain reation (RT-PCR) testing ended up being the most popular diagnostic methods, with antigen tests used for rapid self-testing and RT-PCR was used as the most reliable test[1;2]. Antigen tests utilize the the binding of antigens and antibodies to identify the virus. RT-PCR on the other hand, replicates the RNA in the sample by using the enzyme reverse transcriptase, which makes it possible to identify that the viral RNA is present. Antigen test are easily available for use and could give a results within a short amount of time, but are not as reliable as RT-PCR testing. The sensitivity of antigen tests vary among brands and depending on the presence of antigens, meaning that where in the course of illness the patient is will affect the sensitivity. RT-PCR could on the other hand give more accurate results, but will often have to be sent from a testing area to a laboratory for further analysis[3]. This means it could take a few days to get the result from the test.

An alternate method of detecting viral infections which is to utilize the unique optical properties of gold nanoparticles (Au NPs) for biosensing. Gold nanoparticles has shown exciting promise as biosensors due to their inert nature, biocompatibility, simple methods of synthesis, optical properties and potential for targeting specific molecules[4;5]. The high demand for detection methods of viral infections makes it natural to study other alternatives. There are drawbacks with the testing methods currently available, and developing new methods could potentially fill a gap in the market[3;2]. Au NPs could be a viable alternative in the future, as they can be tailored to target specific viral strains with few modifications needed[5]. The surface of the nanoparticles have the ability to bind molecules which again can bind specific targets, making Au NPs easily adaptable. If a new strain of the virus develops or a new virus emerges, the targeting ligand can easily be switched out with another one.

Different methods of synthesizing Au NPs have been developed, with Turkvich, J. et al. reporting synthesis of spherical Au NPs already in 1950[6]. In 2001 Jana, N.R. et al. reported synthesis of rod-shaped Au NPs and their method has later been adapted to synthesize NPs of many different shapes[7;8;9]. Star-shaped or sea-urchin like Au NPs have also been thoroughly studied and many different synthesis methods have been developed to achieve these shapes[6;10;11;12]. Hence, there are many alternatives when using Au NPs as biosensors and the biosensing performance could be very different based on the shape and size of the Au NP used[4]. Direct comparisons of different gold nanostructures in viral

RNA biosensing have not been performed before, or are at least not known of within this research group.

This thesis studies how the size and shape of Au NPs affect their performance in viral detection to contribute to a greater understanding of the subject. This with the hope that the findings could translate to other virus strains and variants of SARS-CoV-2 and therefore serve as an aid in choosing a Au NP which could detect viral infections high accuracy. Better knowledge on this subject could help make Au NPs a viable alternative to other biosensors.

1.2 Aim

The aim of this thesis is to study the performance in RNA detection when using sea-urchin like, rod-shaped and spherical Au NPs, while also establishing a repeatable and functional root of synthesis and functionalization for all these shapes. This will be done by utilizing and adapting existing methods for synthesis and functionalization, and finally comparing their biosensing performance.

In the first step of the experimental work, Au NPs of different shapes an sizes will be synthesized based on reported methods. These nanoparticles will characterized and studied to examine the repeatability of the synthesis methods, the stability of the particles, and the optical and physical properties of the particles.

To make the particles functional, different methods will be tested to link the Omicron RNA-binding oligonucleotides based on the capping agent already present on the NPs surface. Some methods will try to utilize the functional groups of the present capping agent, whereas other methods will exchange the capping agent with the Omicron RNA-binding oligonucleotides.

Finally, testing of the detection sensitivity will be done by investigating the change in optical signals of the functionalized NPs not bound to Omicron RNA to that of NPs bound to Omicron RNA. Then, the sensitivity of all particles will be compared to find out which shapes and sizes of Au NPs have the highest potential to be used as optical biosensors.

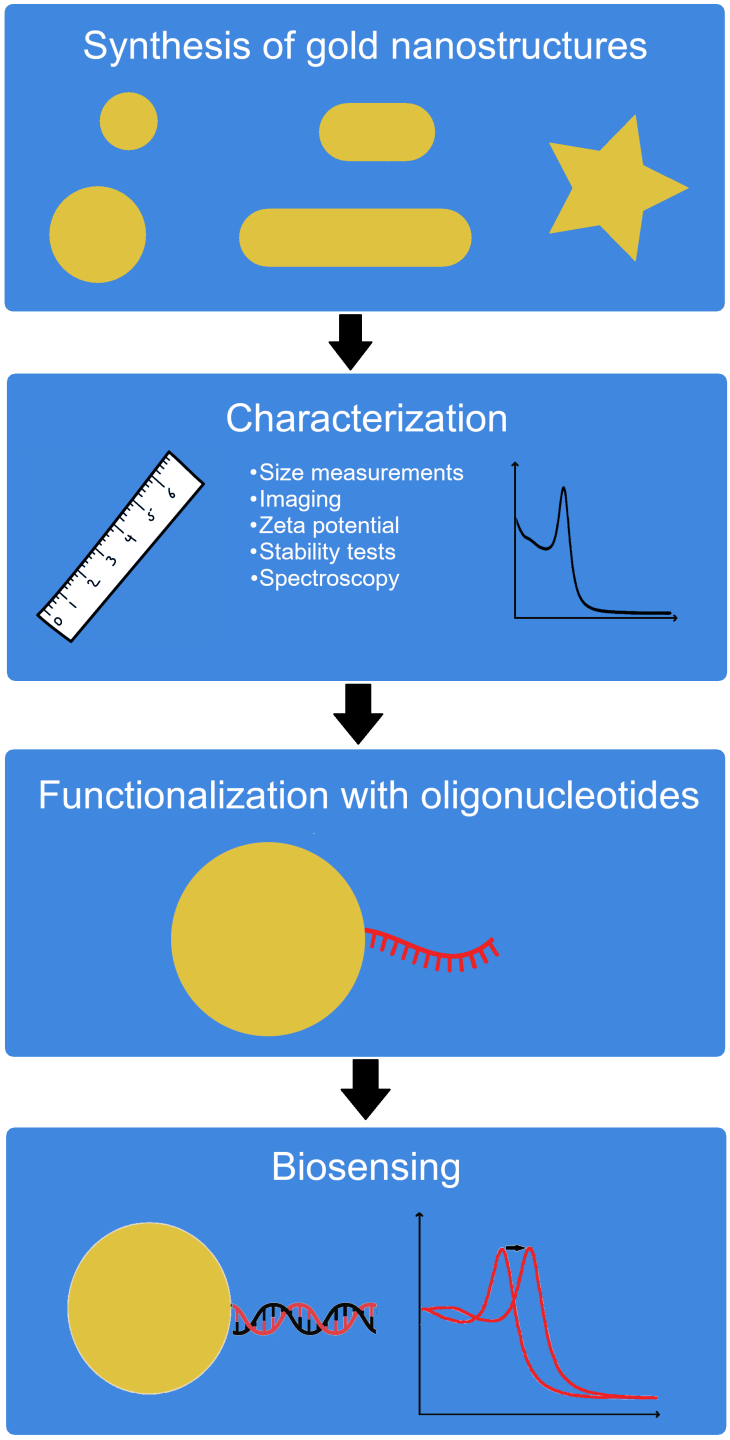

Figure 1.1: Schematic of the workplan of the thesis. The four main steps in the process are synthesis, characterization, functionalization and biosensing.

2 Theoretical background

In this section, the theory and literature relevant for the thesis will be presented to understand the experimental work of the thesis. Firstly, crystallization theory of Au NP synthesis and literature describing reported methods of synthesis will be set forth, with select data of the nanoparticle characterization these authors did. Further, important principles in nanoparticle functionalization and related methods to achieve this will be presented, before finally coming on to the principles of biosensing in general and Au NP biosensing specifically.

2.1 Gold nanoparticle synthesis

In recent years, the syntesis of gold nanoparticles (Au NPs) have been thoroughly studied due to their biocompatibility, optical properties and the many simple methods of synthesis which can give a variety of different shapes such as spheres, rods and stars[13]. This chapter will therefore look into the mechanisms of Au NP formation and the optical properties which make them usable as biosensor. In addition, several reported synthesis methods will be presented, which all give particles of different shapes and sizes.

2.1.1 Mechanisms of nanoparticle nucleation

The thermodynamic driving force in Au NP syntheses is supersaturation[14]. This term describes a system where the concentration of the crystal monomer is higher than its solubility. In a supersaturated system the monomers starts to crystallize, which lowers the degree of supersaturation and finally reach saturated state. To create a supersaturated system in regards to gold, the monomer Au^0 needs to be present in a solution[15]. It is currently not known whether gold ions bind each other first before being reduced or if they are first reduced completely before bonding. The reduction of the gold ions is however usually done by creating an aqueous solution of a gold salt such as gold(III) chloride and adding a reducing agent, e.g. ascorbic acid or sodium citrate, to reduce Au^{3+} to Au^0[15;16;17].

After a high degree of supersaturation has been established, nucleation is initiated[15]. At this point in the synthesis, the nuclei will form and dissolve during a period of time, until nuclei of a certain size are formed. This size is defined as the critical radius (r_c), which is the size where the total Gibbs free energy of the system starts to turn negative. According to the LaMer model, which describes the concentration in a supersaturated system as a function of time, the degree of supersaturation has to be high enough for nucleation to happen[18]. This principle is shown in figure 2.1, where the monomer concentration is plotted as a function of time. In area I in this graph, the concentration rises to the minimum concentration required for nucleation. Once the monomer concentration reaches this value, nucleation is the predominant crystallization mechanism (area II) and in area III the monomers are disposed onto the nuclei, which results in crystal growth. This happens until the monomer concentration reaches its solubility and

regains a stable state.

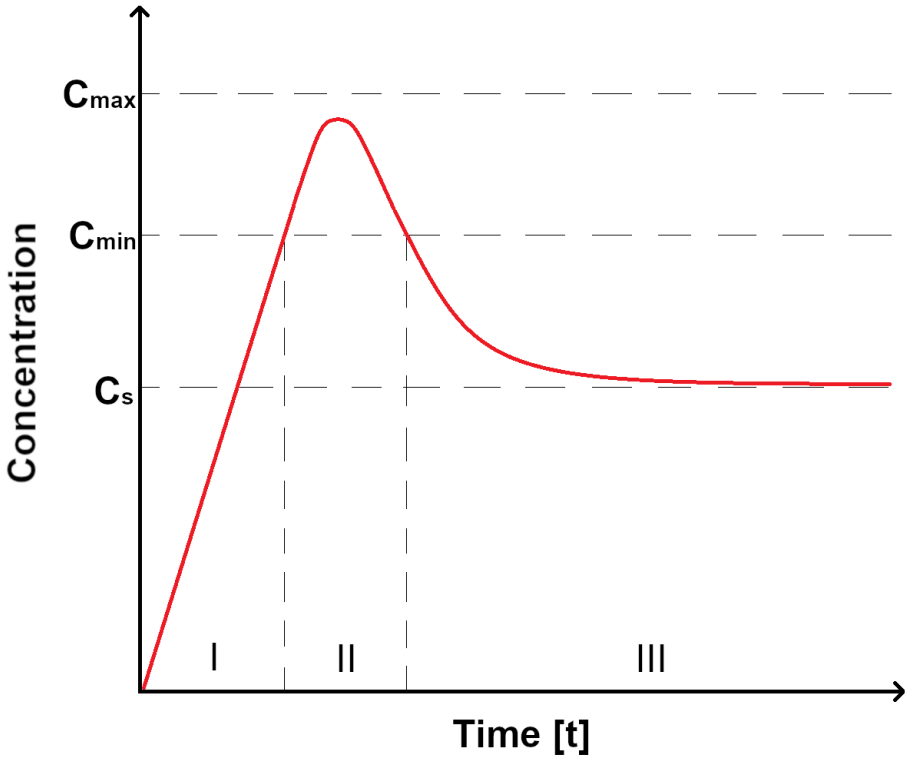

Figure 2.1: Schematic representation of the LaMer model in crystallization. Area I shows the period where monomer concentration is increased, in area II nucleation is occurring and in area III particle growth is the predominant mechanism.

The degree of supersaturation is however not the only variable used obtain stable nuclei, as higher temperatures also can affect the system [15]. The contributions to the total Gibbs free energy of the system are shown in equation 2.1. As seen in this equation, temperature and supersaturation affects ΔG_V, which is the necessary energy required to form a solid-liquid interface. The other contribution to the total Gibbs free energy, ΔG_S, is the excess free energy of the metastable solution over the solid deposition.

$$\Delta G = \Delta \mathrm{G_V} + \Delta \mathrm{G_S} = V \mathrm{G_v} + \gamma A = 4\pi r^2 \left(\frac{-k_B r T ln(S)}{3v} + \gamma\right) \tag{2.1}$$

2.1.2 Nanoparticle growth and aging

As more nuclei form, the degree of supersaturation decreases with the lowering monomer concentration[19]. According to the LaMer model the favourable process in the system at this point will be growth rather than nucleation, as this is more energetically favourable[18]. It requires less energy to add the monomer to an already present particle than for it to form a new nucleus with other monomers[19]. This principle is often utilized in seeded growth, a technique which allows for better control of the growth[19;20]. In this method small crystals are used as seeds for new monomers to dispose on, in a solution with specific conditions and growth affecting chemicals present to allow for control of the crystal growth.

As the monomers deposits on the particle surface, spherical particles will usually form as this is the most favourable shape energetically[20]. In seeded growth however, which is when nanoparticles are added to serve as the starting point for further growth, the degree of supersaturation will affect the morphology of the particle[19]. At higher degrees of supersaturation (but less than what is required for nucleation) more irregular forms of growth such as branching will occur. On the other hand, lower degrees of supersaturation will favour more isotropic shapes.

Furthermore, other shapes can also form by using shape influencing substances or capping agents, or adjusting other parameters in the crystallization reaction[20]. In gold nanorod synthesis, a seeded growth method, use of silver nitrate is for example known to affect the aspect ratio of the rod and the use of other capping agents such as oleic acid will also favour different shapes than spheres[8;9]. In addition, the concentration of reducing agent, pH and seed concentration will also influence the final shape[20;9].

After the synthesis is done, the growth process is still not completely finished. During storage, aging will occur[19]. The are several aging mechanisms, such as phase transformations, which is a process where a metastable crystal will form initially, before a phase transformation causes it to reach a stable phase. Another important mechanisms of aging is one called Ostwald ripening. Ostwald ripening is a process where smaller particles start to dissolve into monomers, which deposits onto the surface of the larger particles. This will over time result in larger particles, but also a more narrow size distribution. These changes are important to be aware of when performing a synthesis.

2.2 Functionalization of nanoparticles

In many Au NP synthesis, the particle will be capped by moieties which are non-functional and potentially cytotoxic[5;21]. Gold nanorods e.g. are mostly capped with CTAB, a substance which is not biocompatible. To make the nanoparticles useful, it is therefore necessary to functionalize the particles with molecules such as for example ssDNA[22]. The functional molecule which is added to the nanoparticle surface can be one capable of binding a specific target, one which is less cytotoxic and increases the stability of the nanoparticle in solution or one capable to enchance imaging, theranostic and therapeutic properties[21;22]. Functionalization can either be done by building upon the current capping agent using chemical reactions or hydrophobic bonds, or by performing a ligand exchange, where the capping agent is replaced with a functional molecule[5].

2.2.1 Ligand exchange

In most established nanoparticle syntheses, the capping agent is important for the size and shape control of the particle and switching it with another may affect the particle[23]. Therefore, it is often desirable to switch the capping agent with another ligand by performing a ligand exchange after a particle has been synthesized. In this reaction the present ligand is usually labeled as the outgoing ligand and the one which is desired to switch is called the incoming ligand.

Some nanoparticles have capping agents which can be displaced easily with molecules which have a stronger affinity to the nanoparticle surface[24]. For instance, Au NPs have a strong affinity for soft ligands, which are acid or bases with stronger polarizability, large atomic radius and low electronegativity[25]. Thiols and phosphines are therefore commonly used to substitute the original capping agent with a functional group. In silver nanoparticles capping agents such as PVP have been shown to be completely replaced by thiols, whereas in gold nanoparticles, CTAB has been completely replaced in a two-step process where PEG-SH and MUA was added to displace the CTAB[26;27].

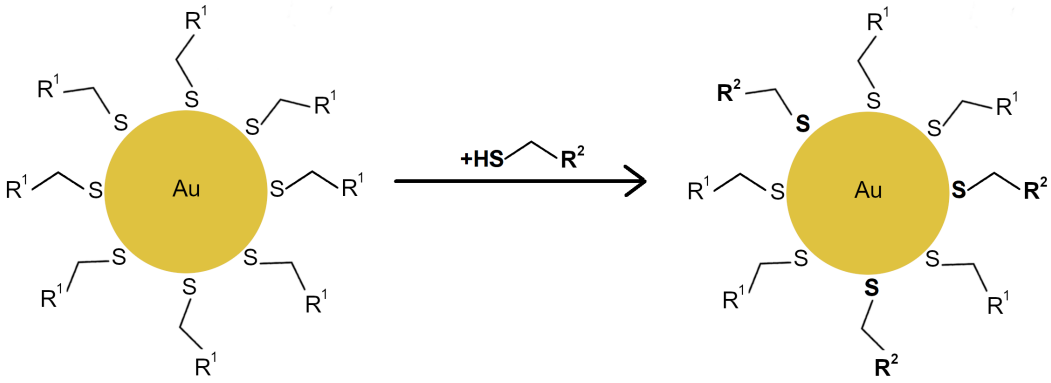

Figure 2.2: Illustration of a ligand exchange where both the incoming and outgoing ligand are thiols[24].

Ligand exchanges can also be used to exchange ligands with the same terminal group, as illustrated with thiols in figure 2.2[24]. This exchange is dependent on several parameters, such as temperature, particle size and the nature of the ligands. These exchanges are mainly non-complete and a much of the outgoing ligand will still be present on the surface due to the similarity in affinity. However, the length of the outgoing chain will affect the exchange. Shorter chained thiols have in some studies been almost completely exchanged in specific conditions, whereas longer chained thiols are not as easily displaced and have a slower exchange rate than shorter chains[28].

2.2.2 Oligonucleotide functionalization

Functional molecules such as oligonucleotides, enzymes and stabilizing molecules can all be used to tailor the nanoparticle complex for specific purposes[29]. If the goal is to target DNA or RNA sequences, the nanoparticle can be functionalized with synthetic oligonucleotide complementary to the target. These oligonucleotides are mainly single stranded DNA (ssDNA) in biotechnology laboratory work, but can also be RNA sequences.

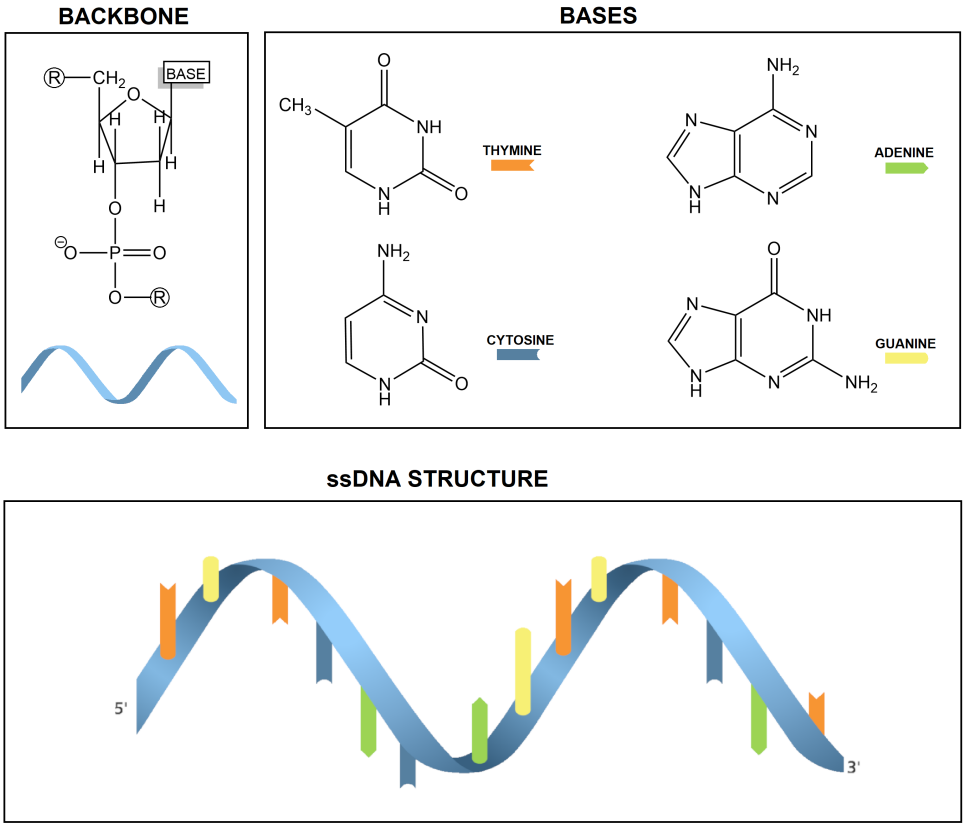

Figure 2.3: The deoxyribonucleic acid backbone structure, bases and overall structure of single-stranded DNA[30].

Oligonucleotides in the form of ssDNA are usually found as intermediates in DNA replication in some biological systems[30]. It is also present in an intermediate step in polymerase chain reactions (PCR), where the double stranded DNA is denatured to form two ssDNA which works as templates for new strands. The structure of an oligonucleotide has a backbone consisting of deoxyribose ssDNA or ribose (RNA). Bases adenine, thymine (uracil in RNA), cytosine and guanine can be bound to this strand, and each base pairs specifically with one of the other bases. The structure of the ssDNA can be seen in figure 2.3, with the chemical structure of the backbone and bases that make up the ssDNA.

Oligonucleotides are mainly synthetically made, and can be modified to be able to bind the nanoparticle[31]. As aforementioned, metal nanoparticles such as Au NPs have a strong affinity to thiols, making thiol modification of oligonucleotides a commonly used method to bind the nanoparticle. The thiol modification can be followed a ligand exchange to replace the capping agent of the nanoparticle with the now thiolated oligonucleotides. The density of thiolated ssDNAs on the Au NP surface is dependent on the curvature of the nanoparticle surface, meaning spherical particles may be able to bind more of the target sequence than a flat surface[32]. Often there may be a linker between the oligonucleotide and the thiol group, but there is no specific one used for all thiol modified oligonucleotides. Figure 2.4 shows how a thiol modified oligonucleotide can be bound to the nanoparticle.

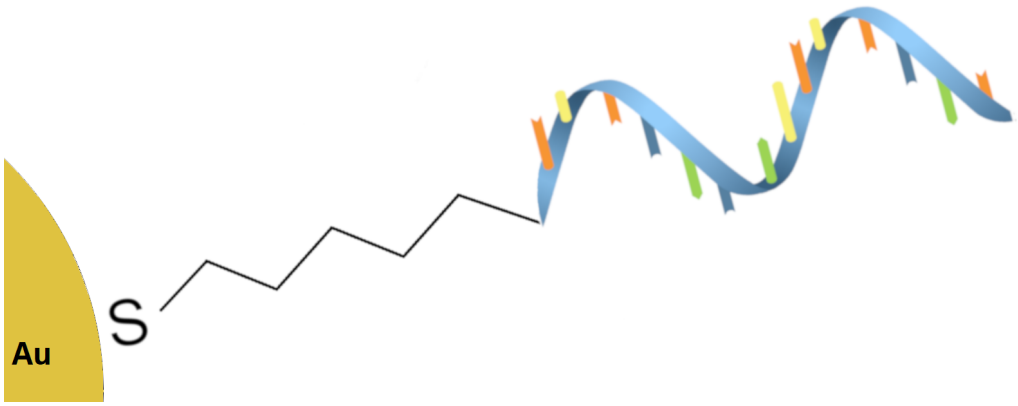

Figure 2.4: Illustration of how a thiol-modified oligonucleotide interacts with the nanoparticle surface. The chain between the sulphur and oligonucleotide in the figure can be several different molecules, and this chain is only an example[32].

2.3 Au NPs as biosensors

Au NPs have a range of potential applications and can for example be used in electronics, drug delivery and for photothermal therapy, and their optical properties also make them very promising as biosensors[4]. They can as formerly established be functionalized with a wide range of functional molecules, making them adaptable too in this field[5]. Biosensors are used for detection of molecules in biological systems and could for instance be used to detect viral infections or concentrations of substances in the body[33]. An example of a common biosensor is the Covid-19 antibody test, where the antibodies (receptors) binds the antigens (target molecule) and causes a red line to appear on the display, which signals that the binding has taken place. Insulin sensors are also biosensors measuring the insulin levels in the body and converting it into a signal.

2.3.1 Biosensing

Biosensing is a process where a receptor is used to bind a molecules found in a biological system, which results in a visible and sometimes measurable signal[33]. This receptor could for example be ssDNA, an antibody or an enzyme, depending on the nature of the target. The binding between the receptor and target molecule is then converted into a signal which can be detected and possibly quantified.

The receptor is very important in a biosensor as it is the main factor affecting the sensors selectivity[33]. If the receptor binds other substances than the analyte, this results in unreliable results, i.e. low selectivity, and it is therefore essential to find a receptor which has a high selectivity in respect to the analyte. The receptor is connected or bound to a transducer, which is the part of the sensor which converts receptor-analyte complex the signal. The transducer is the most important part of the complex in terms of sensitivity. A biosensor with high sensitivity gives a noticeable signal in samples with low analyte concentrations. In many cases an amplifier is used to increase the signal to make it easier to identify for the instrument processing the signal, but finding a sensitive transducer is essential when making a biosensor.

There are several different types of biosensors which can be categorized based on their receptor and their transducer. The receptor could be based on DNA bindings, antigen-antibody interactions, enzyme bindings and more[34]. If the biosensors are categorized by their transducing element on the other hand, they can be labelled as either acoustic, thermal, electrochemical or optical biosensors[35]. In acoustic biosensing the analyte-receptor complex changes the physical properties of an acoustic wave, which can be measured to detect the binding. Thermal biosensors are based on the analyte-receptor binding reaction causing heat to be absorbed or released, making it possible to demonstrate the analyte by changes in the temperature. There are many types of electrochemical biosensors, but their common principle is that ions and electrons are involved in the analyte-receptor reaction which causes electrical changes the can be measured.

Finally, optical biosensors are based on light how the complex is affected by or affects light. Au NPs are examples of optical biosensors, and they are based on the binding between the receptor and analyte causing changes to the refractive index of the Au NP[36].

2.3.2 Au NP-based biosensing

Some of the most important qualities of Au NPs are their optical properties, which are the result of a phenomena called localized surface plasmon resonance (LSPR)[4]. This phenomena occurs when light interacts with particles of lower sizes than the wavelength of the light[36]. When exposed to white light, the surface electrons of the nanoparticle will start to oscillate with a specific resonant frequency, which depends on the shape and size of the particle[4]. nanospheres (NSs) will for example have one peak in an absorbance spectrum due to its isotropic nature, whereas nanorods (NRs) will have different properties in different directions[36]. The rod has one short axis and one long axis, which results in one peak each in their absorbance spectrum. Sea urchin-like particles or nanourchins (NUs) will on the other hand have one absorbance peak similarly to spheres, but will have a broader peaks at higher wavelengths due to the spikes[11;12]. These three examples are illustrated in figure 2.5.

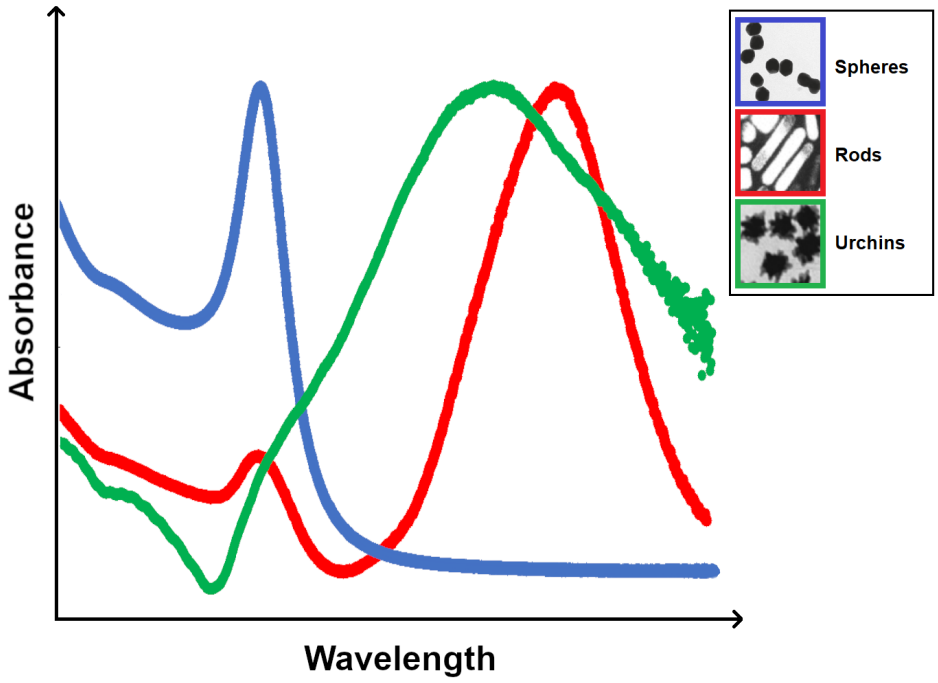

Figure 2.5: Example absorbance spectra for nanospheres (blue), nanorods (red) and nanourchins (green) with representative TEM images. The spectra and images are adapted from reported literature[10;8;12].

Au NPs can be used as biosensors by binding the receptor to the particle surface

as presented in the functionalization chapter[37]. Because of the NPs optical properties, they can be utilized to convert the binding into a measurable signal[36]. When the functionalized particle binds the target molecule the local refractive index will change, causing a shift in the absorbance spectrum. This could either be in the form of a red-shift towards higher wavelengths, but blue-shifts have also been reported in some studies[4;38] Functionalization can also have this affect the cause this shift, if the new incoming has a very different refractive index than the outgoing one[4]. By identifying this shift it is possible to identify the presence of the target molecule in a sample, thereby making the Au NP the transducer of the biosensor complex. This analysis could for example be done by UV-Vis, as illustrated in figure 2.6. The shift in the absorbance spectrum shows how sensitive the sensor is, and if the shift is hard to identify at low concentrations the sensor does not have a good performance. Also, an increase in peak absorbance intensity is also often observed in biosensing experiments[39;40]. These principles allow for detection of viruses, DNA/RNA and many other biomolecules[41]. Viruses such as HIV-1 and influenza-virus have been detected even at low concentrations[39;40]. Oligo-functionalized Au NPs have also been shown be functional to sense complementary strands[38]. In many of these methods, the nanoparticle is immobilized on a surface and functionalized in situ.

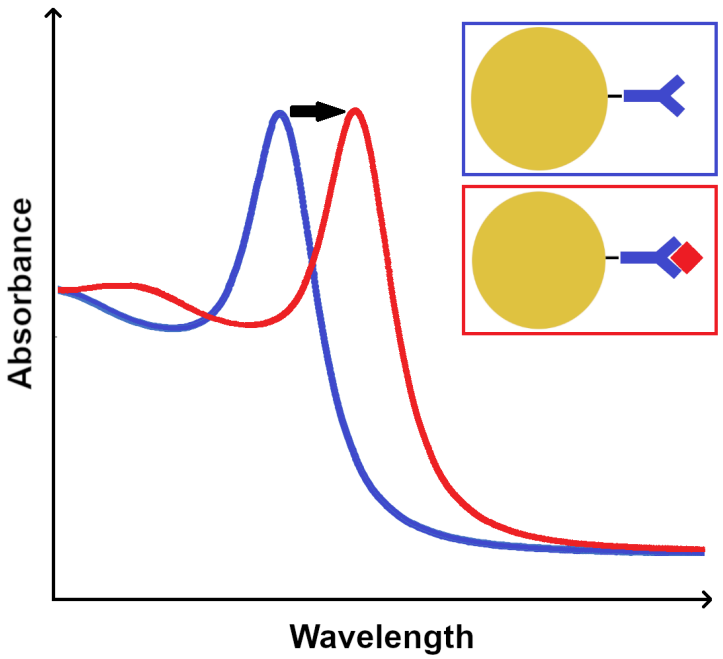

Figure 2.6: Illustration of the change that may be observed in an absorbance spectrum when a functionalized nanoparticle binds the target. The blue plot represents the nanoparticle complex not bound to the target and the red plot represents a target-bound complex[37].

The absorbance peaks at higher wavelength which can be observed in nanorods and nanourchins are also interesting from a biosensing standpoint, as these wave-

lengths are close to or in the near infrared (NIR) area of the absorbance spectrum[12;8;42]. NIR wavelengths have the potential of penetrating human tissue, which could make it possible to do in-vivo biosensing, which could be done by Surface Enhanced Raman Spectroscopy (SERS)[42]. Au NPs are also mainly biocompatible and inert, which adds to the potential of in-vivo biosensing. However, in terms of biocompatibility, the size is important and particles of sizes above 100 nm can have cytotoxic effects[43]. Likewise, the lower concentrations of Au NPs injected will also reduce the risk of developing blood clots[44].

Au NPs can be used as biosensors in other ways than just pure LSPR-based biosensing[41]. In some cases the binding between analyte and receptor on the Au NP surface can cause the particle to become less stable and therefore start to aggregate and agglomerate. This is a method of biosensing in which clear colour changes are observed in the nanoparticle solution, making it a possible to observe with the naked eye. Furthermore, Au NPs can as mentioned be used in SERS biosensing as they have the ability to enhance the light scattering signals in SERS. SERS give information about specific chemical bonds, making it a biosensing method with high specificity. Lastly, Au NPs can also be used to quench or enhance fluorescence due to its optical properties. When the gold nanoparticle is located close to a fluorescent molecule, one of them may transfer energy to the other one in a process called Förster Resonance Energy Transfer (FRET). This causes fluorescence to either enhance or be quenched depending on if the Au NP is the donor or the acceptor.

2.4 Au NP characterization

Nanoparticle characterization is essential to determine the size, shape and surface charge of the particles among other properties. This is important to verify that a synthesis based on an existing protocol has been successful or to examine the properties of a newly developed synthesis. There have been developed several different techniques and instruments for this purpose, and the properties can be therefore be measured in several different ways. In this section some of the main methods of determining shape, size, surface charge and optical properties are presented, in addition to methods of quantification. This will mainly focus on the methods which are going to be utilized later in this project.

2.4.1 Size and shape determination

The size of nanoparticles is very important for its biocompatibility, as particles larger than 100 nm may have cytoxic effects and lower cellular uptake[43]. There are several methods of measuring nanoparticle size which are based on different principles[45]. Two of the most common methods utilized in nanoparticle size determination are size determination based on Transmission Electron Microscopy (TEM) imaging and TEM, but many other analytical methods such as particle tracking analysis and centrifugal liquid sedimentation can be utilized for size determination.

Particle tracking analysis uses scattered light scattered by the particles to determine their size[46]. The function of this technique will be discussed further in the particle quantification chapter. Centrifugal liquid sedimentation on the other hand uses measurements of the particle solution over time while its being centrifuged[47]. During centrifugation, particles will move towards the outer rim of the centrifuge and will continuously be measured to find the rate of sedimentation. These measurements could for example be absorbance or transmittance measurements, as less particles will be present over time to absorb light.

In TEM imaging, electrons are transmitted through the sample to create an image of the sample[48]. This allows for both shape and size determination of the nanoparticles. The main components of the instrument are a electron source which can transmit the electrons and electron apertures, condenser lenses and objective lenses to control the electron beam[49]. When the electrons are sent through the sample, the interactions cause them to scatter, and this scattering is detected and used to generate an image on the computer screen[48]. A simple schematic of some of the main parts of a TEM microscope is shown in figure 2.7 and an example of a TEM image taken using bright-field imaging.

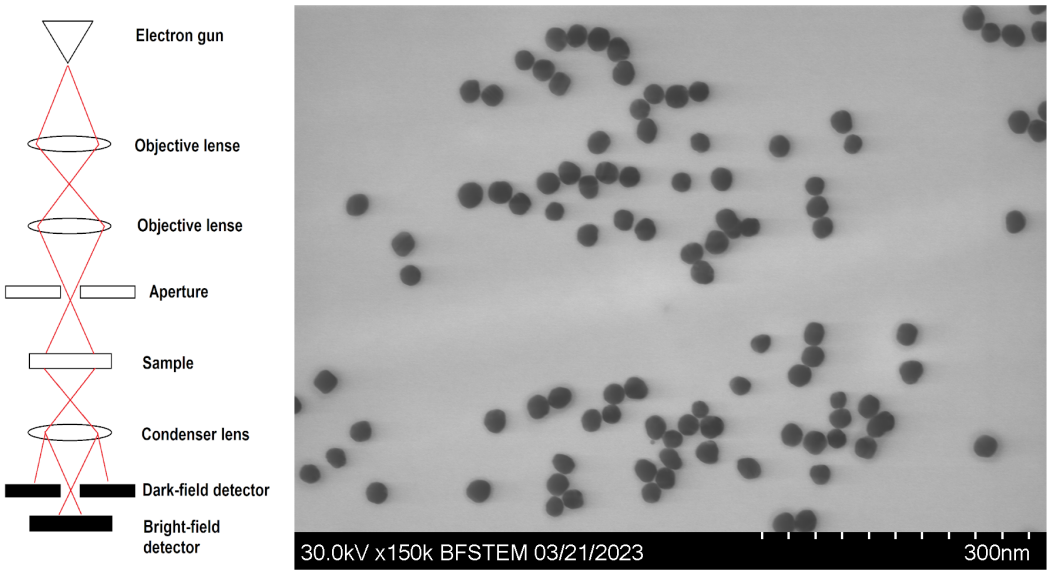

Figure 2.7: Example schematic of the most important parts of a TEM instrument can be distributed along the path of the beam. An image taken in the bright-field mode is also included.

After TEM imaging has been performed the images have to be analyzed to determine the sizes[45]. This can be done using image analysis software, such as for example ImageJ. These types of software uses the scale in the TEM image as a reference to determine the particle size. One limitation of TEM based size determinations is that a very small portion of the nanoparticle population is analyzed[50]. If the images are not representative of the population, there may be significant errors in the estimated size.

DLS can also be used for size determination, and builds on a different principle where the intensity of scattered of light is measured over time[51]. The fluctuations in the light scattering intensity over time are caused by the Brownian motion of the particles. The intensity fluctuations in the measurements can therefore be used to measure the Brownian motion of the particles. Interactions of nanoparticles with solvent molecules causes this motion and it is dependent on size, temperature and solvent viscosity. Therefore the viscosity of the solvent needs to be known and the temperature should be fixed to obtain accurate size measurements. This can be seen in the Einstein-Stokes equation (equation 2.2), which also shows that the hydrodynamic radius (D_h) can be derived if the translational diffusion coefficient (D_τ) is known. This coefficient can be derived from how rapid the fluctuations in scattering intensity is. Larger particles move slower in solution and scatter more light, whereas smaller particles move faster and scatters less light, which causes differences in the fluctuations in scattering intensity.

$$D_\tau = \frac{k_B T}{6\pi\eta R_h} \qquad \Rightarrow \qquad R_h = \frac{k_B T}{6\pi\eta D_\tau} \tag{2.2}$$

The size that is calculated from the scattered light is the hydrodynamic size, and it is therefore important to understand what this size tells us. The hydrodynamic size is the size of a hypothetical sphere that diffuses at the same rate (same D_τ) as the measured particle including the capping agent that stabilizes it[51]. This makes measurements of particles with anisotropic shapes more uncertain than measurements of spherical particles. As TEM sizes are estimated based on the particle alone, the measured hydrodynamic size will be larger than the measured TEM size. The hydrodynamic radius will therefore be dependent on which capping agent is used and how stretched out it is in the solvent.

Other than the issue of measuring anisotropic particles, there is also one important issue even when measuring the size of isotropic structures[52]. If there are few large contaminants present in the sample, they may have a large influence on the measured size since DLS measures the scattering intensity. Larger particles or contaminants will scatter more light than smaller ones, making them measure higher intensities compared to the nanoparticles, even though they may be significantly outnumbered.

2.4.2 Zeta Potential measurements

Zeta potentials can give information about the electrostatic potential of what is referred to as the slipping plane[53]. A nanoparticle in solution will have ions of opposite charge of the surface bound to them. The particle and the strongly bound ions form the Stern layer and other both positive and negative ions will be loosely associated to this layer. An illustration of what constitutes the Stern layer and the slipping plane can be seen in figure 2.8.

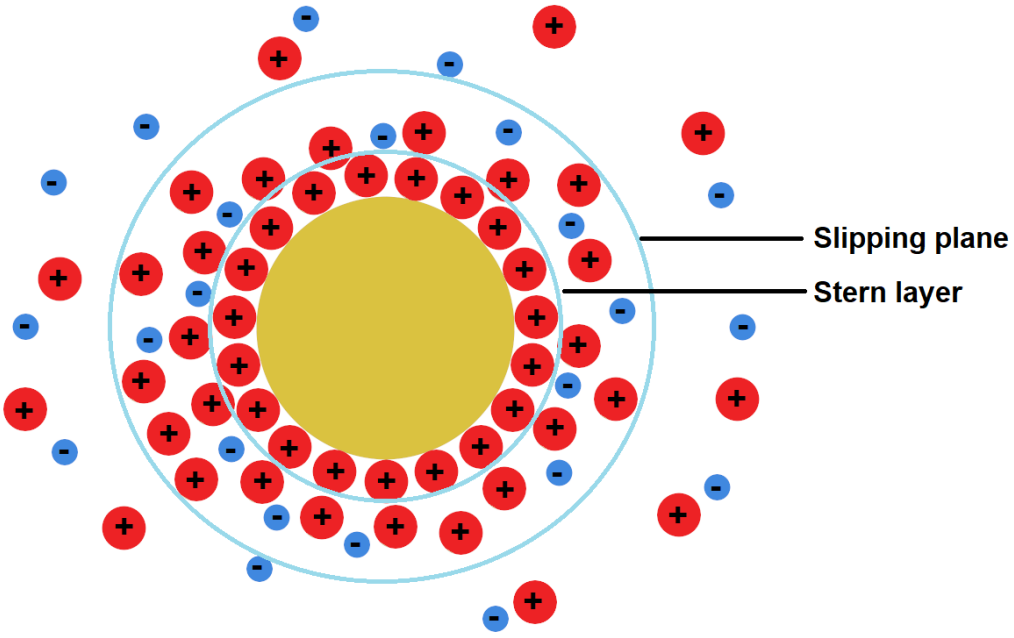

Figure 2.8: Illustration of the Stern layer and slipping plane included of the nanoparticle.

When the nanoparticle solution is analyzed with regards to zeta potential, an electrical field is applied and the particle will start to move from one of the electrodes in the cell to the other[53]. The loosely associated ions which move along with the nanoparticles in the solution form the formerly mentioned slipping plane. The movement of the particles is measured by Electrophoretic Light Scattering (ELS), a technique where a laser beam is scattered by the particles in the solution[54]. The frequency of the scattered light is measured and the difference in this and the frequency of the laser is proportional to the movement speed of the particles. The higher the electrophoretic mobility of the particle is, the higher the zeta potential will be and the speed of the particles can therefore be used to determine the zeta potential.

2.4.3 Spectroscopic analyses

Au NPs absorb specific wavelengths in the visible, near-infrared and infrared region of the electromagnetic spectrum, depending on its shape and size[36]. Spectroscopic analyses such as UV-Vis spectroscopy can show the wavelengths the particle solutions absorb, and other methods can even be used to find the structure of the molecules present in the sample[55]. Raman spectroscopy and Fourier Transform Infrared (FTIR) spectroscopy for example, uses the vibrations in the chemical to give information about its structure. The former measures the energy of the light scattered by the sample, whereas the latter measures how much light is absorbed at specific wavelengths within the infrared region.

To find the absorbance spectra of a Au NP population in these regions, Ultraviolet visible (UV-Vis) spectroscopy can be used as a tool[56]. In this method, light is dispersed into its constituent wavelengths by a prism, allowing for the instrument to analyze specific wavelengths individually. Only light with that specific wavelength is let through the sample, and the instrument measures how much of it is transmitted through the sample. A schematic of this can be seen in figure 2.9. The intensity of the light after the sample is divided by the intensity of the light before the sample, giving the transmittance of the sample. The absorbance is then found by calculating the negative logarithm of the transmittance.

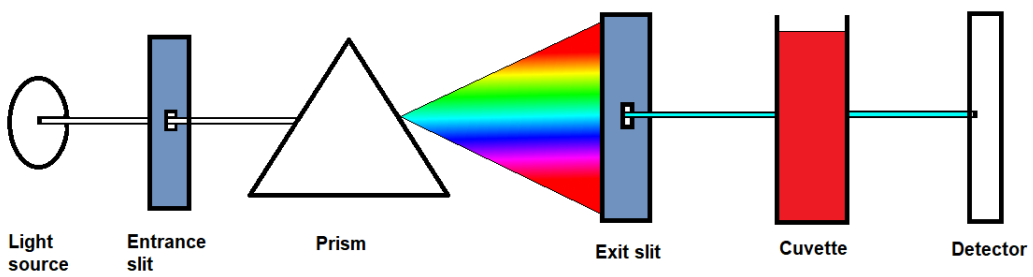

Figure 2.9: Schematic of a typical UV-Vis setup, showing how the absorbance of specific wavelengths of light is analyzed.

Other spectroscopic analyses can also be utilized to learn more about the nanoparticles. FTIR spectroscopy is a method where organic molecules can be identified based on which wavelengths they absorb[57]. Vibrations from specific bonds in a chemical structure will cause the chemical to absorb specific wavelengths, making it possible to identify these groups in a sample. Carboxylic acids will for example often have a peak in the range of 1700-1725 cm^{-1}, mainly because of the vibrations of the C=O bond. Different carbonyls will have peaks at slightly different wavenumbers because of the atoms bound to the carbon. This principle makes it possible to identify functional groups in the spectra.

2.4.4 Particle quantification

Particle Tracking Analysis (PTA) can as previously mentioned be used for size estimations of a nanoparticle population, but it can also be used to determine the concentration of nanoparticles[46]. In PTA, the Brownian motion of individual nanoparticles is tracked based on the light they scatter. The particles are injected into a cell, and are then exposed to a thin sheet of light, which causes them to scatter light. The scattered light is focused onto a camera, which creates an image on the computer screen. Here, the particles will be seen as dots moving along the screen, as can be seen in the illustration in figure 2.10. The centre of each individual particle is identified and tracks it over a certain amount of frames[58].

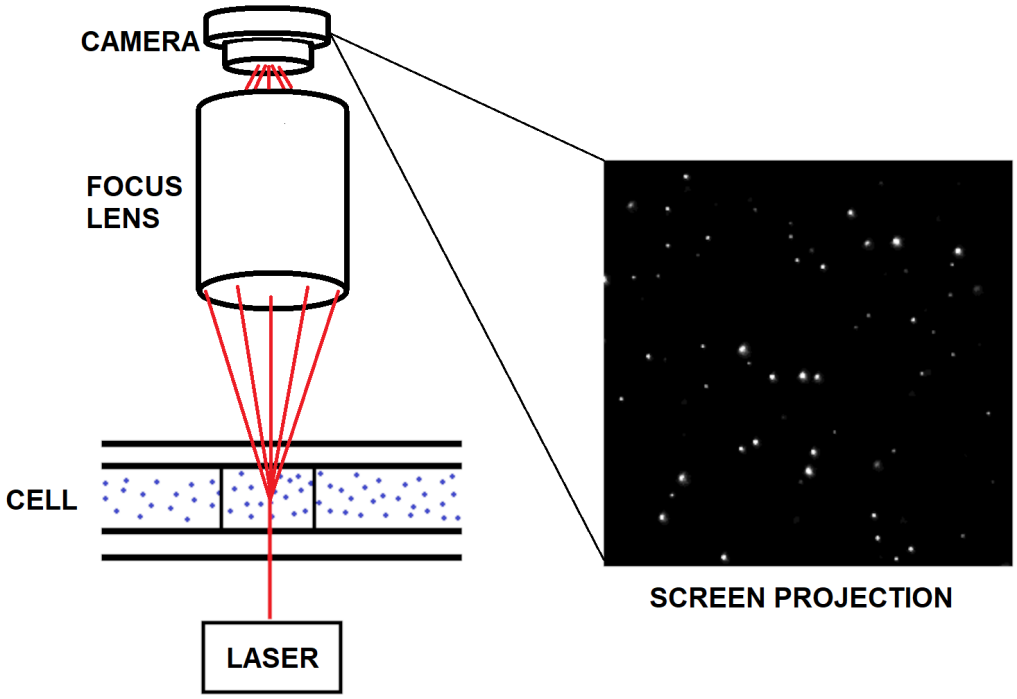

Figure 2.10: Schematic of how PTA works, with an example image of how the particle solution could look on the image projected on the screen.

The camera is focused on a very small area of the cell with a known volume, which makes it possible to measure the amount of particles present in this area[58]. This can be translated to the concentration per mL by scaling, and this number can be used to find the concentration of an undiluted sample by using the dilution factor.

There are however some issues with using PTA. As the particles are being tracked over a number of frames, movement of the particles can cause errors in the measurements[46]. Firstly, if the particle move closer to or further away from the camera they can go out of focus and therefore not be measured properly. Furthermore, if two particles are located close together their intensity peaks could be mistaken as each others, which could lead to errors in the size determination. The samples also generally have to be diluted significantly, which could be a source of error[58].

3 Literature review

3.1 Methods of gold nanoparticle synthesis

Au NP synthesis can be carried out using several different methods based on the desired shape. A seeded approach is commonly utilized to obtain the wanted shape and size, as this allows for larger degree of growth control [20]. The most commonly used methods utilize three main reactants; a salt containing gold, a reducing agent and a capping agent to stabilize the synthesized particles [8;11;10]. Additionally, some syntheses use shape-inducing agent such as silver nitrate to get the desired shapes [8;11]. These agents and varying reaction parameters such as pH can affect the final shape of the nanoparticles [9]. Figure 3.1 is a schematic representation of the main steps the in seeded Au NP synthesis, mainly seed synthesis and growth.

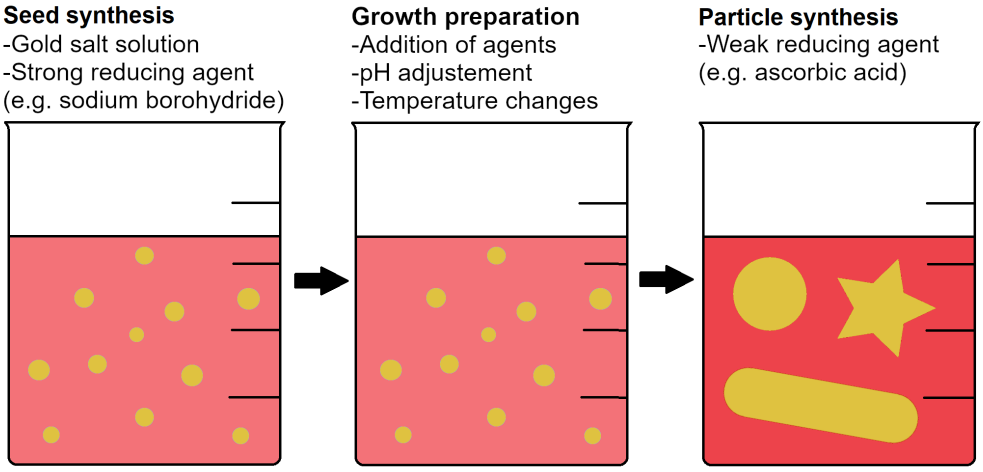

Figure 3.1: Schematic of the main steps in seeded Au NP synthesis, including seed preparation, growth preparation and the final particle synthesis.

3.1.1 Methods of gold nanosphere synthesis

Spherical Au NPs can be synthesized directly in a system, meaning seeding is not necessary. Synthesis of spherical and quasi-spherical nanoparticles have been known for a very long time and one of the most used methods was developed in 1951 by Turkevich et al., and is still used in different variations today [6].

The Turkevich method is a direct method of Au NP synthesis, but the particles obtained can be used for seeded growth to obtain larger spheres or different shapes [6;10]. In this method, a chloroauric acid solution is heated to boiling before adding sodium citrate. During the minutes after sodium citrate addition, the solution will obtain a blue-gray colour before finally turning wine red. Using this method, Turkevich et al. reported gold nanoparticle sizes of 20 $\pm$ 2 nm.

Another well established method is the Brust method, in which gold nanospheres in the range of 1.5-5.2 nm can be obtained [29]. This methods utilizes tetraocty-

lammonium bromide to transfer gold from its aqueous solution to toluene[59]. Then, aqueous sodium borohydride and dodecanethiol is added and gold colloids will form. In the crystallization, sodium borohydride plays the role of the reducing agent and the particles are stabilized by dodecanethiol.

An example of a seeded method of gold nanosphere synthesis is a method developed by Bastús et al[10]. In this method the authors first synthesized Au NS seeds by heating sodium citrate (2.2 mM) to 100 ℃ before adding chloroauric acid (25 mM) and stirring the solution for 10 minutes. The seeds were then used for further growth by two additions of chloroauric acid. Following this, the sample was diluted by removing some of the sample and adding MQ water and sodium citrate solution. This solution was again used as seeds, and the process was repeated as many times as wanted. The first generation they synthesized were 18 ± 1 based on TEM measurements, and the following three generations were measured to be 2 ± 2, 31 ± 3 and 36 ± 2, respectively. These generations corresponded to absorbance peaks of 521.5 nm, 523.5 nm, 525.5 nm and 527.5 nm.

3.1.2 Seeded method of gold nanorod synthesis

One common method of nanorod synthesis is a two-step process developed by Nikoobakht and El-Sayed, which involves an initial synthesis of a seed solution followed by further growth to obtain nanorods[8]. In the seed synthesis three components are used. Firstly, chloroauric acid which is the source of gold in the solution. In the solution, gold will initially exist in the form of Au^{3+}. The second component is sodium borohydride, a strong reducing agent which reduces the Au^{3+} to Au^0. Due to its strong reduction potential, nucleation will be favourable as the solution is highly supersaturated in regards to gold. The final component is Hexadecyltrimethylammonium bromide (CTAB), which works a the capping agent of the gold seeds, stabilizing the particles in solution.

In the second step of the synthesis, chloroauric acid and CTAB is used as in the seed preparation, but silver nitrate is also used[8]. Nikoobakht and El-Sayed found the concentration of silver nitrate to be a determining factor of the final nanorods aspect ratio. They found that by increasing the volume of silver nitrate added, the rod aspect ratio would increase up to over 4. Above a certain concentration the aspect ratio would start to decrease. These particle solutions gave absorbance spectra with two peaks, one at around 510 nm and another one which moved to higher wavelengths and had higher intensities with increasing silver nitrate concentration used in the synthesis.

In addition, ascorbic acid is used as the reducing agent at this point. This is a weaker reducing agent than sodium borohydride, which allows for a lower degree of supersaturation and therefore prevents new nuclei from forming. The formerly synthesized seeds are added into the solution, the reduced gold of the solution is deposited on the surface of the seed, causing an increase in nanoparticle size and a change in shape from spherical rod-like.

3.1.3 Seeded methods of gold nanourchin synthesis

Several different methods have been developed to synthesize sea-urchin like or star-shaped Au NPs. These are mainly seeded approaches, where small, spherical nanoparticles are first synthesized. The desired shape is then obtained by either adding other reactants to the mixture or using specific solvents.

One such approach is one developed by Li et al., where hydroquinone was used to induce branching during the growth [60]. Their hypothesis was that increasing hydroquinone concentration would make deposition of monomers on the (111) lattice planes more favourable and thereby a higher degree of branch growth. Their seeds were synthesized using a Turkevich-based nanosphere synthesis, meaning the seeds were capped by citrate [6]. Citrate, $HAuCl_4$ and hydroquinone were the only reactants used in the seeded growth and they could tune the size and degree of branching by adjusting the amount of each reactant [60]. They were therefore able to synthesize particles with sizes between 55 and 200 nm and absorbance maximums between 555 and 702 nm.

Kumar et al. developed a method of synthesizing sea-urchin like Au NPs [12]. The seeds of these particles were synthesized by first coating spherical Au NSs (15 nm) with polyvinylpyrrolidone (PVP) and dispersing them in ethanol, a procedure developed by Graf et al [61]. Afterwards, Kumar et al. dissolved PVP in DMF, before mixing it with chloroauric acid and finally adding the Au NS solution [12]. After 15 minutes of mixing the solution achieved a blue colour and the resulting particles had an absorbance peak at 764 nm, with a shoulder peak at around 550 nm. The average size of the final particles synthesized using PVP with $M_w = 24\ 000$ was 69.0 ± 7.9 nm, whereas the average size of the final particles synthesized using PVP with $M_w = 10\ 000$ was not given.

Other reported methods use several different chemicals to induce spike formation or synthesize other types of seed, such as one reported by Qin et al [62]. The seed synthesis is done by using poly(diallyldimethylammonium)chloride (PDDA), ethylene glycol, silver nitrate and the seeds are dispersed them using a CTAB-solution. The sea-urchin shaped nanoparticles are then formed by mixing CTAB, $HAuCl_4$ and ascorbic acid before adding the seeds and glutathione and mixing for two hours. In a protocol developed by Li et al., gold/silver seeds can be prepared by mixing silver nitrate and $HAuCl_4$ and reducing the metal ions with ascorbic acid [11]. By then adding more $HAuCl_4$, they managed to form urchin-shaped nanoparticles.

3.2 Methods of nanoparticle functionalization

In Au NP syntheses, the capping agents are predominantly molecules with only a stabilizing function[5]. Therefore, many ligand exchange methods have been reported on different types of particles. Some of these methods are direct exchanges where the particle is mixed with the ligand of interest, whereas some are two-step processes where a partial exchange is done prior to the exchange with the ligand of interest[24;27;26].

3.2.1 Direct ligand exchanges

Ligand exchanges can sometimes be performed directly, if the affinity of the original ligand is sufficiently lower than the incoming ligand[63]. In these exchanges, the ligand is added to a nanoparticle solution and mixed for a certain amount of time. Then, the nanoparticles can be washed to remove the original ligand from the solution.

Xia et al. compared the efficiency of direct ligand exchange with o−[2−(3−mercaptopropionylamino o′−methylpolyethylene glycol (PEG-SH) in several different types Au NPs with different capping agents[64]. They found that citrate capped nanoparticles could be easily replaced by the PEG thiols, but that CTAC and CTAB on nanospheres and nanorods were only replaced to a very low degree. PVP on gold nanocages were not as easily replaced as citrate, but were replaced to a higher degree than CTAC and CTAB.

Direct ligand exchange of PVP on nanocubes has also been studied in silver nanocubes (Ag NCs) by Horan et al[26]. In this study, PVP was replaced with cysteamine and mPEG-SH by mixing equal volumes of Ag NCs ($5 * 109$ particles per mL) and thiol (1 µM). They then studied the removal of PVP by taking aliquots out of the reaction mixture at different times in the reaction, and analyzing them using SERS. They observed that the intensity of the PVP-peak in the SERS spectra decreased the longer the reaction went on and therefore concluded that the ligand exchange was successful with both cysteamine and mPEG-SH.

The method of the ligand exchanges are generally just to mix the incoming ligand with nanoparticle solution, but when working with specific ligands it can be important important to note how the ligand will affect the dispersibility of the nanoparticle. In their aptamer based ligand exchange, Huang et al. used a direct approach, but had to redisperse the particles in a sodium citrate solution with bovine serum albumin (BSA) to avoid aggregation of the nanoparticles. In this ligand exchange thiol-modified aptamers were the incoming ligand and the nanospheres used were capped with citrate.

3.2.2 Two-step ligand exchanges

Many methods use two-step approaches to exchange the original capping agent of the particle, especially when this capping agent has a high affinity to the surface[63]. This first step can either be done to partially exchange the capping agent or to remove excess capping agent in the solution. In the second step, the wanted ligand is added to the solution and replaces the original capping agent.

Gold nanorods are often synthesized with CTAB, which is cytotoxic, as the capping agent[21]. Thierry et al. reported one method where CTAB is replaced with o−[2−(3−mercaptopropionylamino)ethyl]−o′−methylpolyethylene glycol (PEG −SH) and 11-mercaptoundecanoic acid (MUA) in a two step process[27]. The structure of these chemicals can be seen in figure 3.2. Firstly, CTAB-capped nanorods were mixed with PEG-SH (1 mg/mL), sonicated and left to react for 2 hours. After this they centrifuged the particles and functionalized them with either MUA and AMTAZ. The particles were first mixed with the chemicals and subsequently sonicated in a water bath at 55 ℃for 60 minutes. Afterwards, the mixture was left overnight, before being sonicated, centrifuged and finally redispersed in water. The pH was adjusted based on which functional molecule was used. The reason the PEG-SH was first used before functionalization with MUA or AMTAZ was that other reported that the direct functionalization was complex and had problems with aggregation and strict reaction conditions[27]. Therefore, using PEG-SH was proposed by Thierry et al. to work as a temporary stabilizer and still be effectively replaced by MUA and AMTAZ.

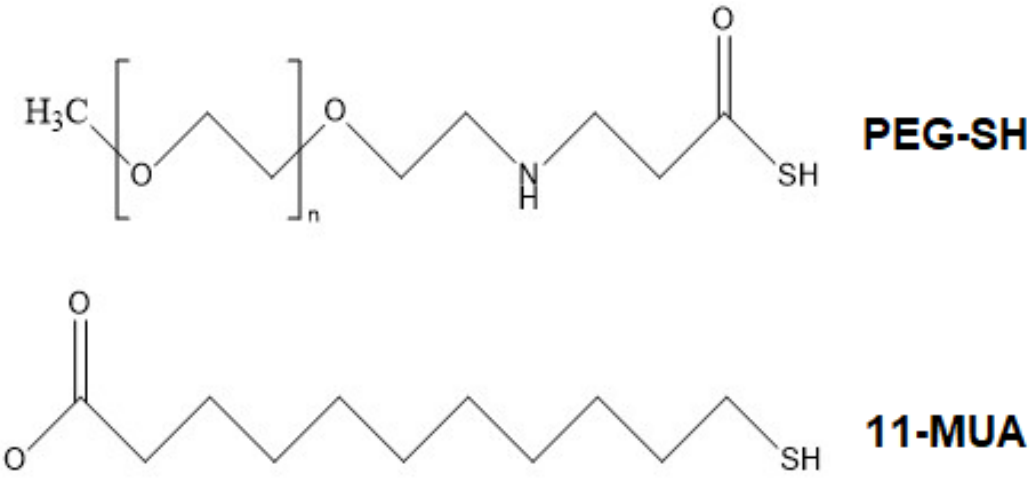

Figure 3.2: The structure of the PEG-SH and 11-MUA used in the Thierry et al. method of ligand exchange for CTAB-capped Au NRs.

Another two-step ligand exchange for CTAB-capped nanoparticles was developed by Dewi et al[65]. In this method, the first step is to remove excess CTAB in the solution by washing with dicholoromethane (DCM). The excess CTAB will after mixing be present in DCM rather than in the aqueous phase. 3-mercaptopropionic acid (3-MPA) is then added to the mixture after DCM is

removed, to replace the remaining CTAB stabilzing the nanoparticles. The thiol group in 3-MPA has a high affinity to the gold surface and can therefore replace the CTAB. CTAC removal on Au NPs is reported by Zhou et al., in a method where silver ions are reduced onto the Au NP surface in a mixture with PVP, which stabilizes the particles[63]. Afterwards, acetone is added and the particles were separated using centrifugation and redispersed in a sodium citrate solution. The particles are then etched using hydrogen peroxide and finally redispersed in sodium citrate, causing the particles to be capped with citrate.

3.2.3 Oligonucleotide functionalization

Functionalization of Au NPs with oligonucleotides has also been studied extensively. Most commonly in gold nanospheres, where citrate is exchanged with a thiol-modified oligonucleotide. Most of these methods are based on a methods developed by Mirkin et al., in which the exchange is done by sequential addition of sodium chloride[66]. The salt masks the charges of both the citrate and the oligonucleotides, which screens the charge-charge repulsion between the particle complex and the oligonucleotides, as well as internally in the oligonucleotide molecule[67]. This allows the oligonucleotides to get closer to the surface and finally replace the citrate.

The direct functionalization is not as common in other shapes, as they are often synthesized with capping agents which have a high affinity for the surface or are dispersible in other solvents than water[24;12]. Therefore, some studies have been focusing on how to use the chemical nature of the capping agent to attach the oligonucleotide. Zhang et al. did for example use N-(3-Dimethylaminopropyl)-N- ethylcarbodiimide hydrochloride (EDC) and N-Hydroxysuccinimide (NHS) to conjugate a amine-modified oligonucleotide to an MUA-capped Au NP[68]. This was the only two commonly reported methods found in the literature search, but there could potentially be other alternatives to these, utilizing other chemical reactions.

4 Materials and methods

In this section, the materials and methods used during the experimental work are presented. Chloroauric acid ($HAuCl_4$, $\geq$ 99.99%), sodium hydroxide ($\geq$ 99.0%, pellets), silver nitrate ($\geq$ 99.0%), sodium borohydride ($\geq$ 98.0%), MUA, PVP (10 kg/mol), NHS (98%), EDC ($\geq$ 98.0%), N,N-dimethylformamide (DMF), HEPES ($\geq$ 99.5%), PEG-SH, sodium chloride (NaCl, $\geq$ 99.5%), Sodium dodecyl sulfate (SDS, $\geq$ 99.0%) and sodium citrate trihydrate ($\geq$ 99.0%) were purchased from Sigma-Aldrich®. CTAB ($\geq$ 99.9%) was purchased from Acros Organics. D-(-)-Isoascorbic acid (98%) was purchased from Alfa Caesar®. Hydrochloric acid (37%) and ethanol (absolute) were purchased from VWR chemicals®. (5'-SH- CCA ATG TGA TCT TTT GGT GT -3') was purchased from GenScript, whereas (5'-NH_2- CCA ATG TGA TCT TTT GGT GT -3') and the FAM-modified complementary strand was purchased from Biolegio.

4.1 Synthesis of gold nanospheres

The synthesis of spherical Au NPs was done by using an adapted protocol developed by Bastus, N.G. et al[10]. Initially the seeds were prepared by adding sodium citrate (2.2 mM, 15 mL) to a round-bottom flask and heating it to 100 or 125 ℃ under vigorous stirring (400 rpm). The solution was stirred for 15 minutes before adding chloroauric acid (25 mM, 0.10 mL) and the solution was stirred for 10 minutes.

The growth steps were done by first lowering the temperature to 90 or 80 ℃ and chloroauric acid (25 mM, 0.10 mL) was added again and the solution was stirred for 30 minutes. Chloroauric acid (25 mM, 0.10 mL) was then added again the solution was stirred for another 30 minutes. Then, 5.5 mL of the solution was removed and MQ water (5.3 mL) was added followed by sodium citrate (60 mM, 0.20 mL). This growth process was repeated multiple times to increase the size further.

4.2 Synthesis of gold nanorods

The seed mediated growth was based on the approach developed by Nikoobakht, B. and El-Sayed M.A[8]. Firstly, CTAB (364 mg) was weighed out in a vial followed by the addition of MQ water (5.0 mL). The CTAB was dissolved by stirring the solution at 90 ℃ and then cooled to room temperature. $HAuCl_4$ (0.50 mM, 5.0 mL) was added and stirred at 750 rpm for 7-8 minutes. $NaBH_4$ (10 mM, 0.60 mL) was diluted with MQ water (1.0 mL) and stirred for 2-3 minutes before the stirring bar was removed. The solution was left for 30 minutes before use.

Then, CTAB (1.2 g) was weighed out in a vial, before MQ water (15 mL) was added. The vial was then put on a heating plate and the mixture was heated to 90 ℃ under stirring to dissolve the CTAB. After the CTAB had dissolved

completely, the solution was cooled down to 35 ℃ and silver nitrate (4.0 mM, 0.75 mL) was added. The solution was stirred for 15 minutes, before $HAuCl_4$ (1.0 mM, 15 mL) was added and the solution was stirred for another 15 minutes.

Ascorbic acid (128 mM, 135 µL) was then added, followed by the addition of Au NP seeds (96 µL). The mixture was stirred at 1000 rpm for 30 seconds, before removing the stirring bar and leaving the solution at 35 ℃ overnight. The following day, the samples were cleaned three times by centrifugation at 14.5k rpm for 20 minutes, and finally redispersed in MQ water (5 mL).

4.3 Synthesis of gold nanourchins

The first step of the process was based on a protocol delevoped by Graf, C. et al., which uses PVP to coat gold nanospheres. Firstly, an Au NS solution (h_d 26 nm, 3.47 mL) was mixed with a PVP solution (25.6 g/L, 0.65 mL) and stirred at 600 rpm for 24 hours. Afterwards, the particles were centrifuged (11.0 rpm, 10 min), the supernatant was removed and ethanol was added to achieve a theoretical gold concentration of 4.2 mM.

Then, PVP (M_w = 10 000, 0.15 g) was dissolved in DMF (15 mL) according to a procedure by Kumar, P.S. et al[12]. Then, the particles solution was mixed with chloroauric acid (164 µL, 25 mM) before PVP@Au NS solution ($7.7 * 10^{10}$ particles) was added quickly. The solution was stirred for 15 minutes before being washed with centrifugation (11k rpm, 10 min) several times using ethanol as the solvent. Finally, the particles were redispersed in MQ water (4.0 mL).

4.4 Replacement of CTAB on Au NRs

The exchange of CTAB on the surface of the Au NR was performed by mixing PEG-SH (2.56 mg/mL, 1.0 mL) with Au NRs ($2.3 * 10^9$ - $3.5 * 10^{10}$ particles per mL, 1.0 mL). This solution was mixed at 400 rpm for two hours, before being washed using centrifugation (14.5k rpm, 20 min) and finally redispersed in MQ water (1.0 or 2.0 mL).

11-MUA was then weighed out and dissolved in ethanol first, before adding an equal volume of water. The 11-MUA solution (10 mM, 0.25 mL) was mixed with the PEG@Au NRs ($9.6 * 10^9$, $4.8 * 10^9$, $2.4 * 10^9$ or $1.2 * 10^9$ particles per mL, 0.50 mL). This mixture was vortexed for five seconds and sonicated for 1 hour at 55 ℃. The particle solution were then centrifuged (14.5k rpm, 10 minutes) and redispersed in MQ water (0.50 mL).

Another approach was also used for the 11-MUA functionalization. In this instance, the nanorods were redispersed in ethanol after the PEG step, before 11-MUA in ethanol (10 mM, 0.25 mL) was added to the nanorod solution ($3.1 * 10^(9)$ - $3.5 * 10^(10)$ particles per mL, 0.5 mL). This was mixed for two hours, followed by centrifugation (14.5k rpm, 20 min) and redispersion in MQ water (1.0 mL) or HEPES (1.0 mL, pH 7.6).

4.5 Replacement of PVP-capping on Au NUs

The removal of PVP on Au NUs was done by adapting a protocol developed by Horan et al[26]. MUA was first dissolved in ethanol to create a 1 µM solution. This solution (0.70 mL) was mixed with an equal volume of Au NU solution in ethanol ($1.5 * 10^{10}$, $7.5 * 10^9$ or $3.8 * 10^9$ particles/mL, 0.70 mL) and stirred for two hours under stirring at 400 rpm.

After this, the sample was transferred to a centrifuge tube and centrifuged at 11k rpm for 10 minutes. The supernatant was removed and the particles were redispersed in MQ water, before being washed once again using centrifugation. Afterwards, the particles were redispersed in MQ water (1.0 mL) or HEPES (1.0 mL, pH 7.6).

4.6 Functionalization of Au NSs with thiol-modified oligonucleotides

Au NSs were functionalized by mixing Au NS solution (0.50 mL), HEPES buffer (pH 7.6, 0.50 mL), thiol-modified oligonucleotides (5'-SH- CCA ATG TGA TCT TTT GGT GT -3') (25 µL, 100 µM) and SDS (1.0 %)[66]. The solution was vortexed for 30 seconds and left for twenty minutes. Then, NaCl (5 M, 10 µL) was added while the sample was sonicated. This was repeated six times with 30 second of vortex and 20 minutes of incubation between each salt addition. After this, the sample was left overnight, before being centrifuged three times (10k rpm, 15 min). The sample was then redispersed in HEPES buffer (pH 7.6, 1.0 mL).

4.7 Functionalization of Au NPs with amine-modified oligonucleotides

Functionalization with oligonucleotides was done based on two protocols developed by Zhang et al. and Kim et al[69;68]. First Au NPs (1.0 mL) dispersed in HEPES buffer (pH 7.6) was mixed with amine-terminated oligonucleotides (5'-NH_2- CCA ATG TGA TCT TTT GGT GT -3') (100 µL, 20 µM). Then, NHS (0.4 M) and EDC (0.2 M) was mixed in equal volumes and added (0.50 mL) to the Au NP mixture. The mixture was stirred at 300 rpm on a shaker plate for 24 hours, with sonication performed a few times during the reaction. The particle solution was then washed by centrifugation three times (14.5k rpm, 20 minutes) and subsequently redispersed in HEPES buffer (pH = 7.6, 1.0 mL).

4.8 Biosensing with Au NPs

Biosensing tests were first performed using a NanoDrop spectrophotometer. Each nanoparticle sample was analyzed three times with varying amounts of target RNA in addition to one blank sample with only Au NPs. The target RNA was isolated from the same strand of the SARS-CoV-2 virus which was first identified

in Wuhan at the start of the pandemic. The amounts of target RNA were set to 100, 500, 1000, 5000 and 10000 copies. A dilution series was made with the mentioned amount of copies per 50 µL.

The samples were prepared by first sonicating and vortexing the Au NP solutions and adding them (40 µL) to a centrifuge tube. Then, the desired amount of copies were added to the mixture (50 µL) and the mixture was vortexed and incubated for 10 minutes before characterization. Three parallels were made of each sample and the average spectrum was calculated based on this. Finally, the spectra were smoothed using SigmaPlot.

Biosensing tests were also performed using a regular UV-Vis spectrophotometer. In this testing, each particle solution was tested with three different target RNA concentrations, which were 10 000, 100 000 and 1 000 000 copies. Au NPs (600 µL) were first sonicated and vortexed, before target RNA (100 µL) was added. The sample was incubated for 10 minutes before being analyzed in the spectrophotometer.

4.9 Characterization

Before characterization, they had to be prepared by using vortex and ultrasonication. Firstly, the particles were sonicated for 1 minute and vortexed for 30 seconds. For absorbance measurements of samples, the Agilent Cary 60 UV-Vis spectrophotometer and ThermoFisher Scientific NanoDrop One was used. The samples were in the former measured at wavelengths between 200 and 1100 nm at a rate of 300 nm/minute in the former and between 300 and 850 nm in the latter.

S(T)EM images were obtained using the Hitachi High-Tech SU9000 Scanning (Transmission) Electron Microscope (S(T)EM). Samples were prepared by adding nanoparticle solution (0.040-0.15 mL) on a carbon-coated copper grid. The size determinations based on the TEM images were done in ImageJ, where between 200 and 500 particles from several different images were used to estimate the size. In the nanorod size determinations, both the short long side was measured individually.

Hydrodynamic size determination were done using the Anton Paar LiteSizer 500, which uses DLS as the basis for the hydrodynamic size measurements. This instrument was also used to measure zeta potential, which is done by using ELS.

To estimate the particle concentration of the samples used in the experimental work the Particle Metrix ZetaView was used, which is a PTA. The samples were diluted to 50-200 particles per frame and the settings used are shown in table 4.1. For nanospheres, the sensitivity was increased to 90 because of the small size.

Table 4.1: The settings used for the particle tracking analysis done by ZetaView.

Sensitivity	70
Frame rate	30
Shutter	100
Trace length	15
Min area	5
Max area	100
Min brightness	25

5 Results and discussion

In this section, results from the experimental work is presented and discussed. The results are divided into three main parts, which are synthesis of gold nanostructures, functionalization of the particles and biosensing. The first part focus on synthesis of the different particles and characterization of the particles which were used later. In the functionalization part, the removal of CTAB and PVP will be discussed, followed by the functionalization with oligonucleotides. Finally, the sensitivity of each biosensor complex is discussed and compared.

5.1 Synthesis of gold nanoparticles

Three different types of particles were synthesized in this experiment. Optimization of the nanosphere synthesis will be discussed in the first section and the characterization of the spheres in the optimized synthesis will be presented. Secondly, the characterization of nanorods will be discussed, focusing on the effect of silver nitrate on the rod aspect ratio. Finally, the synthesis of nanourchins is presented, with focus on repeatability of the synthesis and stability of the particles.

5.1.1 Initial synthesis of Au NSs

The synthesis of gold nanospheres was performed in two different ways. The first one followed the protocol of Bastus, N.G. et al., where the seeds step was done at 100 ℃ and the growth steps were done at 90 ℃. This was repeated three times, and in all three experiments four generations of particles were synthesized, including the seeds. The average hydrodynamic size of each generation is shown in table 5.1.

Table 5.1: The hydrodynamic radius of each generation of the three first nanosphere syntheses. In these syntheses the seeding was done at 100 ℃ and the growth step were done at 90 ℃.

Generation	First synthesis	Second synthesis	Third synthesis
1st gen.	24 ± 0 nm	23 ± 0 nm	31 ± 1 nm
2nd gen.	29 ± 0 nm	24 ± 1 nm	36 ± 1 nm
3rd gen.	34 ± 0 nm	26 ± 0 nm	37 ± 1 nm
4th gen.	39 ± 0 nm	31 ± 0 nm	41 ± 0 nm

There were a couple of challenges with these syntheses. The first step of the synthesis, when nucleation is occurring, particles of very different sizes were synthesized. This can be seen in table5.1 by comparing the measured sizes of the first generation particles. Consequently, the method seemed to have a low degree of repeatability due to the lack of size control. Due to this problem, a simple measure was taken in the subsequent syntheses. The temperature during seeding was increased to 125 ℃ to make nucleation favourable and therefore

get seeds with less variations in size[15]. If the total Gibbs free energy is too low during the nucleation, growth may be favoured and therefore cause larger particles. The 1st generation sizes are different, which may be the result of too low temperature. By increasing the temperature, the total Gibbs free energy of the nucleation can be increased, as seen in equation 2.1. The temperature in the growth steps was also lowered as a pre-emptive measure to avoid secondary nucleation in the next syntheses. Higher temperatures increase the Gibbs free energy in a nucleation process, and can therefore induce nucleation[15]. Hence, decreasing the temperature to 80 ℃ would make secondary nucleation less likely than at 90 ℃.

5.1.2 Modified synthesis of Au NSs

The NPs of the 1st generation in each synthesis were measured using DLS and the hydrodynamic sizes were measured to 21 ± 1 nm, 19 ± 1 nm and 26 ± 2 nm, respectively. The size distributions of the 1st generation in the third synthesis can be seen in figure 5.1, where the left plot of the image portrays the size distributions of the as-prepared 1st generation sample in one of the syntheses. The right plot shows the size distributions of the same sample after it was filtered using a 0.20 µm filter.

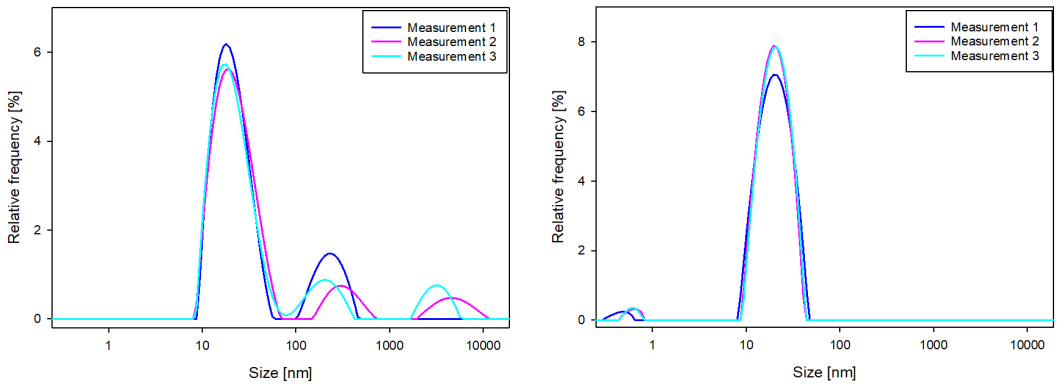

Figure 5.1: The size distributions of the unfiltered (left) and filtered (right) 1st generation sample of the third synthesis. The filtration was done using a 0.20 µm filter and the sample was measured in series of three measurements both before and after filtration.

The dissimilarity in hydrodynamic size between the three samples seemed to indicate that there still were issues with the synthesis. However, as can be seen in figure 5.1, the 1st generation had several peaks in its size distribution plot, while the prevalence of these kinds of peaks decrease for each generation. It was therefore hypothesized that these peaks were caused by aggregates, external contamination or the higher concentration of the first generations. Aggregates makes sense based on DLS theory, as even a small number of aggregates would give give off a large signal in DLS, as larger particles are more heavily weighted

than smaller particles[51]. The higher particle concentration of the earlier generations could also be an explanation, as this causes the particles to be located closer together, which is known to cause issues when tracking their motion. This would also explain the trend of the decreasing signals at later generations, since the growth solution is diluted during the synthesis. The samples were filtered to find out if this was the case. After filtration at 0.20 µm the peaks were eliminated, as can be seen in the right plot of figure 5.1. This makes it likely that aggregates or too high concentration of nanoparticles likely caused the issues. The hydrodynamic sizes of the filtered samples of the 1st generations were used, as they were thought to be a better representation of the particle size than the unfiltered samples.

The hydrodynamic sizes of all the samples in the modified synthesis are shown in table 5.2. The samples marked with a star were filtered before the measurements. A table showing the hydrodynamic sizes before filtration can be seen in appendix A.

Table 5.2: The hydrodynamic radius of each generation of the three syntheses in which seeding was done at 125 ℃ and the growth step were done at 80 ℃. Samples with signals above 200 nm in their first measurements were re-measured after filtration using a 0.20 µm syringe filter.

Generation	First synthesis	Second synthesis	Third synthesis
1st gen.	19 ± 0 nm	17 ± 0 nm	19 ± 0 nm
2nd gen.	25 ± 0 nm	24 ± 0 nm	27 ± 0 nm
3rd gen.	30 ± 0 nm	28 ± 1 nm	29 ± 0 nm
4th gen.	35 ± 0 nm	30 ± 0 nm	33 ± 0 nm

Based on the results presented in table 5.2, the repeatability of the synthesis seems to be better when using the modified temperature program. The first generation particles are fairly close in hydrodynamic size, but the size increase for each generation seems to vary slightly between the three syntheses. This culminates in a size difference of 5 nm between the smallest and largest samples in the fourth generation samples. In all the other generations the gap between the syntheses is 2-3 nm, which is a significant improvement to what was observed in the former temperature program. However, as some of the samples were filtered before the DLS measurements there are some potential errors. If the hypothesis that the other peaks in the size distribution plot were caused by excess sodium citrate is wrong, characterizing the filtered samples would give a faulty image of the particle population. Hence, these numbers should to be compared with the results of other size determining methods, and size measurements based on TEM images could give a better indication of the nanoparticle sizes than the DLS measurements of the hydrodynamic size.

The measured sizes based on TEM images of the nanospheres are shown in figure 5.2. This bar chart shows how the size of each generation compares to the same generations in the other syntheses. The specific sizes are shown in

appendix A, and all measured samples were unfiltered. Histograms of the TEM size measurements of the particles from the last synthesis can be seen in appendix B.

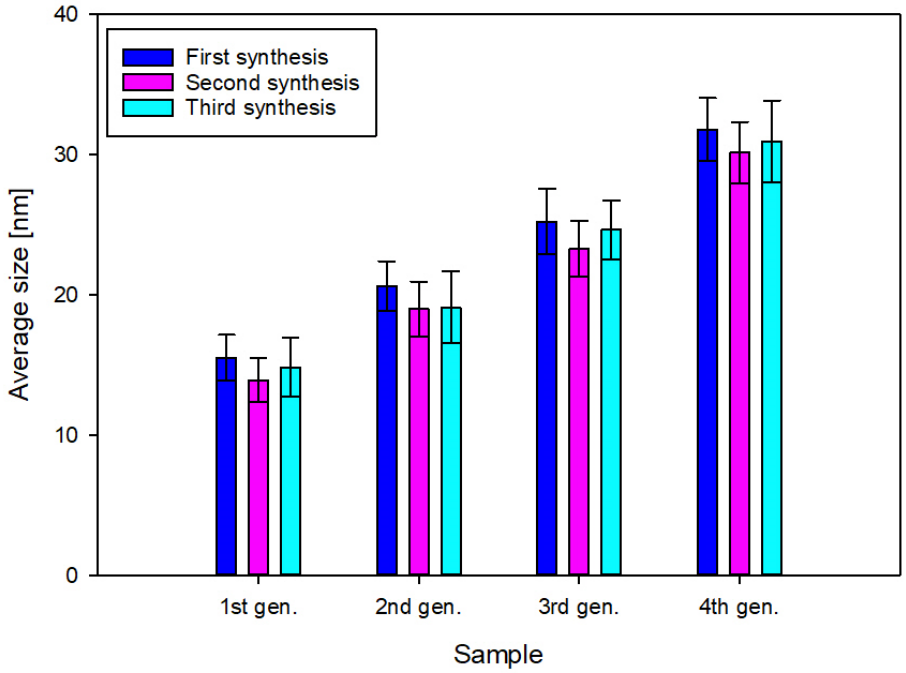

Figure 5.2: The TEM measured TEM sizes of all generations in all three repeats in the synthesis where seeding was done at 125 ℃ and the growth steps were done at 80 ℃.

The results from the TEM image measurements show that the size differences between the three synthesis are not very large. This indicates that it was correct to filter the samples before DLS measurements, as the TEM sizes are more similar to the filtered samples than the unfiltered samples. As expected, the TEM sizes are slightly lower than the hydrodynamic sizes as it only includes the particle itself[51]. DLS on the other hand, tracks the motion of the particle complex in solution, which also includes capping agents. Further, the TEM sizes show that there is a systematic increase in size of the particles, which is similar between all three syntheses. The sizes TEM sizes are not exactly what Bastús et al. reported and the increases are not as significant, but this could be attributed to small variations in how the synthesis was performed and differences in equipment and slight differences in sodium citrate or chloroauric acid concentration[10]. The differences between the reported particles and the particles synthesized in this project are however not immense and the size increase trend is quite similar, which means that the replication of the synthesis was fairly successful.

Representative images of the four generation of particles are included in figure 5.3. These images are from the particle generations of the third synthesis. Image A shows particles of the first generation, the second generation is depicted in image B, while C and D are images of particles of the third and fourth generation, respectively.

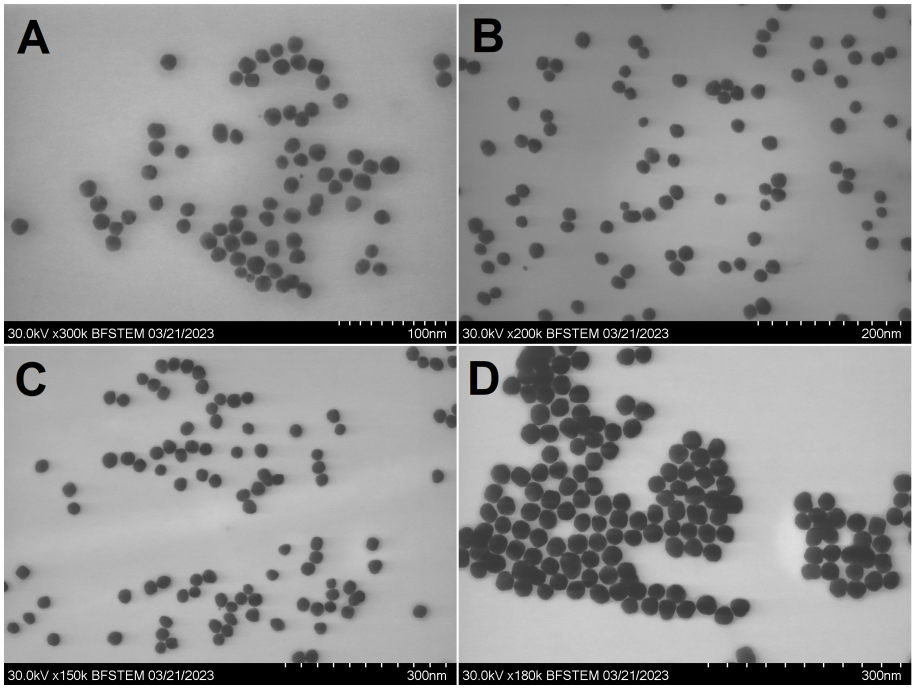

Figure 5.3: Four generations of Au NS from the third synthesis. A shows a representative image of the first generation, image B is representative of the second generation, image C shows the third generation and D shows some of the particles of the fourth and final generation.

The absorption spectra of each generation was obtained using UV-Visible spectroscopy. The spectra the four generations in the third synthesis are shown in figure 5.4. The absorbance peak wavelength increases from 517.5 nm in the first generation, to 519.0 nm, 520.5 nm and 522.0 nm in the second, third and fourth generation.

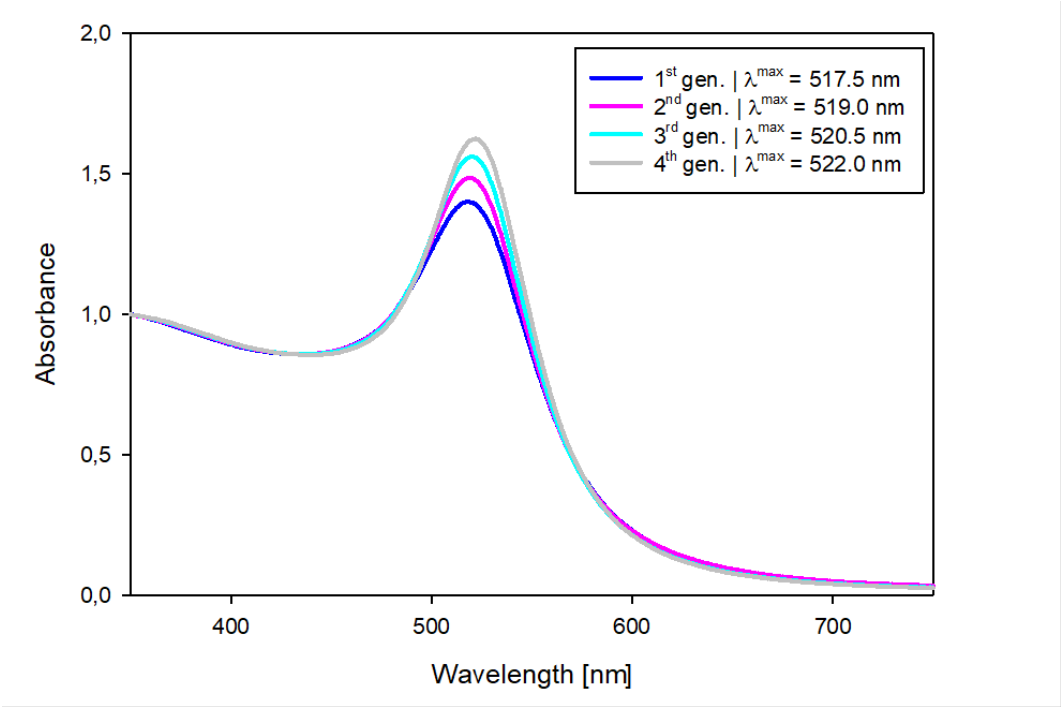

Figure 5.4: The absorption spectra of the four generations of particles obtained in the third synthesis. The legend contains the absorbance peak wavelength, which increases with each generation of particles. Each sample is normalized to itself at 350 nm.

The characterization of particles presented in figure 5.3 and 5.4 shows representative TEM images and UV-Vis spectra of each generation. The former figure shows how the particle size increase significantly from the first to the fourth generation. The latter figure can work as a reference for further work, as there will likely occur changes in the absorbance during the functionalization [4].

The absorbance spectra in figure 5.4 show that there is a slight increase in the wavelength of the absorbance peak for each new generation, which is consistent with the trend observed by Bastús et al [10]. The reason increasing size causes this red-shifts in the spectrum is that the electrons will oscillate over a larger area, which causes the resonant frequency to lower [4]. The trend observed in this work is therefore consistent with the theory. Yet, the absorbance peak wavelengths in this experimental work are consistently lower than the ones reported by the source [10]. This should however not have any effect on the performance, and is therefore not an important factor to consider. Au NSs synthesized using the Turkevich method or methods which use the same reactant are known to be very stable in solution, so further tests to investigate this was not performed [6;10].

5.1.3 Synthesis of Au NRs

The particle length, width, aspect ratio and zeta potential of the three different syntheses, where different volumes of silver nitrate (SN) was used are presented in table 5.3. The length and width are averages based on TEM images of just over 200 particles for each sample, whereas the aspect ratio is calculated based on these size averages. Histograms of the aspect ratios, lengths and widths are shown in appendix B. Rod yield was calculated by dividing the number of rods with an aspect ratio of 1.2 or more to the total number of particles.

Table 5.3: The particle size and aspect ratio based on TEM imaging and zeta potential of the three Au NR solutions. The yield of rods is also included, and all particles with a AR of over 1.2 are counted as rods.

	250 µL SN	500 µL SN	750 µL SN
Avg. particle length	33 ± 8 nm	41 ± 9 nm	45 ± 9 nm
Avg. particle width	16 ± 3 nm	13 ± 3 nm	12 ± 3 nm
Avg. aspect ratio	2.2	3.2	3.9
Rod yield	91 %	96 %	94 %
Zeta potential	12 ± 2 mV	24 ± 1 mV	26 ± 1 mV

TEM images of the these samples are shown in figure 5.5, where A is a representative image of the particles synthesized using 250 µL silver nitrate, while image B and C depicts the particles synthesized using 500 and 750 µL silver nitrate.

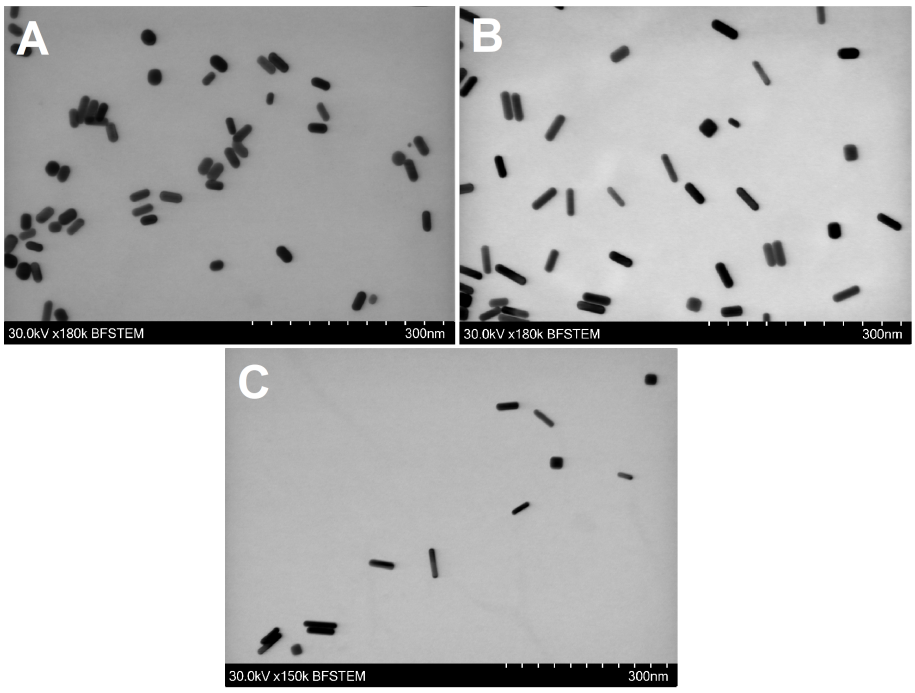

Figure 5.5: TEM images of the three nanorod samples. A is a representative the particles synthesized using 250 µL, whereas B and C are a representative images of particles synthesized using 500 µL and 750 µL.

An important aspect to consider in the size and aspect ratio data presented in table 5.3 is the polydispersity which can be observed in figure 5.5, something which is reflected in the standard deviations in average length and width, shown in table 5.3. Although most of the particles in the images are rod-shaped, there are also several spherical and quasi-spherical particles present in the samples. The aspect ratio of the rods will be underestimated as the spherical particles are also taken into account in the size measurements. This means that the aspect ratio is an average of the entire population, rather than only rod shaped particles.

In the size determinations it is evident that with increasing silver nitrate content, the length of the rods increased whereas the width decreased. In the literature it is suggested that silver ions form complexes with CTAB during the synthesis, which forces the Au NPs to grow into rod shapes[]. Still, these size determinations has a margin of error since only about two hundred particles were analyzed, which is what Nikoobakht and El-Sayed used for their estimations[8]. It is however less than what was used in the Au NS size determinations, and this is because of the difficulty of the shape. Since it was of interest to measure both the length and the width of each particle, automatic size determination based on the 2D area of the particles was not possible. This made the process more time consuming, and all measurements were done manually, which makes human bias or error a potential source of uncertainty. However, these number should still give a fairly good estimation of the populations, both in terms of the sizes and aspect ratios. They could still be somewhat affected by bias and chance, but not to a very high degree. These numbers and the TEM images show that we seem to have achieved three different populations, with different sizes and aspect ratios. This means that the effect of aspect ratio on biosensor sensitivity can be further examined in the biosensing experiments.

On the other hand, the rod yield calculations are more uncertain because of the number of analyzed particles. A few spheres could make a significant difference in the yield, and it is likely that these numbers would have been slightly different, had more particles been analyzed. These numbers are therefore only included to show that there are spheres and quasi-spheres in the population even as the aspect ratio increases. In these calculations, an aspect ratio of 1.2 and above is required for a particle to be counted as a rod. This ratio was set to also include quasi-spherical particles, but makes for some uncertainty as adjusting the ratio by 0.1 either way would affect the rod yield significantly. It is difficult to find exactly the exact aspect ratio which separates a sphere from a rod. Therefore, these numbers are not a perfect representation, but rather an approximation of the rod yield.

Zeta potentials of the AR4 and AR3 nanorods were similar with a zeta potential of around 25 mV and the AR2 nanorods had a zeta potential of about half of that, but all did at least have positive values. This shows that CTAB is on the surface as it should give a positive charge on the particle surface as the positively charged head groups in the adsorbed bilayer[70]. This fact can be utilized in further work.

The zeta potentials are important for functionalization since different capping agents will affect the zeta potential. This makes it possible to use the zeta potential as one of the ways of verifying that CTAB has actually been removed and replaced from the particles.

The UV-Vis spectra of the gold nanorods are plotted in figure 5.6. The blue plot shows the absorbance of the particles synthesized using 250 µL silver nitrate, whereas the the purple plot and Turkish blue plot shows the absorbance of the particles synthesized using 500 and 750 µL silver nitrate, respectively. All samples have similar peaks at in the 510-520 nm range. Their second peaks are very different, as the blue plot has a peak at 650.5 nm, the purple plot has a peak at 764.5 nm and the Turkish blue plot has a peak at 839.0 nm.

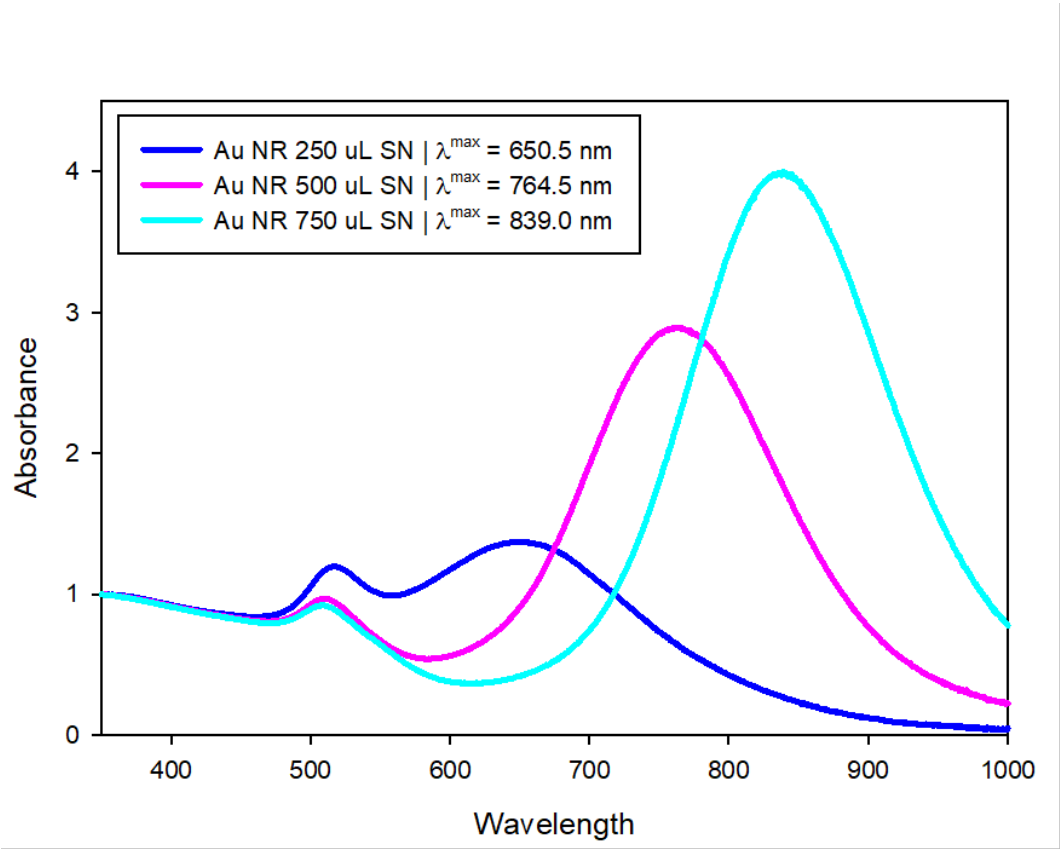

Figure 5.6: The UV-Vis spectra of the Au NR syntheses. The legend shows the SN volume used in each synthesis, which was the only variable between the syntheses. Each sample is normalized to itself at 350 nm.

The UV-Vis spectra in figure 5.6 show that the intensity of the second peak increases as the silver nitrate volume used in the synthesis (and calculated aspect ratio) increases. These UV-Vis spectra prove that we have three different populations, and that the calculated aspect ratios are fairly correct. Also, the wavelength of the second peak is shifted to higher wavelengths with increasing aspect ratio. This synthesis is based on the one reported by Nikoobakht and El-

Sayed, and it is therefore natural to compare these UV-Vis spectra to theirs[8].

For the third synthesis, the absorbance peak is observed at similar wavelengths, as they also reported a peak at just under 840 nm[8]. In the first and second synthesis however, the absorbance peak is observed at slightly lower wavelengths than in the source. Nikoobakht and El-Sayed did not do syntheses which used the exact same concentrations of silver nitrate, but their report contains one synthesis with concentrations which can be used as a reference for this work. By doing interpolation between their results, the absorbance peaks in this work is well in line with what was reported in the source. It should be noted that the exact peak averages achieved by Nikoobakht and El-Sayed were not given, but were read from a graph. This means there is a small margin of error in the estimations. The aspect ratios were also compared to the source and was found to be fairly similar. Therefore, it is likely that this synthesis is easily repeatable. The nanorod samples will from this point be labelled based on their calculated aspect ratios, rounded to the closest integer (CTAB@Au NR AR2, CTAB@Au NR AR3, CTAB@Au NR AR4).

The differences between the Nikoobakht and El-Sayed syntheses and the syntheses in this project are negligible. However, it is important to note that small variations in the concentration of reactants or external influence on the reactants could be the source of these minor differences, as silver nitrate for example is light sensitive[71]. It is therefore important in this synthesis to be aware of these factors to reproduce it. The aim of synthesizing rods of different aspect ratios was achieved, and the synthesis seems to be very repeatable. Hence, these particles were deemed to be suitable for further CTAB removal and oligonucleotide functionalization. There are clearly different populations with different aspect ratios, which makes them suitable to investigate how the aspect ratios affect the Au NRs sensitivity as biosensors.

5.1.4 Synthesis of Au NUs

The synthesis of nanourchins was done three times to find out if the procedure was reproducible. In the two final syntheses, the same gold nanosphere solution was used as the seeds whereas the first synthesis used a different nanosphere solution as seeds. The concentration of these solution is also given.

Table 5.4: The hydrodynamic radius and zeta potential of the three Au NU solutions, and the concentration of the seed solutions used to synthesize the particles.

	First synthesis	Second synthesis	Third synthesis
Hydrodynamic size	145 ± 2 nm	141 ± 3 nm	183 ± 15 nm
Zeta potential	22 ± 2 mV	22 ± 1 mV	22 ± 2 mV
C_{seeds} (particles/mL)	$1.8 * 10^{12}$	$1.8 * 10^{12}$	$7.5 * 10^{11}$

The UV-Vis spectra of three different syntheses of gold nanourchins are presented in figure 5.7. The particle solution of the first synthesis has an absorbance peak 832.5 nm, the second has a peak at 852.0 nm and the third and final has an absorbance peak at 874.5 nm.

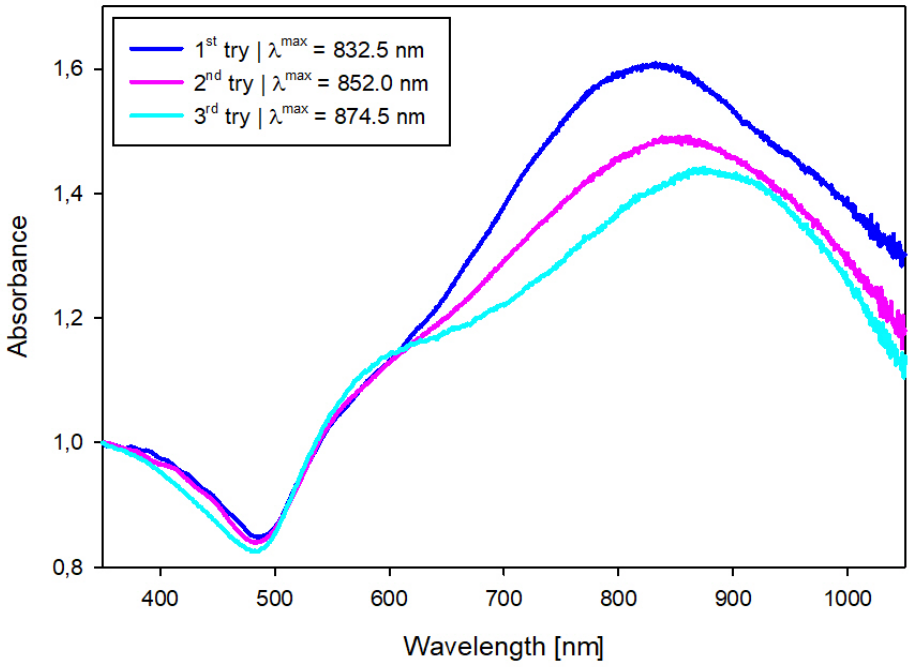

Figure 5.7: UV-Vis spectra of the three Au NU samples. A and B shows the first and second sample, which were synthesized using the same seed solution. C shows the third synthesis, which used a different seed solution. The legend also shows the absorbance peak of all three samples. Each sample is normalized to itself at 350 nm.

In figure 5.8, TEM images of the three nanourchin solutions are shown. Image A shows particles from the first synthesis, particles from the second synthesis are shown in image B and image C shows particles from the third synthesis.

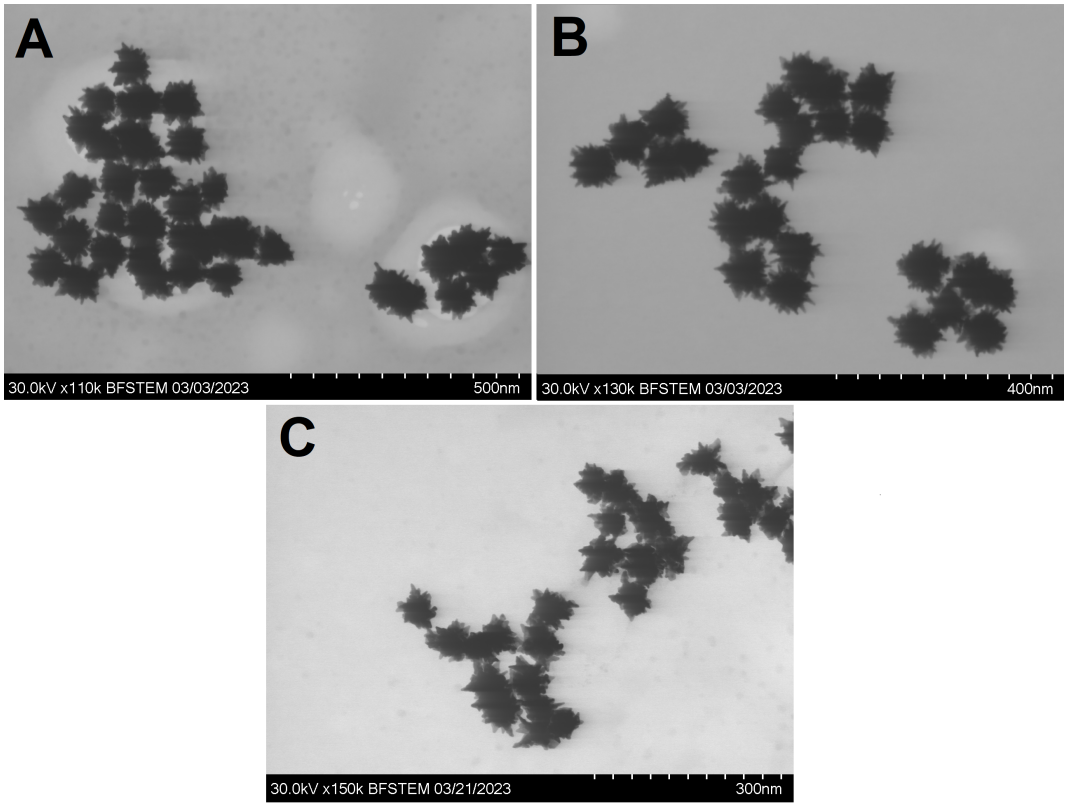

Figure 5.8: TEM images of the three Au NU samples. A and B shows the first and second sample, which were synthesized using the same seed solution. C shows the third synthesis, which used a different seed solution.

A comparison between the hydrodynamic sizes of the three samples given in table 5.4 shows that there is a slight difference between the the first two and the final sample. This could potentially be attributed to small differences in the concentration the seed solutions used in the syntheses. If the particle concentration measurements were slightly off, that could have a notable effect on the growth. If there were less seeds in the solution available for growth but still the same concentration of gold, the particles should theoretically grow larger. In addition, the degree of supersaturation would be higher and could cause a higher degree of diffusion-controlled growth, which means that there would be a higher degree of irregular growth (branch growth)[19]. This seems to be the case when comparing the TEM images in figure 5.8, as the particles in image C seems to be a bit less dense and have a more inconsistent shape than the particles in image A and B. However, this is based on a small sample size and is based on subjective observations, which makes it difficult to draw a definite conclusion.

Further, the UV-Vis spectra in figure 5.7 is also consistent with the size differences, as there is a notable difference between the two first and the final sample. The shoulder peak of the third sample is significantly more prevalent than that of the first two, which supports the hypothesis that there is a morphological difference between the samples. The shape and size of gold nanoparticles cause differences in the absorbance, which should mean that the third sample is different from the former two[4].

There are also differences in absorbance around the peak wavelengths between the second and first sample, but this could be expected in a growth process which favours irregular growth. It could be caused by difference in diffusion rate if the particles were added more or less quick to the mixture, it could be caused by microscopic differences in seeds added as discussed earlier or potentially just be naturally occurring variations in this process. The differences are however within a satisfying range considering the irregular growth, and all three samples have fairly similar absorbance spectra, with only the shoulder peak of the third sample standing out as a significant deviation.

There process is hence be seen as fairly repeatable, and the most significant change could be done differently to obtain less variation it is to use one seed solution for all syntheses, since this would avoid larger differences in supersaturation in the reaction mixture. The particle tracking analysis could give slightly different concentrations every time since the samples have to be very diluted, which could also be a source of error[58]. Still, the solutions from these syntheses were deemed to be usable for further analyses and functionalization as the differences between them was not enormous and all had the desired sea-urchin like shape.

5.1.5 Verification of surface capping on Au NUs

An FTIR analysis was also performed to investigate the particles during the synthesis process. For reference, sodium citrate and PVP were measured individually, followed by measurements of the citrate coated seeds, the seeds after treatment with PVP and the particles after the growth process. The FTIR spectra of all these samples are shown in figure 5.9. Some of the spectra have been amplified to make them easier to compare with the other spectra. The the bonds attributed to each peak are added based on literature[57;72;73;74].

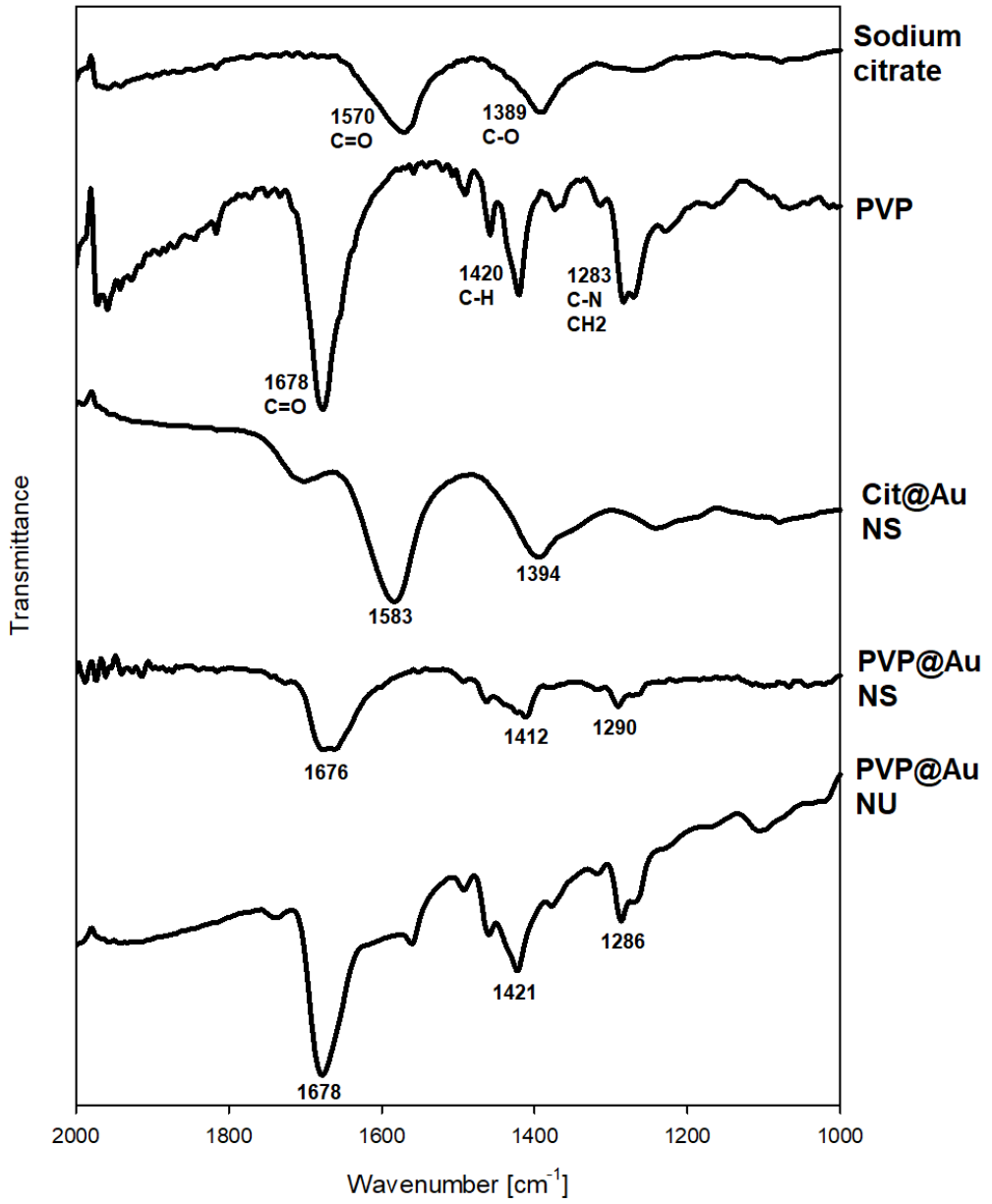

Figure 5.9: The FTIR spectra of the particles from the synthesis, in addition to the references sodium citrate and PVP. The three analyzed particles solution are citrate coated nanospheres, PVP-treated nanospheres and the final nanourchins.

The FTIR spectra ca be used to verify that the correct capping agent is actually present in each step of the process. By comparing the spectra of pure sodium citrate with that of the citrate capped Au NSs from the Au NS synthesis used in this project. Sodium citrate has two clear peaks, one at 1570 cm^{-1} and another at 1389 cm^{-1}, which are also present in the spectra of the Au NSs. Based on the Coates guide on how to interpret FTIR spectra, carboxylates will have peak at between 1610 and 1550 cm^{-1} and in the range 1420-1300 range[57]. Wang et al. also specify that the signal former represents a C=O bond and the latter represents the C-O bond in the carboxyl group[72]. This shows that the citrate shows the expected results in the spectra and can be used as a comparison for the other samples. The citrate-coated nanospheres which were used as seeds has similar peaks in its spectrum, but one of the peaks is at about 1685 cm^{-1}, which is a bit higher than in the sodium citrate measurement from this sample, but still within the Coates range of carboxylates[57]. Hence, the results can be seen as a verification that citrate is actually stabilizing the nanoparticle.

PVP on the other hand has three large peaks, one at 1678 cm^{-1}, one at 1420 cm^{-1} and one at 1283 cm^{-1}. The one at 1675 cm^{-1} is the most prevalent, whereas the others have several sub-peaks at nearby wavelengths. Coates states that tertiary amines should have a peak between 1360 and 1310 cm^{-1}. The nitrogen atom in PVP is bound to three carbons and is therefore tertiary, but none of the peaks are in this range[57]. The final peak (1285 cm^{-1}) is just out of this range, but is within the range of primary and secondary aromatic amines. Therefore, other articles were reviewed, and similar spectra to the ones obtained in this work were observed[73;74]. These articles identified peaks similar to the one at 1675 cm^{-1} as a C=O stretching band. Further, the peaks similar to the 1285 cm^{-1} peak were identified as signals from CH_2 wagging and C-N bonds. The last peak, at 1420 cm^{-1} was in the reviewed sources said to represent the C-H bending. All of these bonds can be observed in the PVP structure, and the spectra obtained in this work was used as reference for the nanoparticle samples.

All of these peaks can be observed both in the PVP-treated Au NSs and the final Au NUs, and it can therefore be seen that the signals from the C=O stretching band, C-N stretch, C-H bending and CH_2 wagging are all present in these samples. The peaks of the PVP-capped nanospheres are not as easily identifiable as the pure PVP and PVP-capped nanourchins, but can still be observed close to the expected wavelengths, with a maximum difference of 8 cm^{-1} between a reference peak and a peak in the nanoparticle samples spectra. This shows that there is likely a presence of PVP in the samples as the mentioned band can be identified in the spectra. These signals could be from residual PVP in the solution, and not PVP on the particle surface. However, the samples were centrifuged several times to remove residual PVP, making it more likely that the signals are from PVP adsorbed on the nanoparticle surface.

It is important to note that some of the spectra were amplified to be able to see the nuances. Many of the samples such as the PVP-treated Au NSs, were

available in small volumes. Therefore, the peaks were difficult to see in their original scale and therefore difficult to compare to the other samples. Still, this should not affect what we can derive from the spectra, as they are only used for a qualitative analysis. Based on the results from this FTIR and TEM images, the particles seem to be successfully synthesized and capped with PVP. However, how stable the particles are with this PVP-capping is unknown and it is essential to investigate this further.

5.1.6 Stability of Au NUs

The nanourchins were analysed by UV-Vis spectroscopy after treatment with sonication and vortex. The spectra from this analysis are shown in figure 5.10. This figure includes the spectra right after treatment, as well as two, ten, twenty and thirty minutes later. The nanourchins from the first synthesis were used for this analysis.

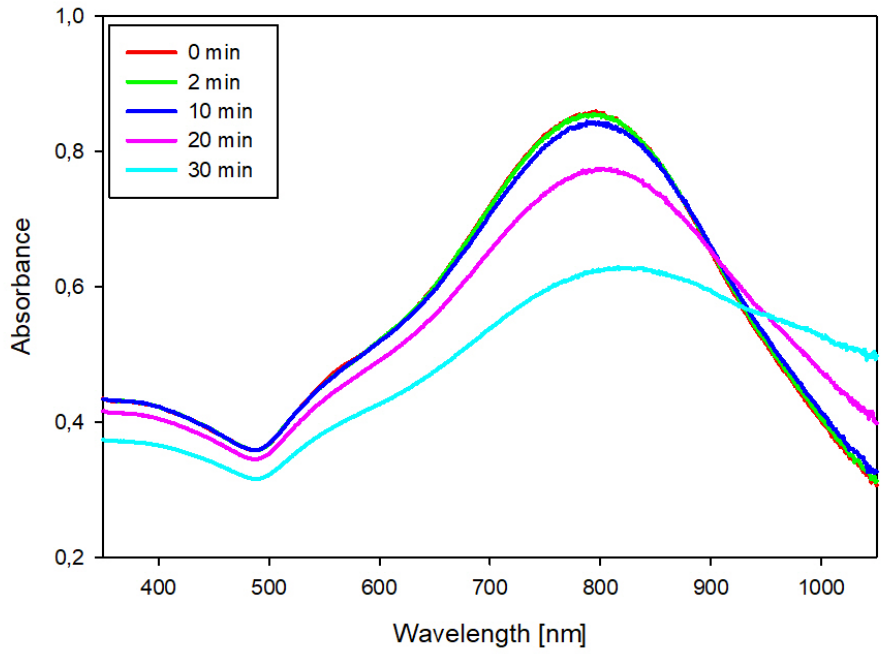

Figure 5.10: The absorption spectra of the nanourchins right after sonication and vortex, and two, ten, twenty and thirty minutes later.

The spectra presented in figure 5.10 shows how stable the Au NUs are in ethanol. This gives an idea of how quickly the particles should be used and if they can be used at all. If the particles were to precipitate immediately, they would be problematic to work with later as they could aggregate and agglomerate during functionalization. This would result in a more polydisperse particle solution and therefore a broader absorbance peak, which could make it more difficult to identify the peak shift during biosensing. Also, larger particles than these could be less biocompatible, which would limit the potential in-vivo application [43].

The figure shows that for the ten first minutes, the particles are fairly stable. However, after twenty minutes the particles have started to precipitate, as can be seen as the peak broadens and the peak intensity is lowered. Thirty minutes after the start, the spectrum had significantly changed from the first one. The peak is much broader and the intensity of the peak has decreased notably, which indicates that a high amount of particles precipitated out of the solution between the twenty and thirty minute mark.

What can be derived from this data is that the particles are stable for a satisfactory amount of time. Within ten minutes, it should be possible to initiate functionalization and it would therefore not be expected to have a high degree of agglomeration or aggregation. However, the particle solution should not be used after twenty minutes seeing as the rate of precipitation seems to increase around this point. This may as previously discussed cause issues with higher polydispersity and lower biocompatibility, making them unsuitable for biomedical applications.

UV-Vis spectroscopy was done on the first particle solution at different times after synthesis, the first being right after synthesis and the final one being after one and a half hour of storage. The absorbance peak wavelength of each analysis was plotted and can be seen in figure 5.11.

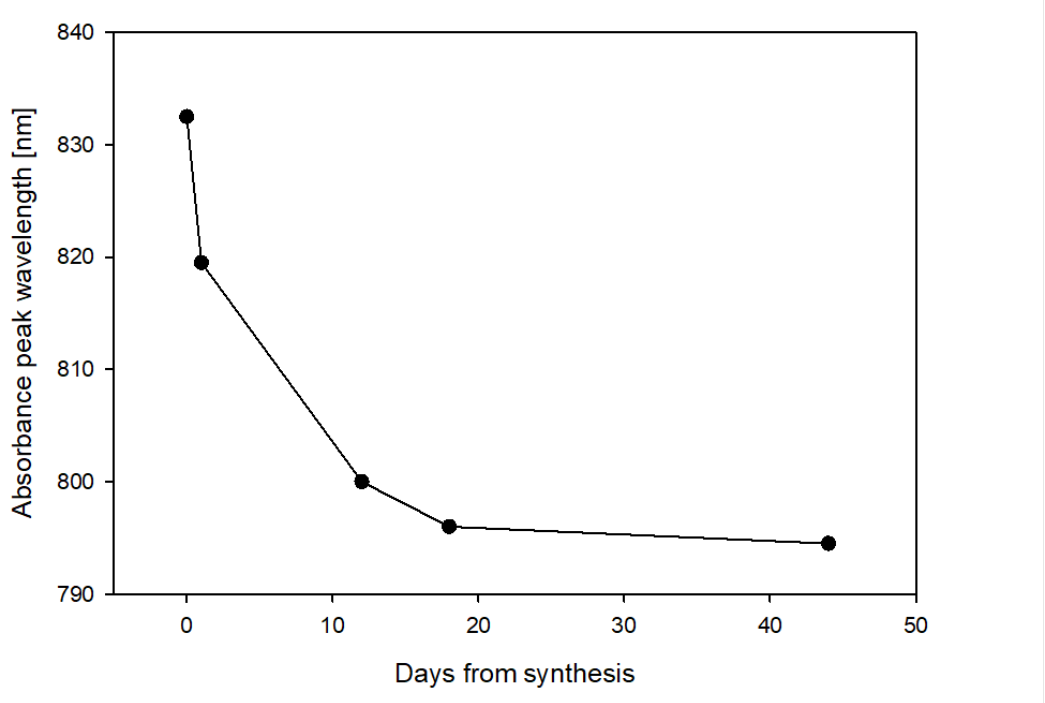

Figure 5.11: The shift of the absorbance peak wavelength over time. The particles of the second synthesis was used to do this analysis. After synthesis, the absorbance peak was at 832.5 nm, but this shifted to 794.5 nm in 44 days.

TEM imaging was also performed of both the the particles after synthesis and after one and a half month of storage. In figure 5.12, image A shows the particles as-synthesized and image B portrays the urchins after 45 days.

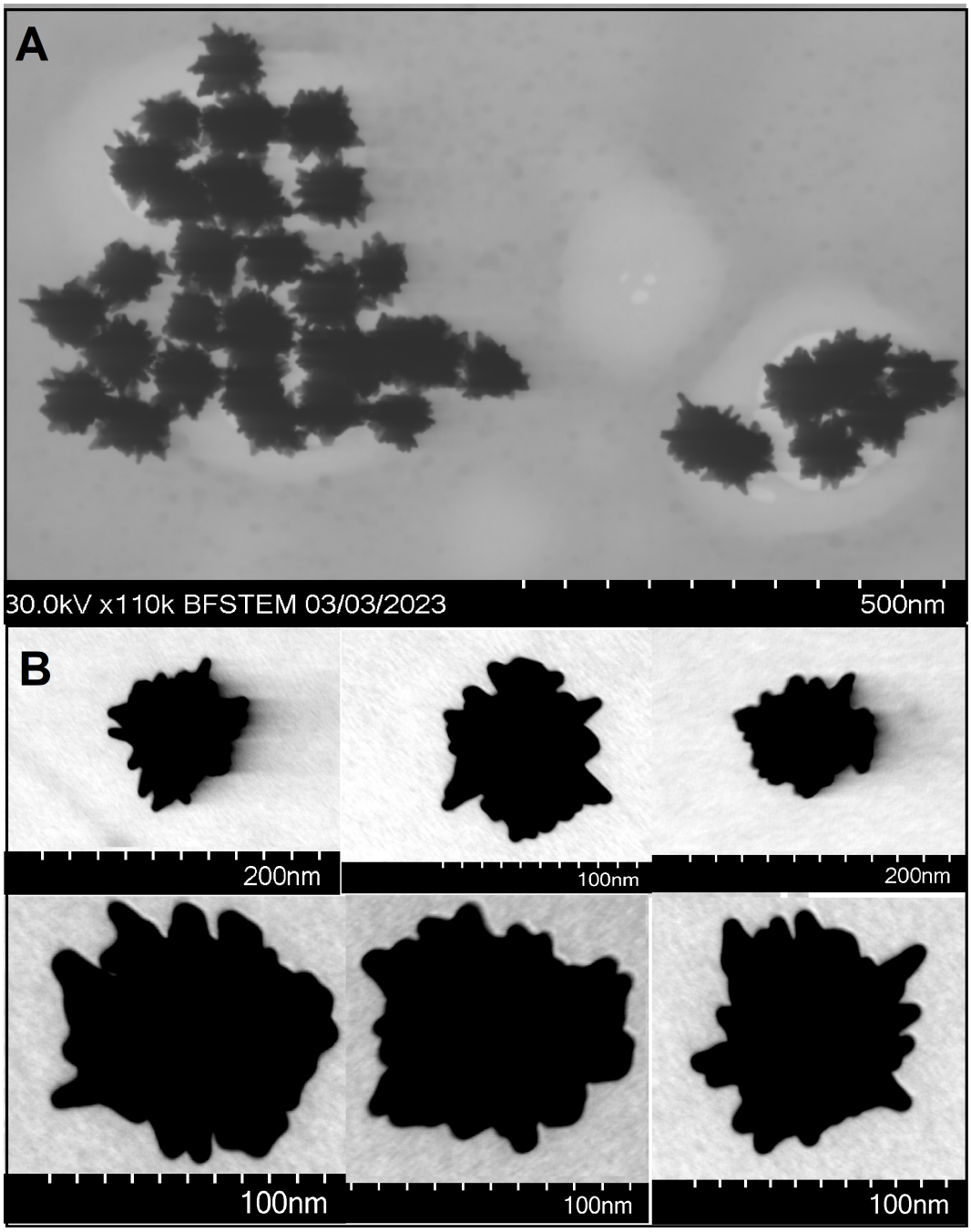

Figure 5.12: TEM images of the nanourchin particles on the day of the synthesis (A) and after one and a half month of storage (B).

Based on figure 5.11, it is evident that there is a significant change during the 10-15 first days after synthesis, as the absorbance peak shifts to lower wavelengths at a high rate. From the day of the synthesis to the day after, there is a shift of

over 10 nm, and in the following ten days it decreases by another 20 nm. After just under 20 days the peak seems to stabilize, with only a shift of about 2 nm in over the next twenty days.

Looking at the TEM images in figure 5.12, the particles do still have very significant spikes after storage. It is difficult to draw any real conclusions about morphological changes, but they seem to be slightly more dense in appearance than initially and the spikes seem to be slightly more blunt. The former difference could be due to differences in the TEM imaging brightness and contrast settings and differences in TEM sizes are difficult to identify due to the irregular shape of the particles. It is also difficult to state if the latter difference is just observed by chance or if the population in general has more blunt edges than right after synthesis.

The trend observed in the peak shift study, shows that to use the particles as-synthesized it is necessary to use them as quickly as possible. The observed change change could be the result of Ostwald ripening, which is the process where smaller particles dissolve and the monomers dispose on the surface of the larger particles[19]. Still, the nanourchins still have a spiky surface after the storage period, meaning they still have the desired shape. The peak is also still at a NIR wavelength after storage, so they still have the potential for in-vivo applications[42].

This begs the question if the particles should be used immediately after synthesis or whether it is better to use them when they have stabilized. It is possible that the Ostwald ripening would still be as significant even if the functionalization was done immediately after synthesis. In that case this could work as a source of error in biosensing, as the rate of the peak shift is very high during the first days after synthesis. Therefore, it may be better to use the particles after some time of storage, as the particles seem to stabilize during this period. Since they also still have their spiky structure and the solution still has a peak in the NIR area, the effect of these particles as biosensors should not be significantly different than if used shortly after synthesis.

5.2 Functionalization of nanoparticles

After the particles were synthesized and thoroughly characterized, functionalization of the Au NPs was done. The functionalization was divided into three main parts. Firstly, CTAB was partially removed from the Au NRs and replaced using first PEG-SH followed by an exchange with MUA. The latter chemical was also used to replace the PVP on the Au NUs. The final step was to cap the particles with oligonucleotides, using amino-terminated oligonucleotides to bind the carboxyl groups in citrate and MUA.

5.2.1 PEGylation of CTAB-capped AU NRs

The concentration of the CTAB@Au NR AR2 was $2.9 * 10^{10}$ particles per mL, whereas the concentrations of the CTAB@Au NR AR3 and CTAB@Au NR AR4 solutions were $1.8 * 10^{10}$ and $1.4 * 10^{10}$ particles per mL, respectively. CTAB@Au NR AR3 solution was used in different concentrations in the reaction with a fixed amount of PEG-SH. The UV-Vis spectra of these three samples after reaction with PEG-SH are included in figure 5.13, with the spectra before the reaction. All spectra are normalized to their absorbance at 350 nm.

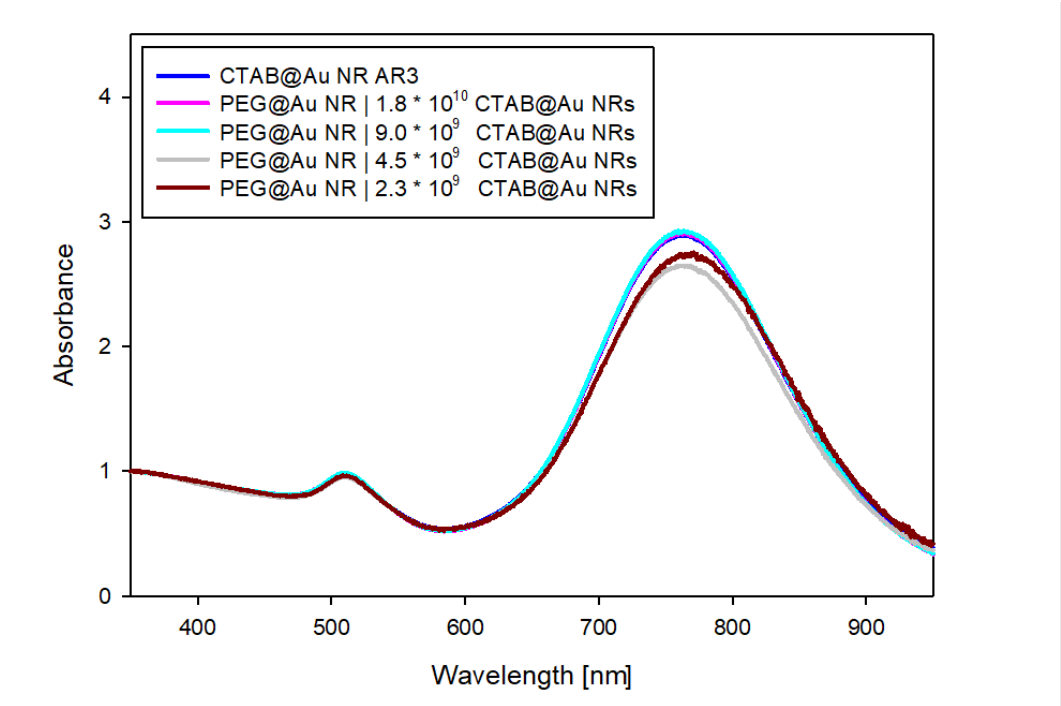

Figure 5.13: The UV-Vis spectra of the CTAB-capped nanorod (blue) and nanorod solutions where CTAB had been exchanged with PEG-SH. The solutions where PEG-SH was added used different concentrations of nanorods, one using the as-prepared CTAB@Au NR AR3 solution (purple) and three which were diluted by factors of two (Turkish blue), four (grey) and eight (brown) from the as-prepared CTAB@Au NR solution. The number of particles used in the PEG functionalization is given in the legend.

The zeta potential of the PEG-treated samples are given in figure 5.14. The zeta potential of the CTAB-capped nanorods is also included for reference and is positive. After the PEG exchange, the zeta potential of all samples is negative.

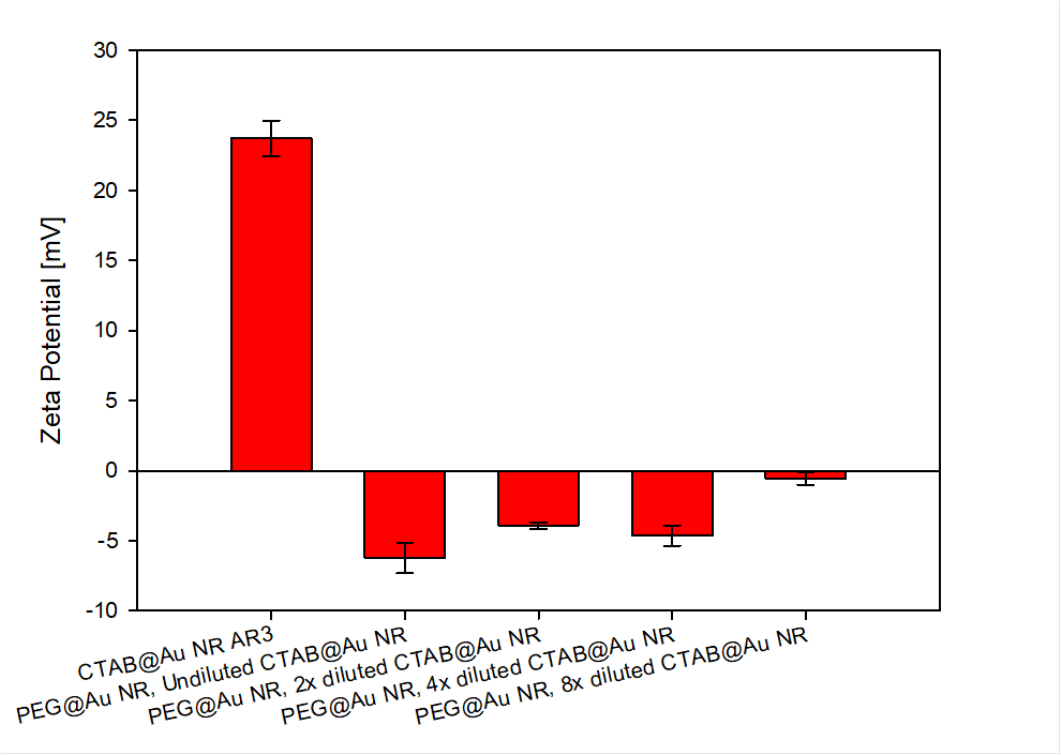

Figure 5.14: The zeta potential of the four different samples which were treated with PEG-SH and the CTAB@Au NR AR3 before the exchange.

The success of the PEG-functionalization can be verified by looking at absorbance spectra and zeta potentials. Firstly, the undiluted and the two times diluted are almost exactly the same as the spectra before functionalization. However, the four and eight times diluted nanorod solution has a slightly lower intensity in the second peak than the CTAB@Au NR. However, these spectra can not alone show if the PEG functionalization was successful, as it is possible that the CTAB is still on the nanoparticle surface rather than PEG. More data is needed to verify that it is actually PEG which is present on the surface.

The zeta potential could be used to verify the PEG functionalization. With CTAB on the surface, the zeta potential should be positive[70]. However, when the PEG is present on the surface the zeta potential should be negative, due to the oxygen atoms in the polyethylene glycol chain[75]. However, this particular PEG also has a nitrogen atom, which could bring the zeta potential closer to a positive value. All samples which were treated with PEG had a slightly negative zeta potential, as can be seen in figure 5.14, which is in line with the theory. The difference in zeta potential before and after PEGylation is very significant, making it fairly certain that there is PEG present on the surface of the nanopar-

ticle. There was therefore not necessary to perform any further characterization to validate that this was the case.

Furthermore, the reason that the dilution series was used in the functionalization to investigate if the particle concentration had an influence on the PEG functionalization. The data from the UV-Vis spectroscopy and and zeta potential measurements shows that the as-prepared nanoparticles could be used directly in the PEG functionalization. There does on the other hand seem to be an issue as lower particle concentrations are used in the functionalization, as the intensity of the peaks lowers. Why this is happening is not certain, but it could be due to an unevenly distributed loss during the centrifugation process. Therefore, the as-prepared CTAB@Au NRs were used directly for PEGylation for the two other samples nanorods solutions.

The other two CTAB@Au NR solutions (CTAB@Au NR AR2 and CTAB@Au NR AR4) were also used for further functionalization. These were treated with PEG undiluted as formerly discussed, and their absorbance spectra before and after PEGylation are shown in figure 5.15. The second peaks have shifted to slightly higher wavelengths, but the intensities are largely unaffected. After PEGylation, these nanorods were redispersed in ethanol.

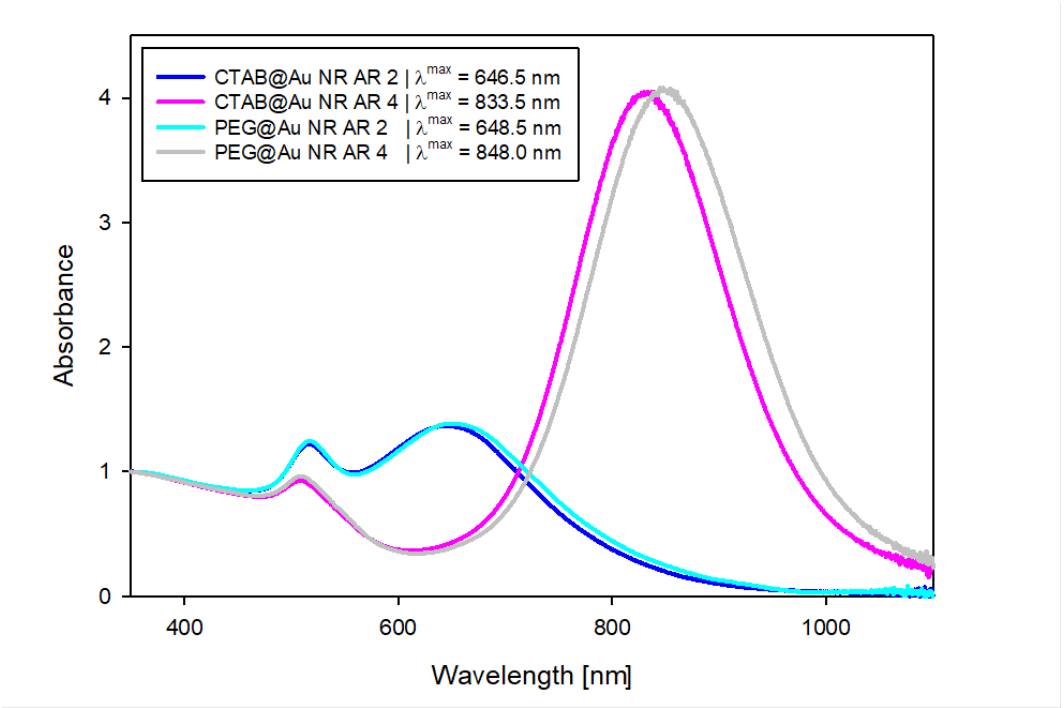

Figure 5.15: Absorbance spectra of the nanorods with the lowest and highest aspect ratio, both before and after PEGylation.

5.2.2 MUA-functionalization of PEGylated AU NRs

MUA-functionalization was done following the Thierry et al. method, using the PEG@Au NR AR3 solution diluted by a factor of two and four and one undiluted solution. After functionalization, the particles were redispersed either in pure MQ water or in water with a pH of 9. The absorbance spectra of all particle solutions can be seen in figure 5.16. The top plots shows the spectra the particle solutions which were redispersed in water with a pH of 7 and the bottom shows the spectra of the particle solutions which were redispersed in water with a pH of 9.

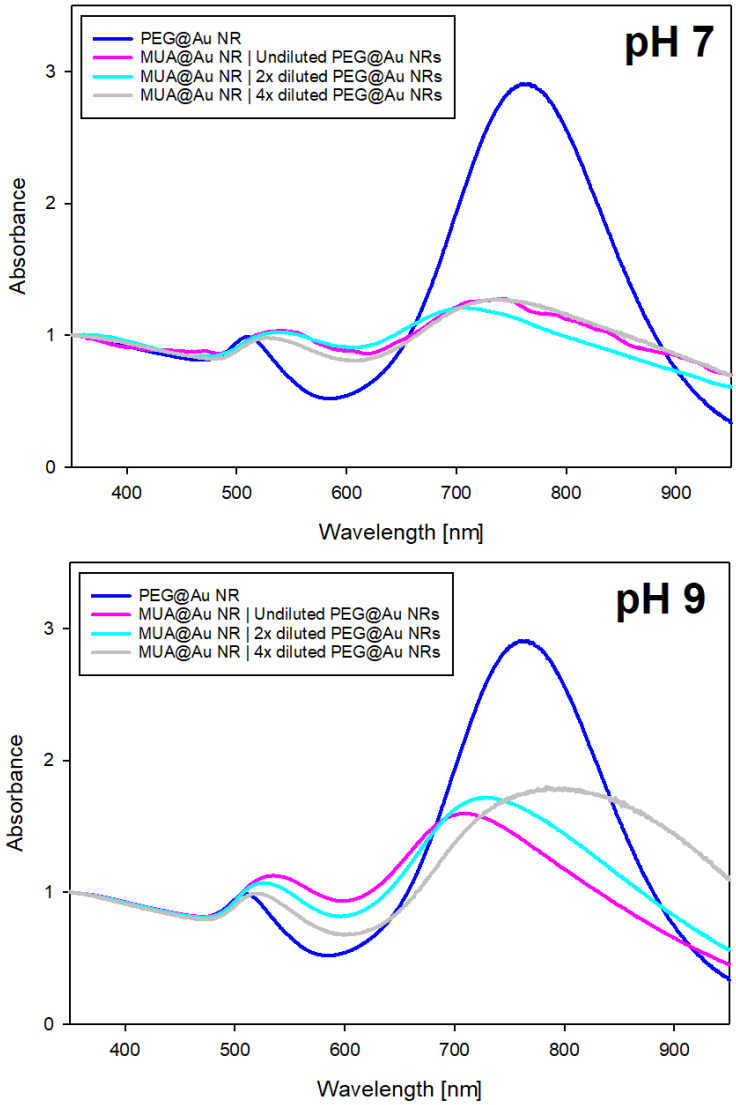

Figure 5.16: Absorbance spectra of the particle solutions dispersed in MQ water with a pH of about 7 (top plot) and in MQ water with a pH of about 9 (bottom plot) after MUA-functionalization. All spectra were normalized to their absorbance at 350 nm.

The absorbance spectra of in figure 5.16 show that pH plays an important role when redispersing the particles after the MUA capping process. This study was done as Thierry et al. redispersed the particles using water adjusted to pH 9. Therefore, it could be that the issues that arose when redispersing the particles in regular MQ water would not be occurring when using basic water for redispersion. These figures show that adjusting the pH helps in maintaining more of the original absorbance fingerprint, but perhaps still not to a satisfying degree. When the particles were redispersed, there was a clear difference in the spectra from the PEGylated solution, both when dispersed using MQ water and basic water.

The small peak at around 515 nm after MUA capping was significantly broader and had shifted to higher wavelengths, whereas the larger peak has lowered notably in intensity and also shifted to lower wavelengths in all but one of the parallels. This means that there must have occurred a change in the population, but it is unlikely that the ligand exchange would have induced any morphological changes in the particles. Therefore, it is more likely that there has either been happening aggregation during the process, despite of the sonication, or that rods with different aspect ratios would have different rates of exchange.

A hypothesis to why these problems was occurring is grounded in the fact that the MUA is soluble in ethanol, but not soluble in water[76]. Even though the PEGylated Au NRs are dispersible in ethanol, they are still highly dispersible in water as observed in the experimental work. References also confirm that PEGs should be soluble in both water and ethanol[77]. This could cause a problem where the contact between the nanoparticles is limited due to the differences in solubility and dispersibility of the incoming ligand and PEGylated nanoparticles. Also, since the functionalization is done using sonication, the particles and MUA will not be mixed as well as if stirring was used. Consequently, the rate of ligand exchange could be affected negatively.

To improve the ligand exchange changes had to be made to the MUA-capping process, which could avoid the mixing problems and therefore make the ligand exchange more successful. Given the hypothesis that the difference in nanoparticle dispersibility and MUA solubility in water and ethanol causing the issue, a change was made based on a method where PVP is replaced on silver nanoparticles[26]. This method is used also used as the blueprint for the Au NU functionalization, which will be presented later. In this method, the PVP-capped nanoparticles are dispersed in ethanol and is mixed with several thiols, also dispersed in ethanol. They report successful exchanges in this paper, but it is important to note that PVP has a lower affinity to the particle surface than thiols[24].

In this context however, thiolated PEG is already present on the surface, which could make the exchange more difficult. Still, a theory that using ethanol as the sole solvent would give higher degree of mixing of the particles was developed based on the findings of this paper. A better mixing rate would potentially make an exchange more likely. The high concentration of MUA compared to PEG

on the surface could make up for this, as the rate of thiol ligand exchanges is dependent on the concentration of the incoming ligand[28].

Therefore, instead of redispersing the particles in water after PEGylation, the particles were dispersed in ethanol. Also, the MUA was dispersed in ethanol instead of a water-ethanol mixture. Furthermore, the exchange was done by stirring at 400 rpm for two hours instead of sonication for one hour. This could provide better mixing of the particles and MUA and potentially improve the contact between them.

5.2.3 Modification of MUA-functionalization in Au NRs

The discussed changes were applied to the protocol and the adapted method was performed, this time using the PEG@Au NR AR4. The absorbance spectra of the functionalized nanorod solutions are shown in figure 5.17. These first three functionalizations used $6.3 * 10^9$, $3.1 * 10^9$ or $1.6 * 10^9$ PEGylated nanorods in the MUA-functionalization. One more functionalization was done after these three, this time using a more concentrated solution of PEGylated nanorods. In addition to these, the spectrum of the nanorods before MUA-functionalization was also included.

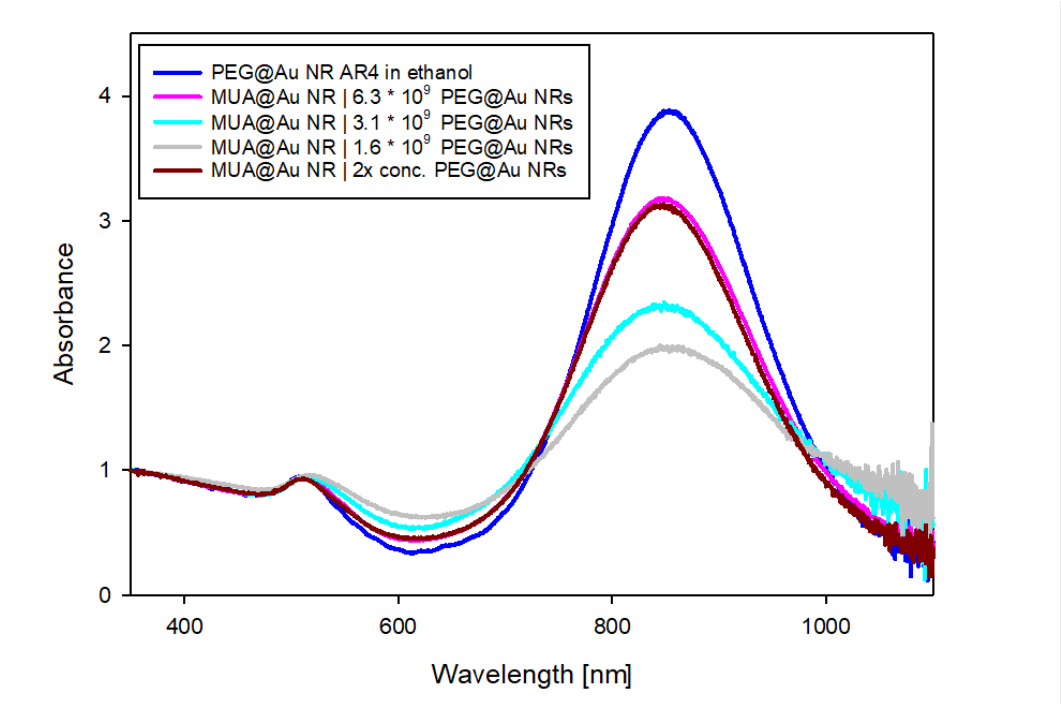

Figure 5.17: Absorbance spectra of the PEG@Au NR AR4 nanorods and four MUA-functionalized nanorod solutions. The four MUA-functionalized samples were prepared using different amounts of PEGylated Au NR AR4 particles, and the number of particles used is stated in the legend. All spectra were normalized to their absorbance at 350 nm.

The zeta potentials of the four samples were also measured and can be seen in figure 5.18. These four samples were functionalized using different dilutions (concentrated, undiluted, two times and four times diluted) of the PEG@Au NR AR4 solution. In the figure, the zeta potentials of the CTAB-capped nanorods and the same solution after PEGylation. The zeta potential of the PEG@Au NR AR4 was -3 ± 1 mV, whereas the zeta potential of the three samples which had undergone MUA-functionalization were -20 ± 9 mV (concentrated PEG@Au NRs), -17 ± 1 mV (undiluted PEG@Au NRs), -4 ± 1 mV (2x diluted PEG@Au NRs) and -8 ± 2 mV (4x diluted PEG@Au NRs).

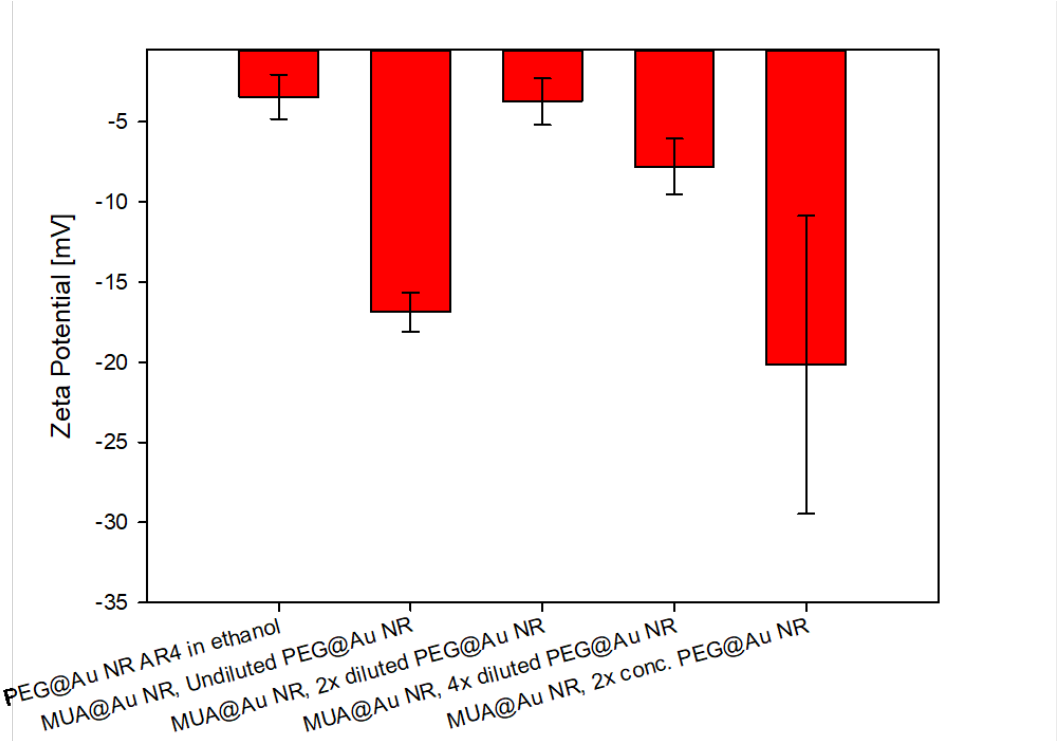

Figure 5.18: Zeta potentials of the PEGylated Au NR AR4 and the four MUA-functionalized samples. The four MUA-functionalized samples were prepared using different numbers of PEGylated Au NR AR4 particles, and these numbers are given in the legend.

Based on absorbance spectra, this way of performing the ligand exchange is notably more successful than the former method. The intensity of the second peak is somewhat reduced after MUA-functionalization, but not as much as when using the Thierry et al. method[27]. The first peak at around 510 nm is almost exactly tracking the peaks of the CTAB-capped and PEGylated nanorods. If the exchange has taken place, the changes made to the method seems to have helped preserve more of the original nanoparticle population. Even though the second peak has a slightly lower intensity than the PEG@Au NRs, it is still a clear improvement of the former method.

The spectra of the MUA-functionalized nanorods show that a high concentration of nanorods should be used to preserve the absorbance fingerprint of the solution, a trend also observed in the PEGylation. It is difficult to argue what exactly causes this, but it could potentially have something to do with the loss of particles during cleaning. When the concentration of particles gets very low, a loss of particles could have larger effects on the population than if the concentration is high. However, these results could potentially just be the product of an unsuccessful exchange. If the MUA has not been able to replace the current capping agents, the particle could still be capped with CTAB and PEG. Therefore, other characterization methods were used to verify that MUA is present on the surface. Furthermore, the concentrated PEG@Au NR solution was functionalized

after the other ones to find out if it was possible increase the peak intensity. This sample was prepared by redispersing the PEG@Au NRs in 1 mL of ethanol instead of 2 mL. This gave very similar results to that of the undiluted PEG@Au NR solution, but resulted in a more concentrated MUA-functionalized nanorod solution. This indicates that the intensity seen in this spectrum may be the limit for the intensity when using this method.

The decrease in zeta potentials from that of the PEGylated nanorods to that of the MUA-functionalized also indicate that MUA is present on the surface. MUA has a carboxyl group on the surface, whereas PEG does not have any charged groups, meaning MUA capped nanoparticles should have a higher negative potential than PEGylated nanorods. This is the case, as the MUA-functionalized nanoparticle solutions have a higher negative zeta potential than the PEGylated particles in all samples. The difference is not very significant in the samples prepared using diluted PEG@Au NR solutions, but the samples functionalized from undiluted and concentrated PEG@Au NR solutions showed a larger decrease in zeta potential. However, there is still one important uncertainty in these number, which is that the PEGylated nanorods were dispersed in ethanol, whereas the MUA-functionalized nanoparticles were dispersed in MQ water. This could cause some of the difference in zeta potentials, as a former thesis have measured the zeta potential of water-dispersed PEGylated nanorods down to about -14 mV [78]. This makes it more difficult to draw any conclusions about the capping of the nanoparticles, and more data was needed to investigate the capping further.

An FTIR analysis was also performed of both the PEGylated nanorods and MUA-functionalized nanorod solution. The spectra of these samples are shown in figure 5.19, with the spectra of pure MUA. The bonds attributed to each peak in the figure are based on reports in the literature[57;73;74]. The bond represented by peak at 1047 in the MUA sample could not be identified based on literature.

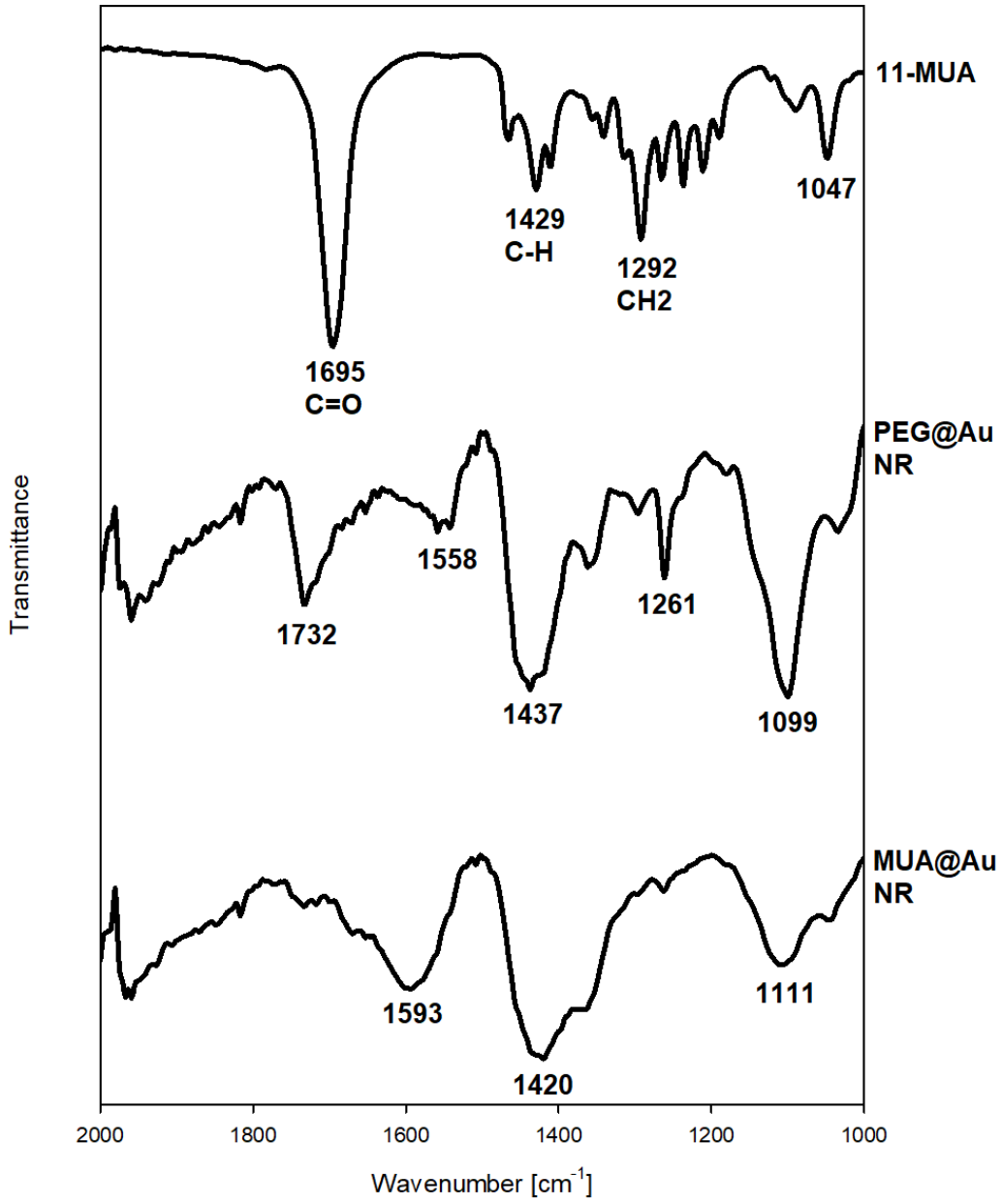

Figure 5.19: The IR spectra of the PEGylated nanorods, MUA-functionalized nanorods and pure MUA. The bonds attributed to each peak in the figure are based on reports in the literature[57;73;74].

The FTIR analysis was done to investigate the the capping agents in further detail. When looking at figure 5.19 it is evident that there are significant differences between the three analyzed samples. Firstly, looking at the PEG-capped nanorods, there are several peaks which can be identified using Coates guide to reading FTIR spectra[57]. The peak at 1732 cm^{-1} is close to, but not quite in the range of amides, which is 1630-1680 cm^{-1}. Still, it is close enough that it is reasonable to assume that it represents the C=O bond in the structure of PEG-SH. Further, the peaks at 1437 and 1261 cm^{-1} are similar to the peaks found in PVP[73;74]. This means the former likely represents C-H bending and the latter represents CH_2 wagging and C-N bonds, which should both be present when considering the PEG-SH structure. Finally, the peak at 1099 cm^{-1} should be caused by the ether groups in he structure[57]. The ether group is found in the repeating unit of PEG-SH, which explains why this peak is the largest in the spectra in the selected range.

After identifying the peaks in the PEG@Au NR spectra, both this and the MUA spectra can be used to verify that the exchange has taken place. Firstly, by comparing the pure MUA spectra to the MUA-capped nanorod spectra several differences can be identified. However, this does not necessarily mean that the exchange has not taken place, as the Coates guide for reading the spectra offers an explanation[57]. Even though carboxylic acid should have peaks at around 1700 cm^{-1}, this is not the case for carboxylates. An example of a carboxylic acid salt from earlier in the thesis is sodium citrate (fig 5.9), which has on peak at around 1578 cm^{-1} and another at around 1389 cm^{-1}. This corresponded well with the given wavenumbers of carboxylic acid salts in the Coates guide, and peaks at very similar wavenumbers are observed in the spectra of the MUA-functionalized nanorods. This means that the signals are likely from vibrations of carboxylates in the samples, meaning it is very likely that MUA is present on the surface. These difference between the FTIR spectrum of pure MUA and MUA-functionalized nanoparticles are observed in other papers too, further supporting that the Au NRs are functionalized with MUA[79;80].

One uncertainty with this analysis is that a high concentration of 11-MUA was used in the functionalization. It is therefore possible that the peak which indicate the presence of MUA are not actually from MUA bound to the surface, but rather free MUA in the solution. There is especially one factor which is important to consider. Firstly, when MUA is not bound to the nanoparticle, it is not soluble in regular MQ water, meaning it would likely just precipitate out[76]. It is however possible that there was some ethanol left in the solution after centrifugation, in which free MUA could exist. Still, there are arguments against this too. Firstly, MUA is a very small molecule compared to the nanoparticles and would still be in the supernatant after centrifugation rather than in the precipitate. This means most of the MUA would be removed after centrifugation. Also, since the spectra has changed from one typical for a carboxylic acid to one typical for carboxylates it is likely that the MUA is in fact on the surface of the particle[57]. If it was just on free the ethanol parts of the solution, it should in theory have

given a spectra more similar to the 11-MUA spectra in figure 5.19 unless it has reacted in other ways during the mixing.

Based on the results shown in the absorbance spectra and zeta potential measurements, two times concentrated PEG@Au NR solutions (redispersed in 1 mL ethanol instead of 2 mL) were used for functionalization of the nanorods. The absorbance spectra after MUA-functionalization are shown in figure 5.20, with their initial spectra (with CTAB-capping) also indcluded as a reference. The intensities of the peaks were lower after functionalization, but there was not observed much of a peak shift in either one. These nanoparticle solutions were used for the subsequent oligonucleotide functionalization.

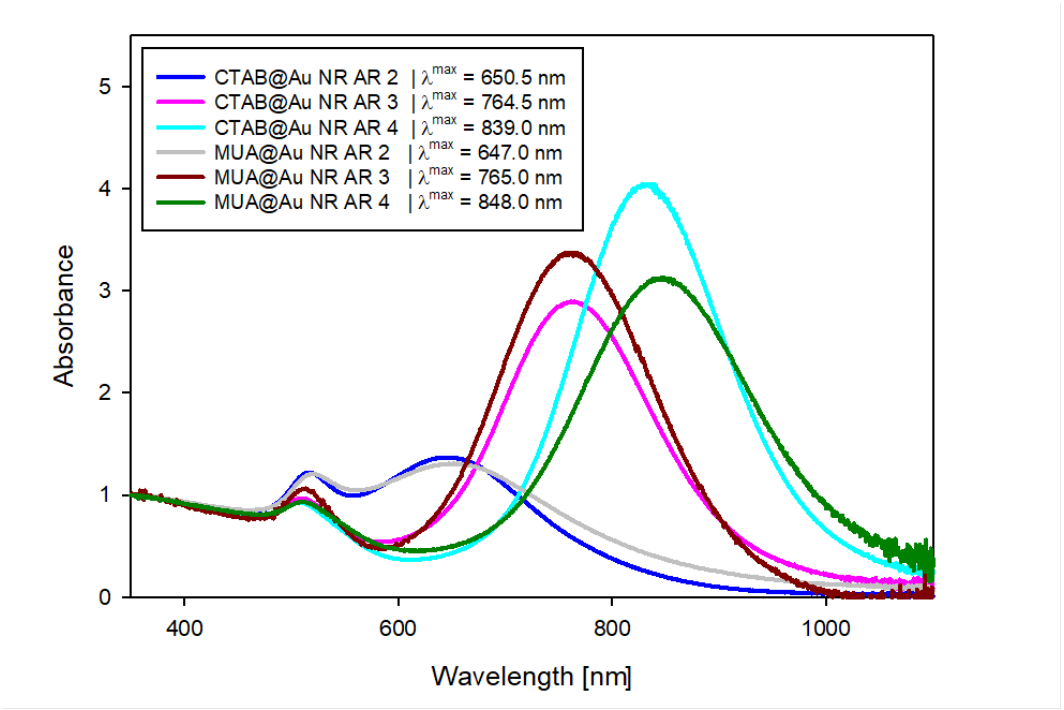

Figure 5.20: Absorbance spectra of the nanorods with the lowest and highest aspect ratio, both before and after MUA-functionalization. All spectra were normalized to their absorbance at 350 nm.

5.2.4 Displacement of PVP in Au NUs

The concentration of the sample used for functionalization was $3.0*10^{10}$ particles per mL. Three different dilutions of this sample was used in the MUA functionalization. One with a dilution factor of two, the second with a dilution factor of four and a final dilution factor of eight. Figure 5.21 shows the absorbance spectra of these three samples after the MUA-functionalization, plus the spectra of the original solution on the day of the functionalization. Dispersion tests were also performed pre and post functionalization. Pre functionalization, the particles were dispersed in water and post functionalization the particles were redispersed in ethanol. These experiments both gave the same result, as precipitation occurred shortly after redispersion.

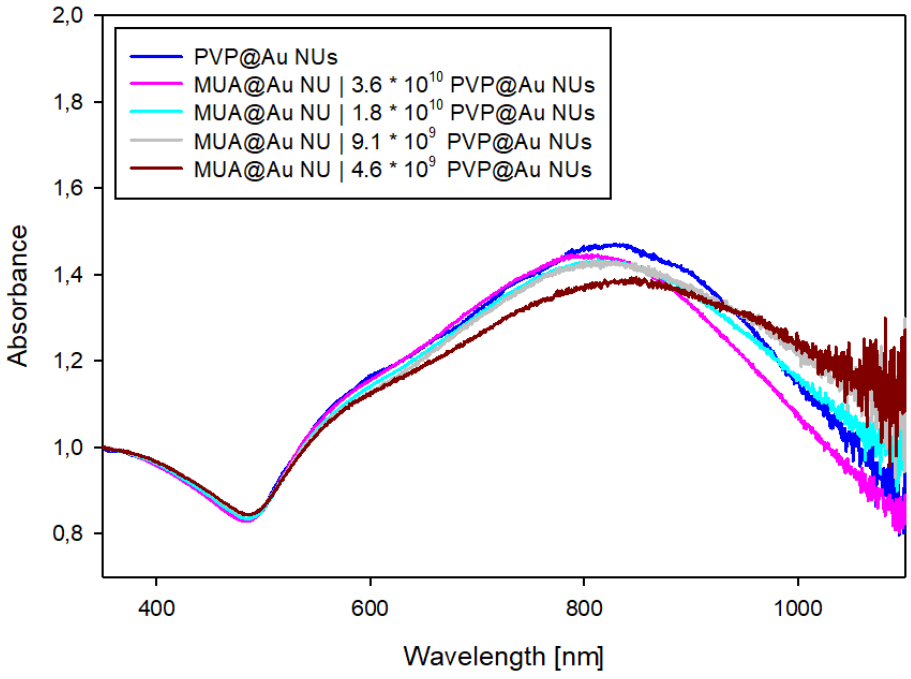

Figure 5.21: The UV-Vis spectrum of the Au NUs after functionalization with MUA. The functionalizations used different amounts of PVP-capped nanourchins, all stated in the legend. All spectra are normalized to their own absorbance at 350 nm.

The zeta potential of the three samples was also measured. Figure 5.22 shows the zeta potential of the three samples after MUA functionalization and the original PVP-capped Au NUs. The zeta potential of the latter was about 20 mV, and in all three MUA-functionalized samples the zeta potential has turned negative.

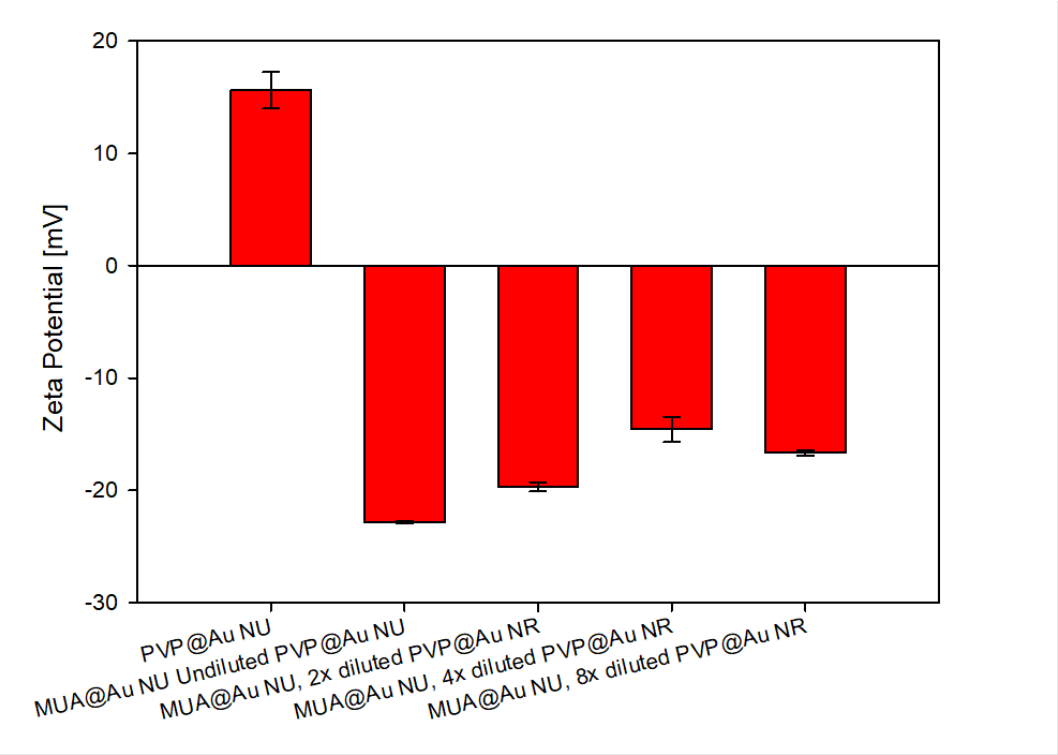

Figure 5.22: Zeta potentials of the PVP@Au NUs and the four MUA-functionalized samples. The four MUA-functionalized samples were prepared using different numbers of PVP@Au NUs, and these numbers are stated in the legend.

The absorbance spectra of the MUA-functionalized nanourchins are fairly similar before and after synthesis. The loss of intensity is negligible in all but the sample which used the least amount of particles in the functionalization. This peak is also broader than all the other peaks, which means we have a similar trend to that observed in nanorod functionalization. As the amount of particles used for functionalization decrease, the spectra changes more. Why this trend is observed was previously discussed to have something to do with particle loss in the centrifugation steps. As this trend is observed in many different types of functionalization, it is likely to have the same root cause.

The zeta potentials are also very indicative of the success of the functionalization, but it is important to note that the particles were dispersed in different solvents before and after functionalization, which could have an influence on the zeta potential. Still, the zeta potential turned from almost positive 20 mV to negative 15-22 mV in all tries, meaning it is very likely that the capping agent has been exchanged, regardless of the change in solvent. Another factor which supports this is the dispersion tests which were done on the particles. The PVP@Au NUs precipitated out when tried redispersed in water, which means they could not be the capping agent of the particles after functionalization, as the particles at this point could only be dispersed in water and not ethanol.

An FTIR analysis was also done on the sample after MUA functionalization and of pure MUA. The spectra of these compounds between 2000 cm^{-1} and 1000 cm^{-1} is presented in figure 5.23. In this figure, the spectra of PVP and the PVP-capped nanourchins which were presented earlier in figure 5.9. The bonds attributed to each peak in the figure are based on reports in the literature [57;73;74].

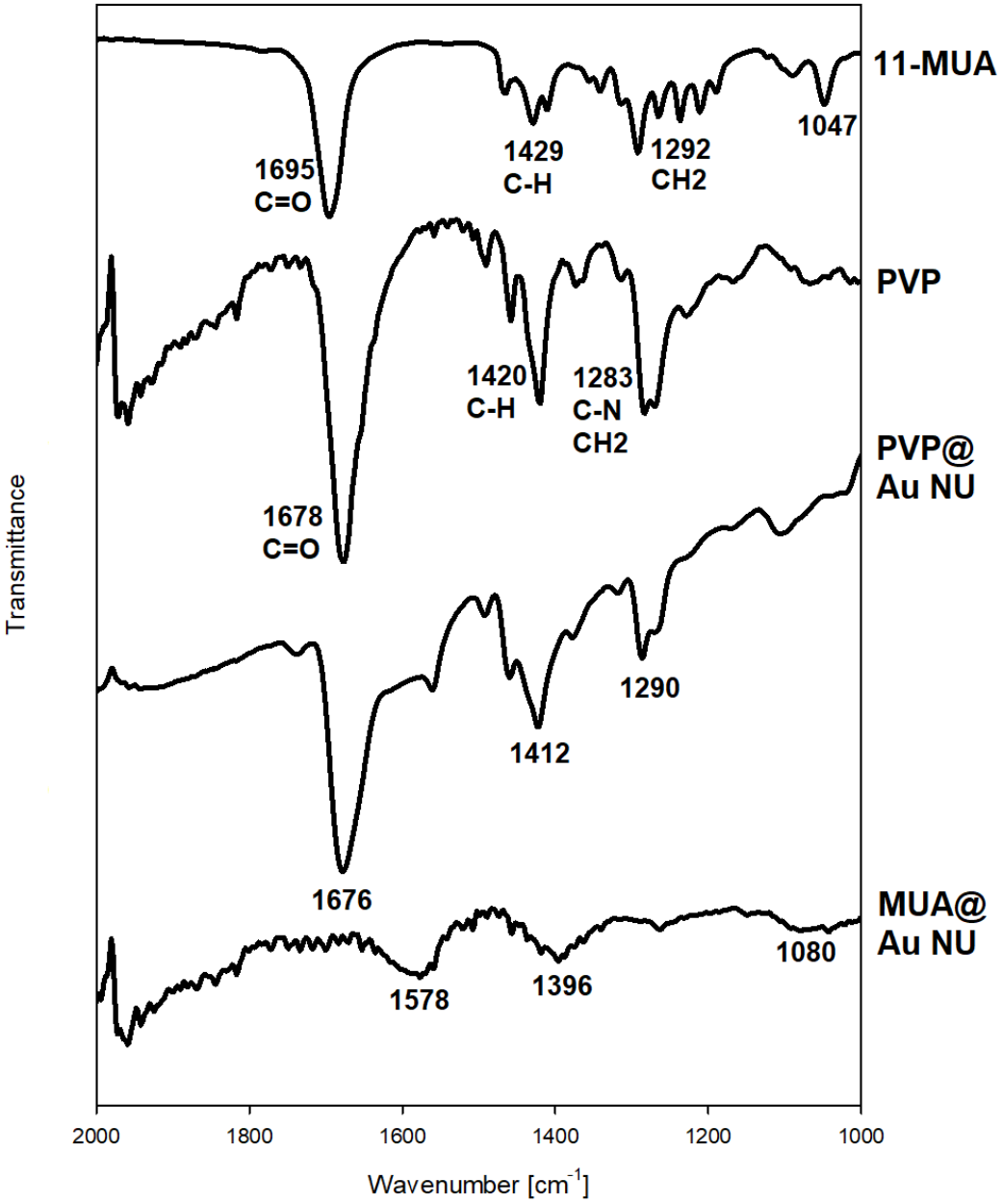

Figure 5.23: FTIR spectra of sodium citrate, PVP, PVP-capped nanourchins and MUA-capped nanourchins. The bonds attributed to the peaks are based on literature.

The FTIR spectra of MUA and PVP have already been discussed in previous sections and will therefore not be explained in detail in this section. However, it should be noted that the structures of these two chemicals indicates that they should have very similar spectra since they contain carbonyl groups and long alkane chains. They should according to the literature both have carbonyl peaks, and signals from C-H bending and CH_2 wagging, which all can be seen in their spectra in figure 5.23[57;73;74]. The easiest way to distinguish these two spectra is by looking at the amide group in PVP. The C=O peak in the PVP spectrum is firstly almost exactly at the value indicating the presence of a tertiary amide, which PVP can be classified as, since the nitrogen atom is bound to three carbons in the PVP structure[57]. In the MUA spectrum the carbonyl peak is at a slightly higher wavenumber, since it is a carboxylic acid rather than a amide. This is the most important distinction between the two in the wavenumber range in the figure. Also, the peak at 1283 cm^{-1} could also represent the C-N stretch, but it is difficult to use this to distinguish it from the MUA-spectrum[73].

Before functionalization the spectrum is very similar to the spectrum of pure PVP, with peaks at almost exactly the same wavelengths. This spectrum was discussed in the nanourchin synthesis section, and it is therefore more interesting to look at the differences in the spectra before and after MUA-functionalization. It is clear that changes have occurred, and the spectrum resembles the spectrum observed after the nanorod MUA-functionalization. The differences between this spectrum and the FTIR spectrum of pure MUA can be explained by potential changes in the carboxyl group, which changes from the form of a carboxylic acid to being in the form of a carboxylate. The peaks are in line with what wavenumbers the Coates guide to reading FTIR spectra states that carboxylic acid and carboxylate peaks should be found at[57]. This is as formerly discussed a trend which is observed in other work where MUA is used to functionalize nanoparticles[79;80].

The characterization of the MUA-functionalized nanourchins indicated that the functionalization was successful, and it was therefore not necessary to adjust the method further. The most concentrated sample of gold nanourchins was used for further functionalization with oligonucleotides. This was the sample in which $3.6 * 10^{10}$ PVP@Au NUs was used in the functionalization.

5.2.5 Oligonucleotide functionalization of Au NPs

After functionalization with oligonucleotides, the nanospheres were characterized by UV-Vis spectroscopy both before and after mixing with a carboxyfluorscein (FAM)-modified complementary strand. For reference, the citrate-capped Au NS solutions which were used for functionalization were also characterized in the same manner. These absorbance spectra are shown in figure 5.24, showing the 1st generation particle spectra in the top plot and the 4th generation particle spectra in the bottom plot.

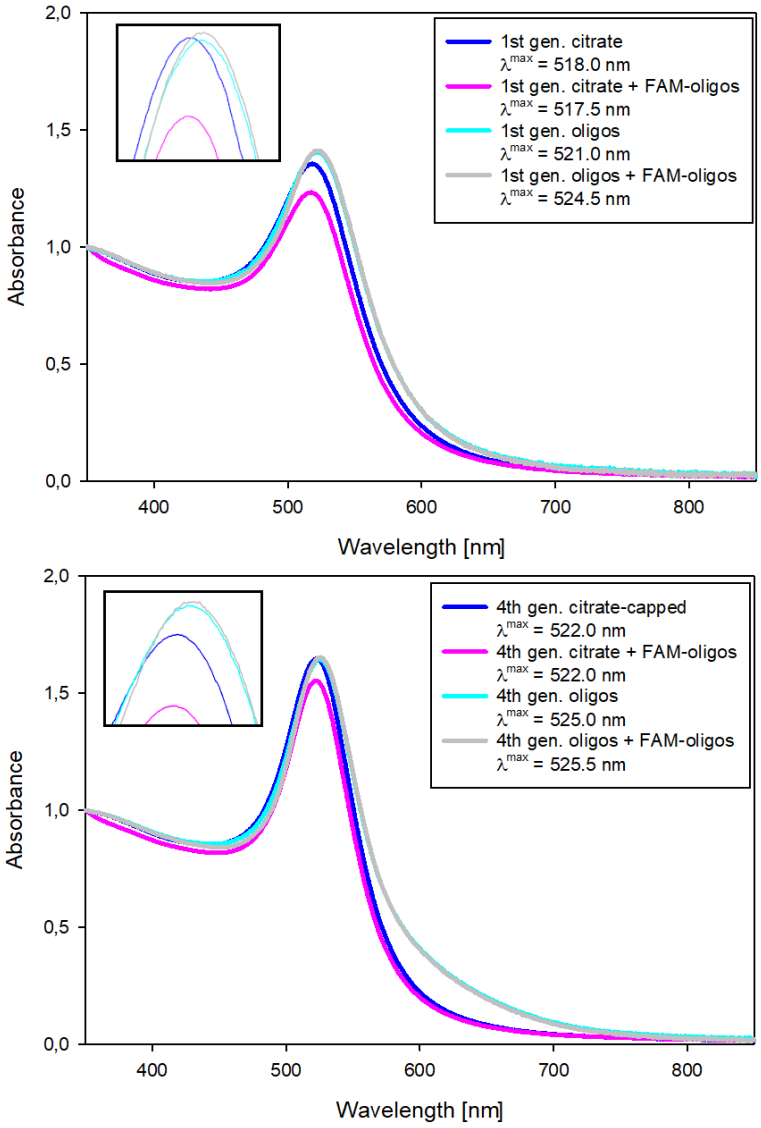

Figure 5.24: Absorbance spectra of the 1st generation (top) and 4th generation (bottom) nanosphere samples before and after oligonucleotide-functionalization, and after mixing both with a FAM-modified complementary oligonucleotide. A zoom in on the peaks is also included. All spectra are normalized to their absorbance at 350 nm.

The oligonucleotide functionalization seems to have affected the samples to a low degree. The first generation particle solution increased slightly in intensity around the peak. The intensity of the fourth generation samples did not change significantly, except between 550 and 750 nm where the intensity also increased slightly after functionalization. The change in this spectrum may have been caused by some aggregation during the functionalization. When salt is added to the oligonucleotide-nanoparticle mixture, the charges of the citrate capping of the nanospheres is screened and the particle is therefore destabilized [67]. This is important, as it makes it gives the thiol-modified oligonucleotides better access to bind the surface of the nanoparticle. There will be a charge-repulsion between the negatively charged oligonucleotide and the citrate-capped nanoparticles, which the salt addition helps to avoid.

In terms of the absorbance peak wavelength which are stated in the legends of figure 5.24, an important difference can be seen when comparing the functionalized Au NSs and the non-functionalized Au NSs. Firstly, there is a shift in both samples after the particles were functionalized. In both the 1st generation and 4th generation Au NSs this was a shift of about 3 nm, which means that the functionalization has caused changes to the oligonucleotide solution. This could be because of the previously discussed aggregation, but it could also be caused by refractive index changes due to the functionalization [4].

When also taking the FAM-modified oligonucleotides analyses into consideration, another important difference in the functionalized and non-functionalized particles is observed. When the non-functionalized nanoparticles were mixed with the FAM-modified oligonucleotides a reduction in the peak intensity was observed in both particles solutions, but no peak shift is observed (0.5 nm blue-shift in the 1st generation sample). In the functionalized samples however, a red-shift is observed in both particle solution with about 3.5 nm in the 1st generation particles and 0.5 nm in the 4th generation particles. The intensity also increases slightly, as can be seen in figure 5.24, but not to a very large degree. This indicates that the functionalization has been somewhat successful, since only the functionalized particles exhibit a shift when the complementary strand was introduced. The changes are very small however, and is therefore not a definite confirmation of the functionalization but rather a solid indication.

The nanorods functionalized with oligonucleotides were characterized by UV-Vis spectroscopy both before and after mixing with a FAM-modified complementary strand. For reference, the MUA-capped Au NR solutions which were used for functionalization were also characterized in the same manner. The Au NR solutions which were used for functionalization were also characterized in the same manner for reference. These absorbance spectra are shown in figure 5.25, showing the AR2 particle spectra in the top plot and the AR3 particle spectra in the bottom plot. The MUA-capped AR2 sample had some noise, and was therefore treated with a smoothing function in SigmaPlot to allow for comparison.

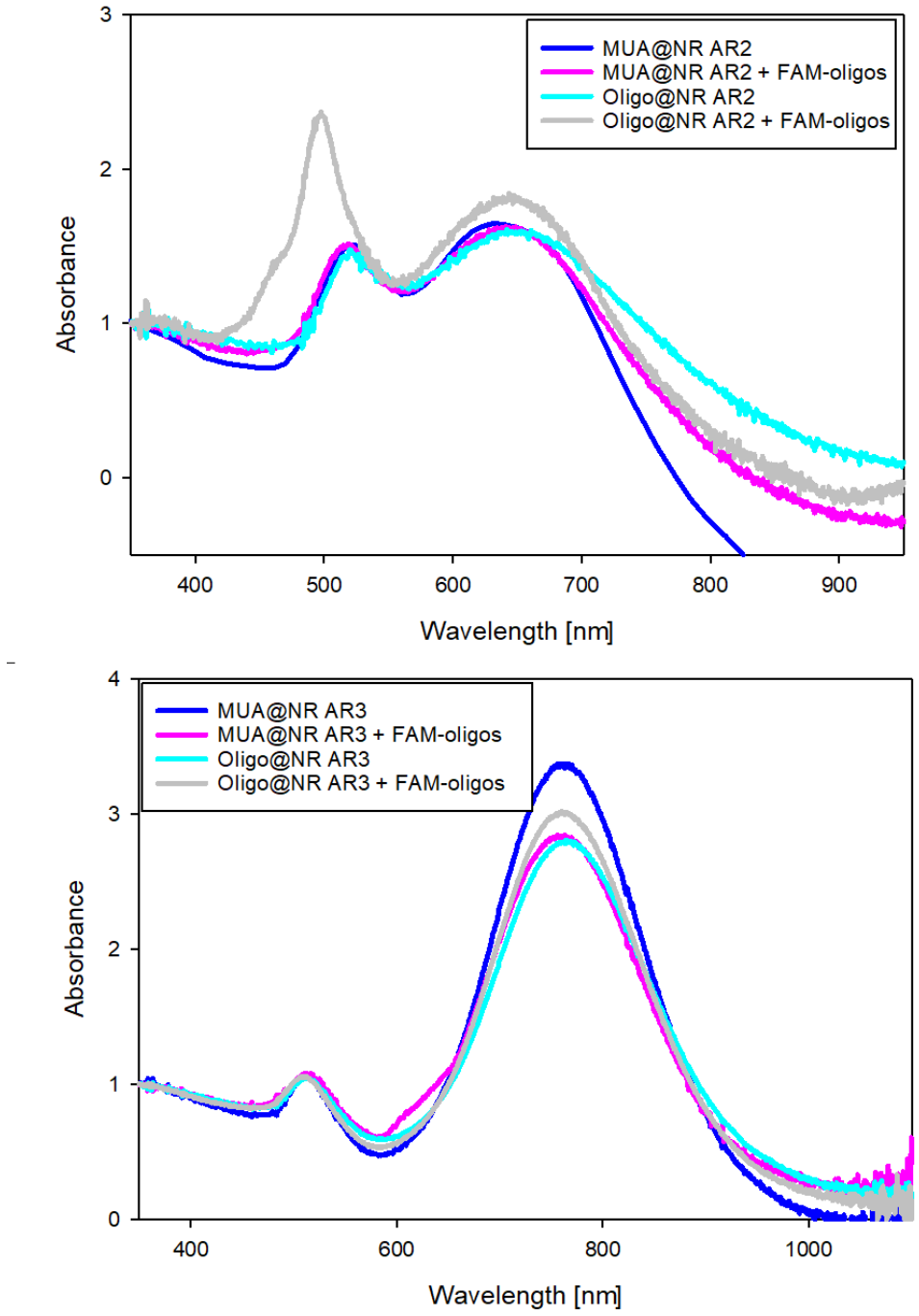

Figure 5.25: Absorbance spectra of the AR2 (top) and AR3 (bottom) nanorod samples before and after oligonucleotide-functionalization. All spectra are normalized to their absorbance at 350 nm.

Due to low concentrations of the AR2 nanorods incubated with the FAM-oligos, this spectra cannot be compared to the other ones with a high degree of certainty. However, the rest of the spectra can be compared with each other and provide greater context to the AR3 spectra. Firstly, the three spectra are fairly similar

which indicates that the oligo-functionalization has not affected the particle population to a high degree or caused agglomeration of particles. Other than that, mixing with FAM-oligos does not seem to have an effect on the MUA-capped AR2 nanorods which could be important to keep in mind in the biosensing section.

The oligonucleotide functionalization of the AR3 nanorods does on the other hand seem to have affected the nanoparticle population, as the peak intensity lowered after functionalization. This is likely due to loss of particles or aggregation during the functionalization. The spectra also show that being incubated with a complementary strand had different effects on the MUA-capped and oligo-functionalized nanorods. The incubation of FAM-oligos with MUA-capped rods caused a decrease in peak intensity, whereas the incubation with oligo-functionalized rods caused an increase in peak absorbance intensity. There is no notable shift in absorbance peak wavelength however, but it could be that the FAM-oligos does not have a high enough effect on the refractive index of the particles. A change in the refractive index is required for a LSPR wavelength shift to occur[4].

It is difficult to use these results as conclusive evidence of successful functionalization, but the difference in effect when MUA-capped and oligo-functionalized were incubated with FAM-oligos strongly indicates that the functionalization was successful. These results are similar to the nanosphere results, where a decrease in peak intensity was observed in the MUA-capped NPs after incubation with FAM-oligos and a slight increase was observed in the oligo-functionalized particles (when incubated with FAM-oligos).

The nanourchins functionalized with oligonucleotides were characterized by UV-Vis spectroscopy both before and after mixing with a FAM-modified complementary strand. For reference, the MUA-capped Au NU solution which were used for functionalization were also characterized in the same manner. The Au NU solution which were used for functionalization were also characterized in the same manner for reference. These absorbance spectra are shown in figure 5.26.

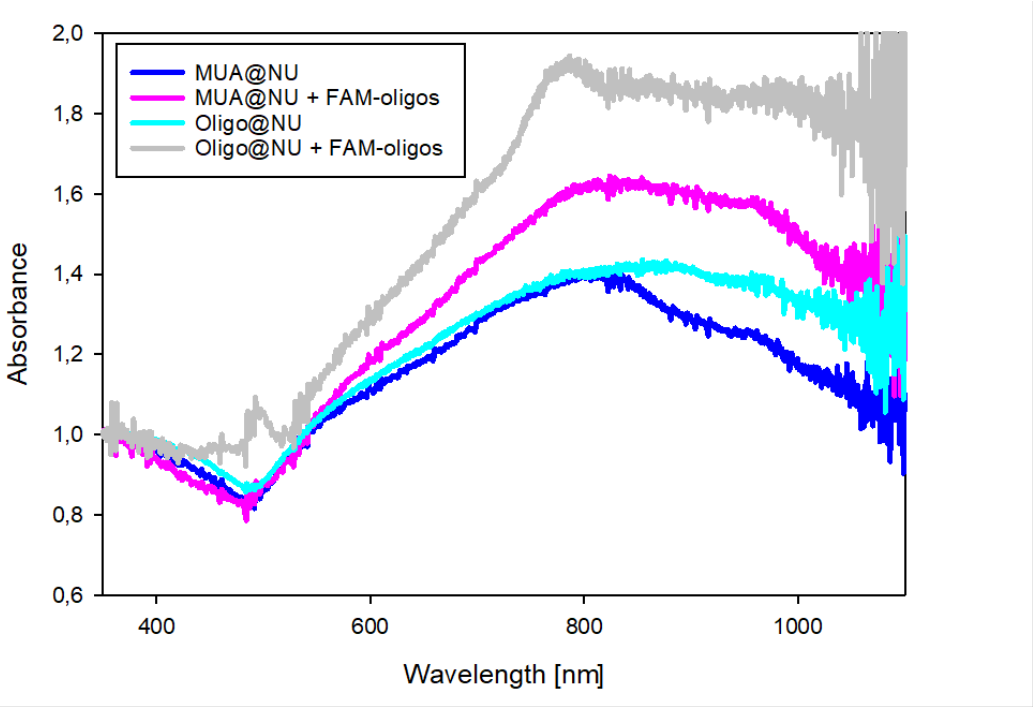

Figure 5.26: Absorbance spectra of nanourchin sample before and after oligonucleotide-functionalization. All spectra are normalized to their absorbance at 350 nm.

The changes which were observed in the Au NSs and the Au NRs are not seen in the Au NUs. Here, an increase in absorbance is observed both when the MUA-capped and oligo-functionalized NUs were incubated with FAM-oligos. It is not certain what can be derived from this information, but it should be noted that the increase in absorption intensity is much higher for the oligo-functionalized NUs than the MUA-capped ones.

Two problems with the Au NUs are also very evident when considering these results. Firstly, the peak is not very defined, especially after functionalization, which would make it difficult to identify LSPR wavelength shifts. Secondly, the noticeable changes in the absorbance spectra before and after oligonucleotide functionalization indicate that there are stability issues with the particles, causing loss of particles when they are functionalized. This makes the absorbance spectra change significantly and the concentration to drop with each washing step.

Although the functionalization of Au NSs, NRs and NUs seems to have been successful based on the results in this section, more testing should have been done to get a conclusive answer. However, time and instrument limitations made it difficult to analyze them further. The original plan with using the FAM-oligos was to look at the difference in fluorescence intensity when oligo-functionalized and non-functionalized Au NPs were incubated with them. Still, the particles were tested out for biosensing, the results of which will also work as an indication of the functionalization success.

5.3 Biosensing performance of Au NPs

Biosensing testing was done using two different spectrophotometers, a NanoDrop and a regular UV-Vis spectrophotometer. The results from these experiments are shown in the two following subsections, with the NanoDrop results being presented and discussed first, followed by the UV-Vis spectrophotometer results. The first analysis used lower concentrations of target RNA, whereas higher concentrations were tested in the latter.

5.3.1 Biosensing using NanoDrop spectrophotometer

The spectra of the nanosphere 1st (A) and 4th (B) generation and the AR2 (C) nanorods are included in figure 5.27. The amount of target RNA the sample each sample was incubated with it shown in the legend. The nanourchin sample and the AR4 nanorod sample are excluded as the highest measurable wavelength of the spectrophotometer was 850 nm, making it difficult to analyze these peaks. The concentration of the former was also too low to analyze.

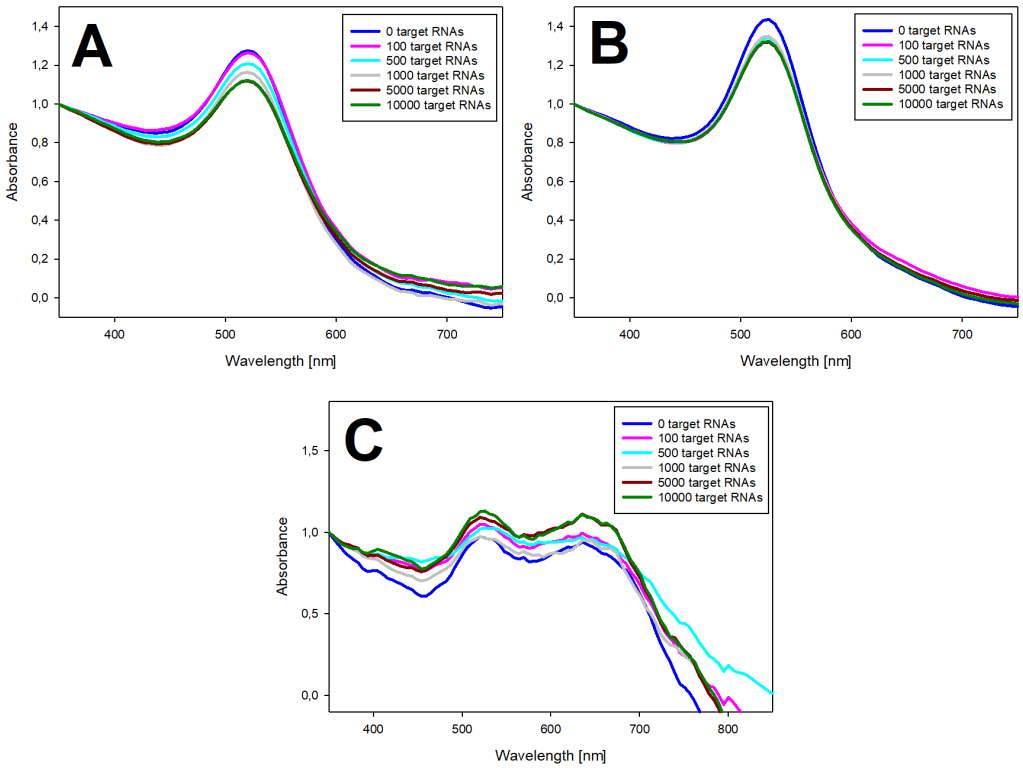

Figure 5.27: Absorbance spectra of the 1st (A) and 4th (B) generation nanosphere samples, and AR2 (C) nanorod samples. The Au NPs were incubated with different amounts of target RNA, which can be seen in the legend.

In the nanosphere samples, the intensity of the peaks decreases as the RNA concentration gets higher. This could either be the result of the specific binding between particle complex and target or it could be an effect the RNA presence,

meaning non-complementary sequence would show the same result. Changes in intensity have been shown to happen when Au NPs bind their target, but this is most commonly in the form of an increase[39;40]. This may mean that the biosensing is unsuccessful overall. Either the binding is not happening or the concentration of target RNA is too low to detect. Either way, this effect is more similar to the one observed in the functionalization chapter, when the non-functionalized nanospheres were mixed with FAM-oligos. The nanorod samples is on the other hand more in line with other reports, and an increase in absorbance intensity can be seen with increasing target RNA concentration. The spectra are however quite unreliable, and can not be used to draw any conclusions.

In the spectra of the nanosphere solutions, a small blue-shift can be observed as the target RNA concentration increases. This is most visible in the 1st generation nanospheres where the shift is about 3-4 nm from the blank to the highest concentrated sample, but in the 4th generation sample a shift of 1-2 nm is also observed. In the nanorod sample, the spectra are too bad to determine any absorbance peaks and this factor is therefore not considered for the AR2 NRs.

There were some clear limitations with using the NanoDrop spectrophotometer for these biosensing tests. Firstly, the range of the spectrophotometer was 190-850 in the UV-Vis method. This meant that when using this, particles with a peak at higher wavelengths can not be thoroughly analyzed. The nanourchins and AR4 were therefore not included in the study since their peaks were close to 850 nm, making it difficult to identify shifts in these two particle solutions. Another challenge with this type of analysis was that there was a large amount of noise in the spectra. Therefore, the plots were smoothed by using a SigmaPlot function. The spectra presented are therefore not perfectly reliable, and this has to be taken into account in the analysis of the results. The fit for the nanosphere samples is fairly good, but the nanorod spectra are not good approximations and can therefore not be used to determine the success of the biosensing. Future tests should focus on having a higher concentration of Au NPs, to get a higher signal-to-noise ratio. The Au NSs were the most concentrated and did therefore give the best curves after smoothing.

These results did not at all provide a good comparison between the three Au NP shapes and did not present any of the nanoparticles as good candidates for biosensing. This could mean that the functionalization was not successful or that the limit of detection is higher than the concentrations used in these experiments. Also, it was concluded that NanoDrop was a bad alternative for nanorods and nanourchins, as it sets a limit to how high absorbance peaks can be analyzed. Therefore, a comparison using a UV-Vis spectrophotometer with higher limits to the upper wavelength is better for a comparison between the shapes.

5.3.2 Biosensing using UV-Vis spectrophotometer

A biosensing experiment was also done using a regular UV-Vis spectrophotometer. In this analysis, all samples were tested after incubation with either 10 000, 100 000 or 1 000 000 copies of viral RNA. Figure 5.28 shows the spectra of the 1st generation (top) and 4th generation (bottom) samples before and after incubation with target RNA.

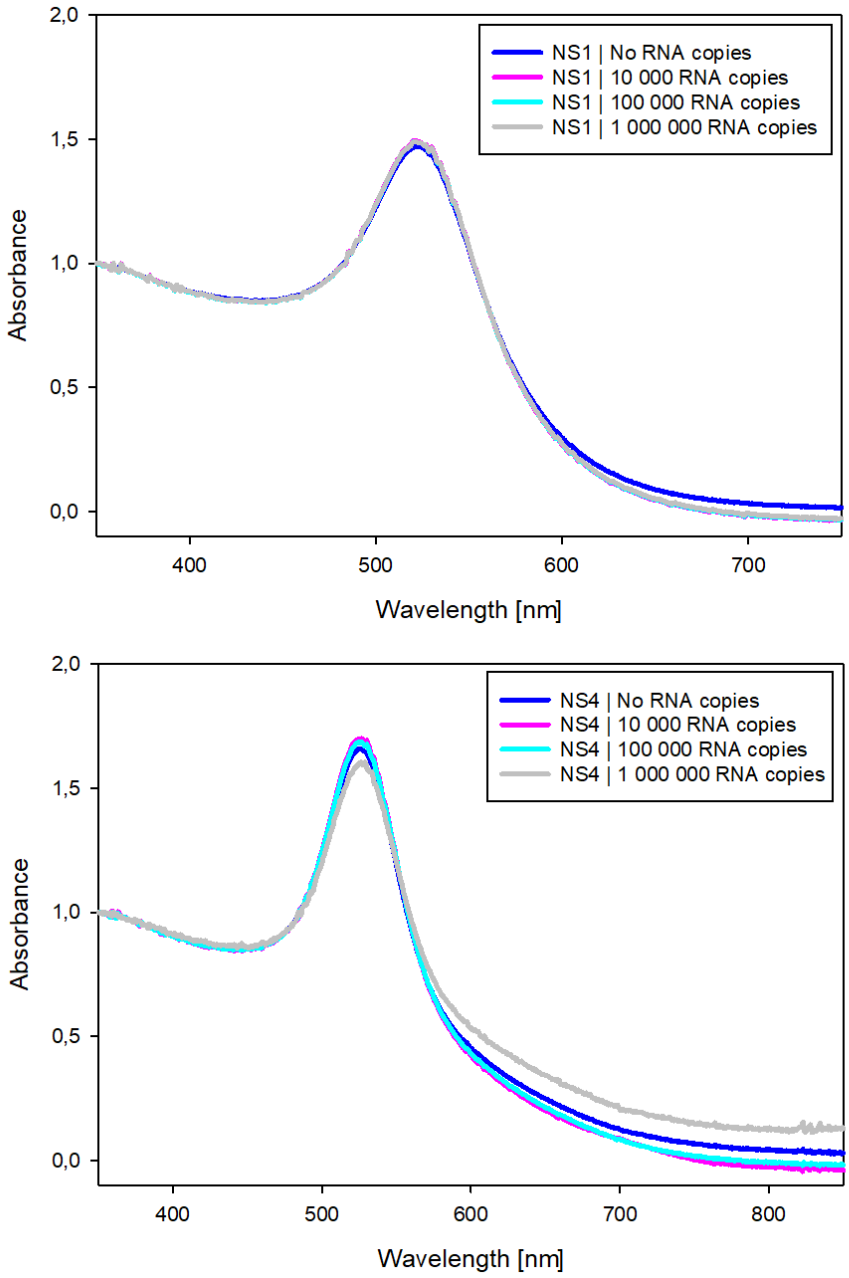

Figure 5.28: Absorbance spectra of the 1st generation (top) and 4th generation (bottom) nanosphere samples before and after mixing with different amounts of RNA copies. The legend shows the amount of RNA copies which the particles were incubated with. All spectra are normalized to their absorbance at 350 nm.

Figure 5.29 is a zoom-in on the peaks in figure 5.28. The peak absorbance intensity of all but one of the samples which were incubated with target RNA, shows an increase when compared to the bare Au NS solution. The peak wavelength is more or less the same in all samples within their own figure.

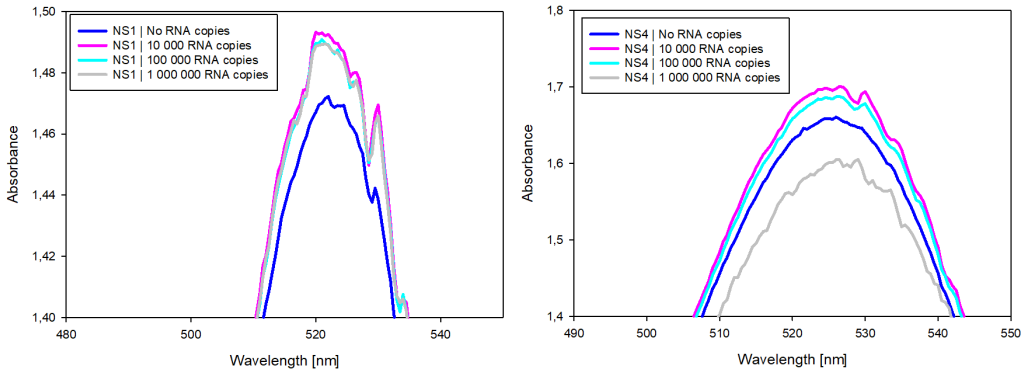

Figure 5.29: Absorbance spectra of the 1st generation (left) and 4th generation (right) nanosphere samples before and after mixing with different amounts of RNA copies, zoomed in around the peak. The legend shows the amount of RNA copies which the particles were incubated with. All spectra are normalized to their absorbance at 350 nm, and the spectra have been smoothed for easier analysis.

The first thing to notice in the spectra in figure 5.28 and 5.29 is that there is no shift in peak wavelength. That means that the presence of target RNA can not be determined by looking at the wavelength of the absorbance peak. This was unexpected, as literature where gold nanostructures have been used as biosensors generally show a slight red-shift after incubation with the target [39;40]. The verification of the oligonucleotide-functionalization also showed a red-shift after incubation with FAM-modified oligonucleotides. It is difficult to answer why the red-shift is not happening, but it could potentially be due to the concentration of the target RNA being too low to affect the refractive index or the incubation time being too short. The concentration of FAM-modified oligonucleotides was significantly higher than the concentration of target RNA, but the size of the RNA strand would suggest that its effect should have been higher.

Still, a difference can be observed when looking at the absorbance intensity of the peak. In all but the NS4 sample incubated with 1 000 000 target RNAs, the intensity increased compared to the sample with only Au NSs. The outlier could potentially be the product of some human error during the analysis or aggregation of particles. It is also the only sample with a slight red-shift, which makes aggregation a very plausible explanation [4]. The other samples however, continues the trend observed in the verification of oligonucleotide-functionalization of both NRs and NSs. This means that this increase in absorbance intensity is the greatest indication of the presence of target RNA for the nanospheres. The intensity only increases slightly in both samples, making it difficult to compare the two nanospheres solutions directly.

Nanorod samples AR2 and AR3 were used for these biosensing experiments. Figure 5.30 shows the AR2 (top) and AR3 (bottom) absorbance spectra before and after incubation with different concentrations of target RNA.

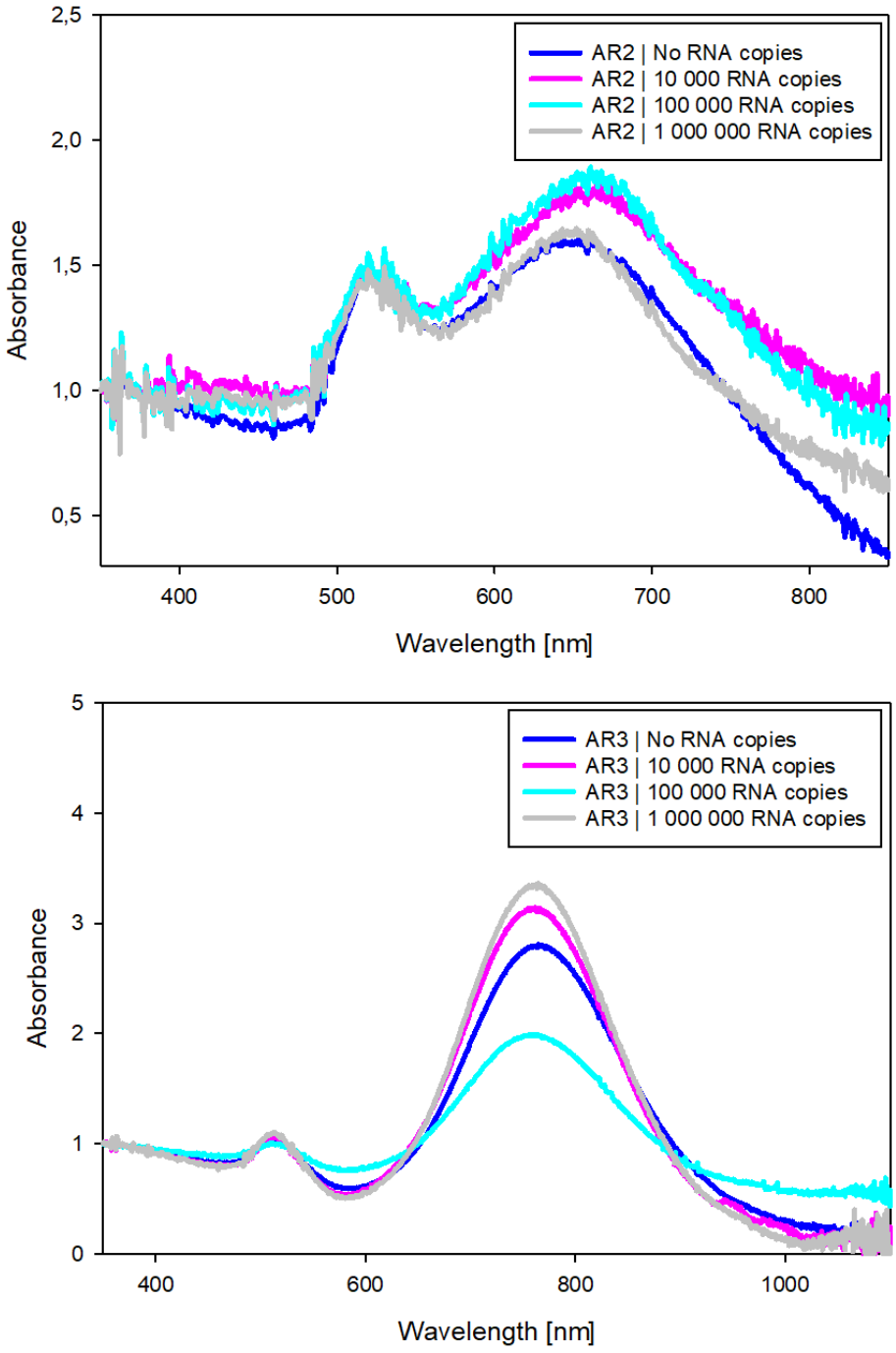

Figure 5.30: Absorbance spectra of the AR2 (top) and AR3 (bottom) nanorod samples before and after mixing with different amounts of RNA copies. The legend shows the amount of RNA copies which the particles were incubated with. All spectra are normalized to their absorbance at 350 nm.

Figure 5.31 shows a zoom-in of the AR4 absorbance spectra which are shown fully in figure 5.30. The peaks of the samples incubated with target RNA have blue-shifted around 5 nm in relation to the bare AR4 nanorod spectra peak. In this figure, the spectra have been normalized to their absorbance at 765 nm.

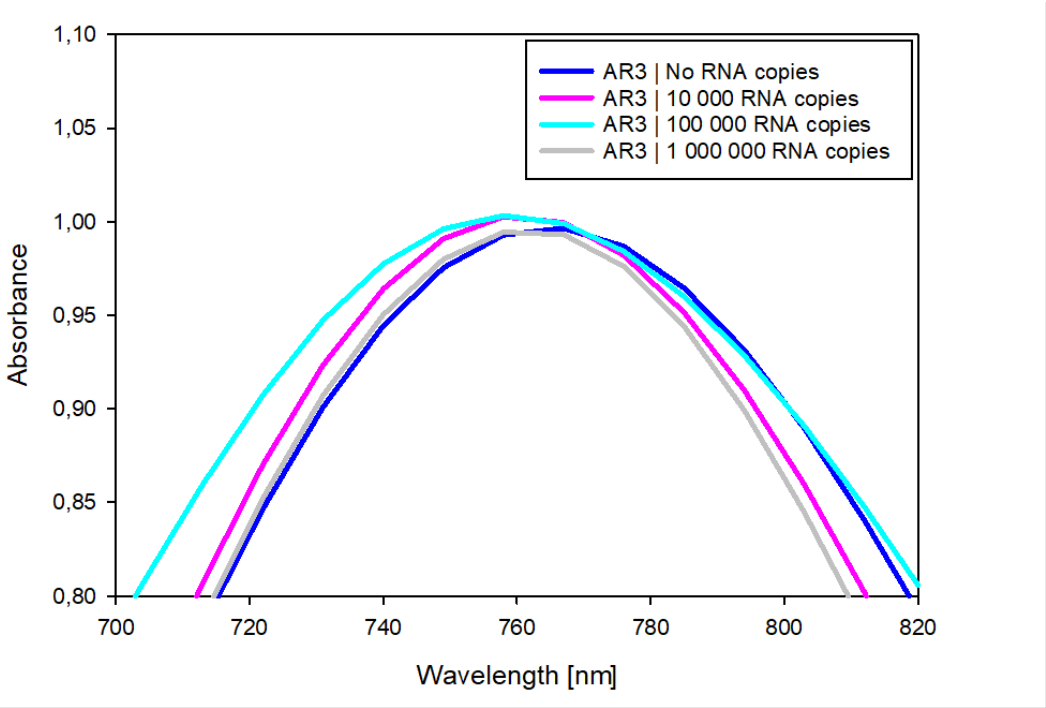

Figure 5.31: Absorbance spectra of the AR2 (top) and AR3 (bottom) nanorod samples before and after mixing with different amounts of RNA copies, zoomed in around the second peak. The legend shows the amount of RNA copies which the particles were incubated with. All spectra are normalized to their absorbance at 765 nm, and the spectra have been smoothed for easier analysis.

Before discussing the spectra presented in relation to biosensing performance, it has to be noted that the AR2 spectra has been edited slightly due to faulty measurements. The absorbance of the samples incubated with target RNA, had were measured to have slightly negative absorbance at wavelengths further form the peaks. The spectra were therefore moved up to have their lowest absorbance at zero, so the samples could be normalized (new samples could not be made due to time limitations). This will be a great source of error, since different adjustments of the spectra will cause different results when normalized. Therefore, the discussion of these spectra has to be viewed critically. Also due to much noise, the spectrum of the bare AR2 nanorod sample was smoothed using a SigmaPlot function.

In both the AR2 and AR3 nanorod spectra, there is generally an increase in absorbance peak intensity after incubation with target RNA. This is with the exception of the AR3 sample incubated with 100 000 target RNA copies. It is uncertain why this is and should be kept in mind in further evaluation of the

results, but like with the nanospheres it may come down to human error in the preparation. In terms of absorbance peak shifts, they can be seen in both the AR2 and AR3 samples. With the exception of the AR2 samples incubated with 1 000 000 RNA copies, a significant red-shift is occurring in the second peak of the AR2 samples. These shifts can be observed very easily, but as due to low NR concentration in these samples and the adjustment of the spectra, these results are not entirely reliable.

The shifts in the AR3 samples are however blue-shifts. Blue-shifts in Au NPs biosensing have been observed in literature, and it may that the refractive index is affected differently due to the shape and optical properties of these nanorods with higher aspect ratios[4;81]. However, in all three of the samples incubated with RNA, the blue-shift is around 5 nm. Seeing as there is both an increase in absorbance peak intensity and a peak-shift, both methods can be used for biosensing. However, it would be interesting to compare these results to a sample incubated to a non-complementary RNA strand. This could be done to get a better understanding of the process, as it can not be verified by these results that the changes are caused by the specific bindings between the Au NP complex and the target RNA.

The nanourchin sample was also tested in the biosensing experiments. The spectra of all the NU samples are shown in figure 5.32.

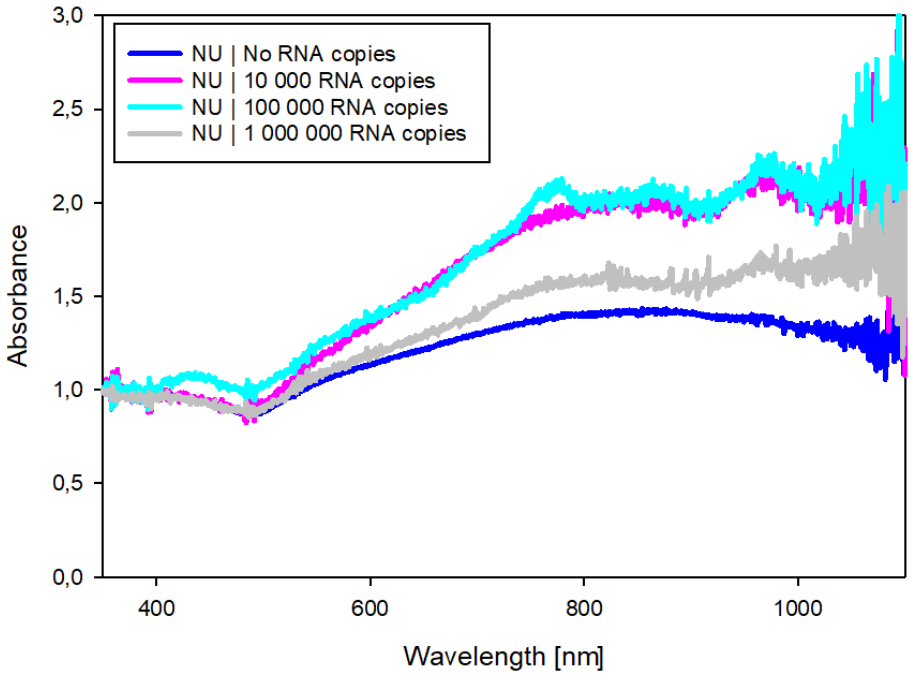

Figure 5.32: Absorbance spectra of the nanourchin sample before and after mixing with different amounts of RNA copies. The legend shows the amount of RNA copies which the particles were incubated with. All spectra are normalized to their absorbance at 350 nm.

The results from the nanourchin biosensing shows one clear limitation with their use. As previously discussed, the lack of clear and narrow peaks make them unusable for biosensing based on peak shifts. On the other hand, the spectra in figure 5.32 suggests that they are very sensitive in terms of absorbance intensity. When incubated with the target RNA, the relative absorbance of the "peak" increases to a very high degree. This suggests that the nanourchins are not entirely unusable as viral RNA biosensors, despite the limitations of broad peaks, changing absorbance spectrum and low stability (compared to the others) which have been discussed in earlier sections.

5.3.3 Comparison of Au NP biosensing performance

The performance of the Au NPs as viral biosensors can be compared in how their peak absorbance intensity changed and the peak wavelength were shifted after being incubated with the viral RNA. Incubation with a non-complementary DNA-strand would have been ideal for comparison, as this would have shown if the changes arose from the specific binding or just the presence of the RNA. However, such a RNA strand was not available at the time of the experiments. These comparisons are therefore done on the assumption that the changes were caused by specific bindings between the Au NP complex and the target RNA.

Firstly, the peak absorbance intensity was the best indicator of target RNA presence. Though seemingly relatively independent of the RNA concentration in all experiments, the peak intensity increased significantly for the Au NUs and Au NRs and slightly for the the Au NS. It is possible that even the lowest RNA concentration used in these experiments was high enough enough to saturate the NP complexes, which could mean that lower concentrations would be possible to distinguish from each other based on the peak absorbance intensity. A couple of samples deviated from the pattern of increased intensity after incubation, but one of them could likely be attributed to aggregation, since this sample was the only one with an observed red-shift. This makes it likely that the other sample with an observed decrease is an outlier caused by some kind of error in the preparation. By comparing the particle shapes directly, it seemed to be the Au NUs which were affected most in terms of absorbance intensity change, followed by the nanorods where the change was also easily noticeable. The change in the nanospheres absorbance was however not as evident, but when zoomed in as small increase was observed.

Furthermore, peak wavelength shifts were only observed in the nanorods, where the lower aspect ratio particles portrayed a significant red-shift (though these results were somewhat uncertain) and the higher aspect ratio particles showed a blue-shift of about 5 nm for all samples. The nanourchins performed the worst in this category as an exact peak was difficult to identify due to its broad appearance. Although the nanospheres did not show any shifts in these biosensing experiments, there was observed a slight red-shift in functionalization verification, where the particles were incubated with a complementary FAM-modified

strand.

The nanorods seemed to perform best as biosensors in these experiments, as they were both susceptible to peak wavelength shifts and increases in absorbance when incubated with the target RNA. Although they have the most complicated functionalization, especially compared to the nanospheres, their performance as biosensors was better than the two other shapes. The results in this work did not show any significant differences based on aspect ratio, and more thorough studies of the influence of aspect ratio could be done in the future.

5.4 Further work

This project has suggested and adapted pathways to synthesize and functionalize three different types of particles for use as oligonucleotide-based biosensors. Still, there are a few elements which would be interesting to a have a look at in future work. Firstly, the MUA-functionalization of Au NRs still had a loss of intensity after the protocol had been adapted. This means there could likely still be made further improvements to this protocol and other protocols should be tested, to keep the absorbance spectra of the solution as close to the original as possible. The FTIR analysis and zeta potential measurements indicated that the particles had been functionalized with MUA, but the ligand exchange rate could be studied even further by for example performing carboxyl group quantification after several rounds of centrifugation.

Furthermore, the functionalization with oligonucleotides of all the Au NPs could be looked at in more detail. In the Au NS functionalization, a study of how the concentration of oligonucleotides added affects the functionalization could have been done to optimize the protocol. Due to time limitations however, this was not done but it would be a natural thing to investigate in further work. Also, if a fluorescence spectrophotometer had been available at this point, a more thorough study of the success of the functionalization could have been performed and this would therefore be an interesting analysis to perform. Other methods of verifying the functionalization could also be investigated.

The biosensing comparison should be looked at in greater detail to investigate the performance of the different particles. Due to the many issues with the nanourchins such a lower stability, worse repeatability and broader peaks, these may not be worth looking further into. To use the NanoDrop spectrophotometer for biosensing analyses, the concentration of the nanoparticles needs to be sufficient enough to get a higher signal-to-noise ratio. This could make the smoothing of the curves more accurate, like the ones observed for the nanospheres. Another interesting aspect to study further is the how a non-complementary RNA strand affects the absorbance and use that as a reference in future biosensing experiments. This could provide an answer to whether the changes observed are caused by the specific bindings between the Au NP complex or just by the mere presence of RNA.

Finally, other variations of Au NP biosensing could be looked at in greater detail. These can for example be to either use a mixture of different oligonucleotides (which are complementary to different sequences in the target) in the functionalization as has been reported in other work or to look at aggregation-based biosensing[82;41]. The latter is a method where the binding between the Au NP complex and the target causes particle aggregation, making it more sensitive than the method used in this project.

6 Conclusion

This project aimed to create a pathway for synthesis and functionalization of tree differently shaped Au NPs (spherical, rod-shaped and sea-urchin like) to make them suitable for biosensing of RNA. The particles were first synthesized and characterized thoroughly to examine repeatability of the syntheses and stability of the particles.

The repeatability was found to be very good for the Au NS synthesis after temperature changes were made to promote nucleation in the nucleation stage and to avoid secondary nucleation in the growth stages. The Au NR synthesis gave similar results to the source material and is an established synthesis in the research group, making it known that this synthesis was very repeatable. Finally, the Au NU synthesis was the hardest to replicate, and slightly different absorbance spectra were achieved each synthesis. This is however the most irregular shape, naturally making it the most difficult to reproduce. In terms of nanoparticle stability, Au NSs and Au NRs have been studied in the research group before and were known to be highly stable for a long time, but the Au NUs were found to be less stable. This was observed both in its short term stability in solution and morphology changes over longer periods of time, causing changes in the absorbance spectra.

The functionalization had to be done differently for each of the shapes. The Au NSs could be functionalized with thiol-modified oligonucleotides directly, whereas the Au NRs and Au NUs had to be functionalized in three and two step methods, respectively. The functionalization of Au NSs seemed to be successful based on a test in which a complementary strand was introduced, and the MUA-functionalization of NUs was also successful based on FTIR, zeta potential changes and dispersibility testing. The Au NRs were first successfully functionalized PEG and then MUA through ligand exchanges after adapting an existing method. The oligonucleotide functionalization of these the Au NRs and Au NUs was done based on basic NHS/EDC chemistry, but the success of this functionalization could not be verified due to lack of available methods and time limitations.

Finally, biosensing testing was tested using a NanoDrop spectrophotometer. Due to low concentrations of nanorods and nanourchins, there was a low signal-to-noise ratio, making it difficult to analyze these samples even after using tools for smoothing the curves. Although there was some noise in the nanosphere samples, their spectra were the easiest to examine and a blue-shift and intensity loss was observed with increasing target concentration.

In conclusion, pathways for synthesis and functionalization of three differently shaped nanoparticles are proposed in this project. Unique pathways of functionalization have been created for Au NRs and Au NUs and many steps in all the processes have also been optimized. This work can therefore be used as a guidebook for preparation of various oligonucleotide-functionalized Au NPs. In terms

of biosensing, the simple analyses in this project shows that nanorods seem to be the most promising in viral RNA biosensing, as they had the clearest intensity changes and absorbance peak shifts when incubated with target RNA. The particles are stable and have the potential of being tailored in terms of aspect ratio, but the functionalization is significantly more complex than that of nanospheres. The lower stability and broad peaks of the Au NUs made them difficult to use, but Au NS could also be investigated further as they too showed some potential in the biosensing experiments.

References

[1] Basant Giri et al. Review of analytical performance of covid-19 detection methods. *Analytical and Bioanalytical Chemistry*, 413:35–48, 2021.

[2] Jacqueline Dinnes et al. Rapid, point-of-care antigen tests for diagnosis of sars-cov-2 infection. *Cochrane Database of Systematic Reviews*, 7, 2022.

[3] Norsk Helsenett Folkehelseinstituttet. Om prøvesvar, 2022.

[4] Eleonora Petryayeva and Ulrich J. Krull. Localized surface plasmon resonance: Nanostructures, bioassays and biosensing—a review. *Analytica Chimica Acta*, 706(1):8–24, 2011.

[5] Gennaro Sanità et al. Nanoparticle surface functionalization: How to improve biocompatibility and cellular internalization. *Frontiers in Molecular Biosciences*, 7, 2020.

[6] John Turkevich et al. A study of the nucleation and growth processes in the synthesis of colloidal gold. *Discussions of the Faraday Society*, 11, 1951.

[7] Nikhil R. Jana et al. Wet chemical synthesis of high aspect ratio cylindrical gold nanorods. *The Journal of Physical Chemistry B*, 105(19):4065–4067, 2001.

[8] Babak Nikoobakht and Mostafa A. El-Sayed. Preparation and growth mechanism of gold nanorods (nrs) using seed-mediated growth method. *Chemistry of Materials*, 15(10):1957–1962, 2003.

[9] Karthik Raghunathan et al. Tuning and tracking the growth of goldnanoparticles synthesized using binary surfactant mixtures. *Nanoscale Advances*, 5:1980–1992, 2020.

[10] Neus G. Bastús et al. Kinetically controlled seeded growth synthesis of citrate-stabilized gold nanoparticles of up to 200 nm: Size focusing versus ostwald ripening. *Langmuir*, 27(17):11098–11105, 2011.

[11] Yuanyuan Li et al. Controllable synthesis of sea urchin-like gold nanoparticles and their optical characteristics. *Applied Surface Science*, 498, 2019.

[12] Pandian Senthil Kumar et al. High-yield synthesis and optical response of gold nanostars. *Nanotechnology*, 19, 2008.

[13] Priyanka Singh et al. Gold nanoparticles in diagnostics and therapeutics for human cancer. *International Journal of Molecular Sciences*, 19(7):1979, 2018.

[14] Sulalit Bandyopadhyay. *Fabrication and Application of Nanomaterials*. McGraw-Hill Education, 2019.

[15] Nguyen T.K. Thanh et al. Mechanisms of nucleation and growth of nanoparticles in solution. *Chemical Reviews*, 114(15):7610–7630, 2014.

[16] Zhe Zhang et al. Sodium citrate: A universal reducing agent for reduction / decoration of graphene oxide with au nanoparticles. *Nano research*, 4:599–611, 2011.

[17] Juan Du et al. Ascorbic acid: Chemistry, biology and the treatment of cancer. *Biochimica et Biophysica Acta*, 1826(2):443–457, 2013.

[18] Viktor K. LaMer and Robert H. Dinegar. Theory, production and mechanism of formation of monodispersed hydrosols. *Journal of the American Chemical Society*, 72(11):4847–4854, 1950.

[19] J.W. Mullin. *Crystallization*. Butterworth-Heinemann, 4 edition, 2001.

[20] Panikkanvalappil R. Sajanlal et al. Anisotropic nanomaterials: structure, growth, assembly, and functions. *Nano Reviews*, 2(10), 2011.

[21] Byung-Sang Choi et al. Removal of cetyltrimethylammonium bromide to enhance the biocompatibility of au nanorods synthesized by a modified seed mediated growth process. *Journal of Nanoscience and Nanotechnology*, 8(9):4670–4674, 2008.

[22] Rukmani Thiruppathi et al. Nanoparticle functionalization and its potential for molecular imaging. *Advanced Science*, 4(3), 2017.

[23] Chi M. Phan and Hoang M. Nguyen. Role of capping agent in wet synthesis of nanoparticles. *The Journal of Physical Chemistry*, 121(17):3213–3219, 2017.

[24] A. Caragheorgheopol and V. Chechik. Mechanistic aspects of ligand exchange in au nanoparticles. *Physical Chemistry Chemical Physics*, 10:5029–5041, 2008.

[25] J. A. Cowan. *Inorganic Biochemistry: An Introduction*. John Wiley & Sons, 2nd edition, 1997.

[26] Christine H. Horan et al. Replacement of poly(vinyl pyrrolidone) by thiols: A systematic study of ag nanocube functionalization by surface-enhanced raman scattering. *The Journal of Physical Chemistry*, 115(44):21852–21857, 2011.

[27] Benjamin Thierry et al. A robust procedure for the functionalization of gold nanorods and noble metal nanoparticles. *Chemical Communications*, 13:1724–1726, 2009.

[28] Michael J. Hostetler et al. Dynamics of place-exchange reactions on monolayer-protected gold cluster molecules. *Langmuir*, 15(11):3782–3789, 1999.

[29] Sundus Jabeen Amina and Bin Guo. A review on the synthesis and functionalization of gold nanoparticles as a drug delivery vehicle. *International Journal of Biomedicine*, 15:9823–9857, 2020.

[30] Benjamin A. Pierce. *DNA: The Chemical Nature of the Gene*, book section 8, pages 207–232. W. H. Freeman & Company, 3 edition, 2016.

[31] Pär Sandström et al. Nonspecific and thiol-specific binding of dna to gold nanoparticles. *Langmuir*, 19(18):7537–7543, 2003.

[32] Haley D. Hill et al. The role radius of curvature plays in thiolated oligonucleotide loading on gold nanoparticles. *ASC Nano*, 3(2):418–424, 2009.

[33] Nikhil Bhalla et al. Introduction to biosensors. *Essays in Biochemistry*, 60(1):1–8, 2016.

[34] Parikha Mehrotra. Biosensors and their applications – a review. *Journal of Oral Biology and Craniofacial Research*, 6(2):153–158, 2016.

[35] S. P. Mohanty and E. Kougianos. Biosensors: a tutorial review. *IEEE Potentials*, 25(2):35–40, 2006.

[36] Jie Cao et al. Gold nanorod-based localized surface plasmon resonance biosensors: A review. *Sensors and Actuators B*, 195:332–351, 2014.

[37] Jeffrey N. Anker et al. Biosensing with plasmonic nanosensors. *Nature Materials*, 7:442–453, 2008.

[38] Leonor Soares et al. Localized surface plasmon resonance (lspr) biosensing using gold nanotriangles: detection of dna hybridization events at room temperature†. *Analyst*, 139:4964–4973, 2014.

[39] Jin-Ho Lee et al. Highly sensitive localized surface plasmon resonance immunosensor for label-free detection of hiv-1. *Nanomedicine: Nanotechnology, Biology and Medicine*, 9(7):1018–1026, 2013.

[40] Tae Jung Park et al. Development of label-free optical diagnosis for sensitive detection of influenza virus with genetically engineered fusion protein. *Talanta*, 89:246–252, 2011.

[41] Jin-Ho Lee et al. Application of gold nanoparticle to plasmonic biosensors. *International Journal of Molecular Sciences*, 19(7), 2021.

[42] Sungje Bock et al. Highly sensitive near-infrared sers nanoprobes for in vivo imaging using gold-assembled silica nanoparticles with controllable nanogaps. *Journal of Nanobiotechnology*, 20(130), 2022.

[43] Jayanta Dolai et al. Nanoparticle size effects in biomedical applications. *ACS Applied Nano Materials*, 4(7):6471–6496, 2021.

[44] Niloofar Ajdari et al. Gold nanoparticle interactions in human blood: a model evaluation. *Nanomedicine: Nanotechnology, Biology and Medicine*, 13(4):1531–1542, 2017.

[45] Stephen B. Rice et al. Particle size distributions by transmission electron mi-

croscopy: an interlaboratory comparison case study. *Metrologia*, 50(6):663–678, 2013.

[46] John G. Walker. Improved nano-particle tracking analysis. *Measurement Science and Technology*, 23(6), 2012.

[47] H. Cölfen and T. Pauck. Determination of particle size distributions with angström resolution. *Colloid and Polymer Science*, 275:175–180, 1997.

[48] Mladenka Malenica et al. Perspectives of microscopy methods for morphology characterisation of extracellular vesicles from human biofluids. *Biomedicines*, 9(6):603, 2021.

[49] Thermo Fischer Scientific. Transmission electron microscopy vs scanning electron microscopy, Unknown.

[50] E. Buhr et al. Characterization of nanoparticles by scanning electron microscopy in transmission mode. *Measurement Science and Technology*, 20, 2009.

[51] Jörg Stetefeld et al. Dynamic light scattering: a practical guide and applications in biomedical sciences. *Biophysical Reviews*, 8:409–427, 2016.

[52] Karl Fischer and Manfred Schmidt. Pitfalls and novel applications of particle sizing by dynamic light scattering. *Biomaterials*, 98:79–91, 2016.

[53] Jeffrey D. Clogston et al. *Zeta Potential Measurement*, volume 697 of *Methods in Molecular Biology*, pages 63–70. Humana Press, link.springer.com, 2010.

[54] Sourav Bharracharjee. Dls and zeta potential – what they are and what they are not? *Journal of Controlled Release*, 235:337–351, 2016.

[55] John R. Ferraro et al. *Introductory Raman Spectroscopy*. Elsevier, 2nd edition, 2003.

[56] H.H. Perkampus et al. *UV-VIS Spectroscopy and Its Applications*. Springer Berlin Heidelberg, 2013.

[57] John Coates. Interpretation of infrared spectra, a practical approach, 2000.

[58] Bob Carr et al. Applications of nanoparticle tracking analysis in nanoparticle research - a mini-review. *European Journal of Parenteral & Pharmaceutical Sciences*, 14(2):45–50, 2009.

[59] Mathias Brust et al. Synthesis of thiol-derivatised gold nanoparticles in a two-phase liquid–liquid system. *Journal of the Chemical Society, Chemical Communications*, 7:801–802, 1994.

[60] Jing Li et al. Controllable synthesis of stable urchin-like gold nanoparticles using hydroquinone to tune the reactivity of gold chloride. *The Journal of Physical Chemistry*, 115(9):3630–3637, 2011.

[61] Christina Graf et al. A general method to coat colloidal particles with silica. *Langmuir*, 19(17):6693–6700, 2003.

[62] Yazhou Qin et al. Controllable preparation of sea urchin-like au nps as a sers substrate for highly sensitive detection of the toxic atropine. *RSC Advances*, 11(32):19813–19818, 2021.

[63] Shan Zhou et al. Enabling complete ligand exchange on the surface of gold nanocrystals through the deposition and then etching of silver. *Journal of the American Chemical Society*, 140(38):11898–11901, 2018.

[64] Xiaohu Xia et al. Quantifying the coverage density of poly(ethylene glycol) chains on the surface of gold nanostructures. *ASC Nano*, 6(1):512–522, 2012.

[65] Melissa R. Dewi et al. A highly efficient ligand exchange reaction on gold nanoparticles: preserving their size, shape and colloidal stability. *RSC Advances*, 64:34217–34220, 2014.

[66] Chad A. Mirkin et al. Oligonucleotide-modified gold nanoparticles for intracellular gene regulation. *Science*, 312(5776):1027–1030, 2006.

[67] Biwu Liu and Juewen Liu. Interface-driven hybrid materials based on dna-functionalized gold nanoparticles. *Matter*, 1(4):825–847, 2019.

[68] Qiang Zhang et al. Study of effiency of coupling peptides with gold nanoparticles. *Chinese Journal of Analytical Chemistry*, 45(5):662–667, 2017.

[69] Hyung Hoon Kim et al. Highly sensitive microcantilever biosensors with enhanced sensitivity for detection of human papilloma virus infection. *Sensors and Actuators B: Chemical*, 221:1372–1383, 2015.

[70] Babak Nikoobakht and Mostafa A. El-Sayed. Evidence for bilayer assembly of cationic surfactants on the surface of gold nanorods. *Langmuir*, 17(20):6368–6374, 2001.

[71] Sigma-Aldrich. Sikkerhetsdatablad: Sølvnitrat, 2023.

[72] Deyin Wang et al. Applicability evaluation of bright green-emitting carbon dots in the solid state for white light-emitting diodes. *Chemistry - An Asian Journal*, 13(3):292–298, 2018.

[73] Yuri Borodko et al. Probing the interaction of poly(vinylpyrrolidone) with platinum nanocrystals by uv raman and ftir. *The Journal of Physical Chemistry B*, 110(46):23052–23059, 2006.

[74] N. Vijaya et al. Structural, vibrational, thermal, and conductivity studies on proton-conducting polymer electrolyte based on poly (n-vinylpyrrolidone). *Ionics*, 18:91–99, 2012.

[75] nanoComposix. Polyethylene glycol (peg) surface.

[76] Selleckchem. 11-mercaptoundecanoic acid, Unknown.

[77] Sigma-Aldrich. Polyethylene glycol (pegs and peos), Unknown.

[78] Astrid Prestegård. *Shape Dependency in Functionalization of Gold Nanoparticles for Biosensing Applications*. Thesis, NTNU, 2022.

[79] Behnam Meschi Amoli et al. Thiocarboxylate functionalization of silver nanoparticles: Effect of chain length on the electrical conductivity of nanoparticles and their polymer composites. *Journal of Materials Chemistry*, 22(37):20048–20056, 2012.

[80] Yongming Guo et al. Stable fluorescent gold nanoparticles for detection of cu2+ with good sensitivity and selectivity. *Analyst*, 137(2):301–304, 2011.

[81] Jing Zhao et al. Resonance surface plasmon spectroscopy: Low molecular weight substrate binding to cytochrome p450. *Journal of the American Chemical Society*, 128(34):11004–11005, 2006.

[82] Parikshit Moitra et al. Selective naked-eye detection of sars-cov-2 mediated by n gene targeted antisense oligonucleotide capped plasmonic nanoparticles. *ACS Nano*, 14(6):7617–7627, 2020.

Appendix A: Particle synthesis data

Hydrodynamic sizes of unfiltered nanospheres

Table 6.1: The hydrodynamic radius of each generation of the three syntheses in which seeding was done at 125 ℃ and the growth step were done at 80 ℃. All samples were unfiltered.

Generation	First synthesis	Second synthesis	Third synthesis
1st gen.	21 ± 1 nm	19 ± 1 nm	26 ± 2 nm
2nd gen.	25 ± 1 nm	26 ± 2 nm	26 ± 0 nm
3rd gen.	30 ± 0 nm	26 ± 0 nm	29 ± 0 nm
4th gen.	35 ± 0 nm	30 ± 0 nm	33 ± 0 nm

TEM sizes of unfiltered nanospheres

Table 6.2: The TEM sizes of each generation of the three syntheses in which seeding was done at 125 ℃ and the growth step were done at 80 ℃. All samples were unfiltered.

Generation	First synthesis	Second synthesis	Third synthesis
1st gen.	16 ± 2 nm	14 ± 2 nm	15 ± 2 nm
2nd gen.	21 ± 2 nm	19 ± 2 nm	19 ± 3 nm
3rd gen.	25 ± 2 nm	23 ± 2 nm	25 ± 2 nm
4th gen.	32 ± 2 nm	30 ± 2 nm	31 ± 3 nm

Appendix B: Size and aspect ratio histograms of Au NRs

Size histograms of 1st generation Au NSs

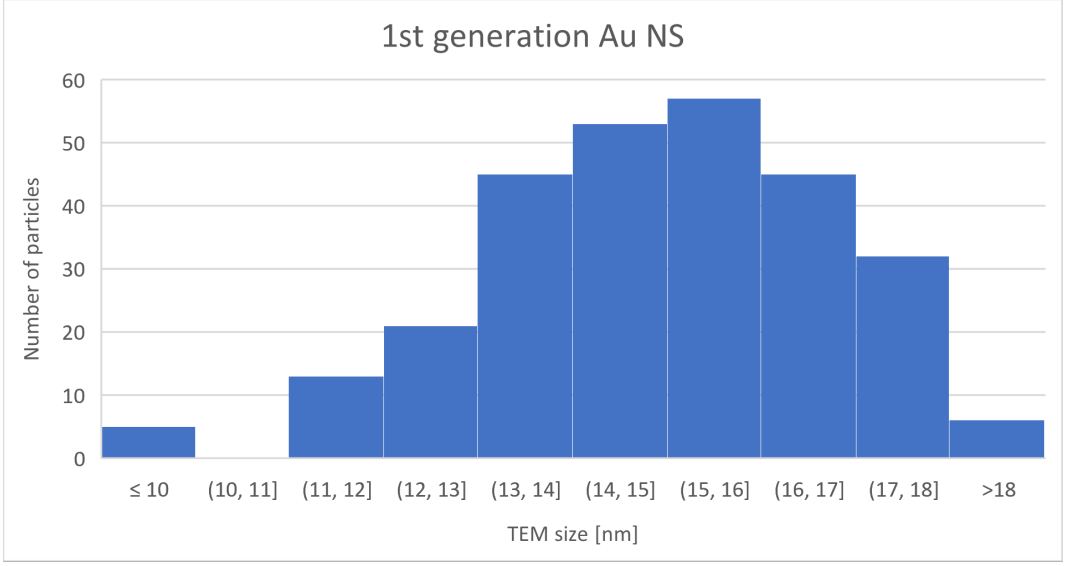

Size histograms of 2nd generation Au NSs

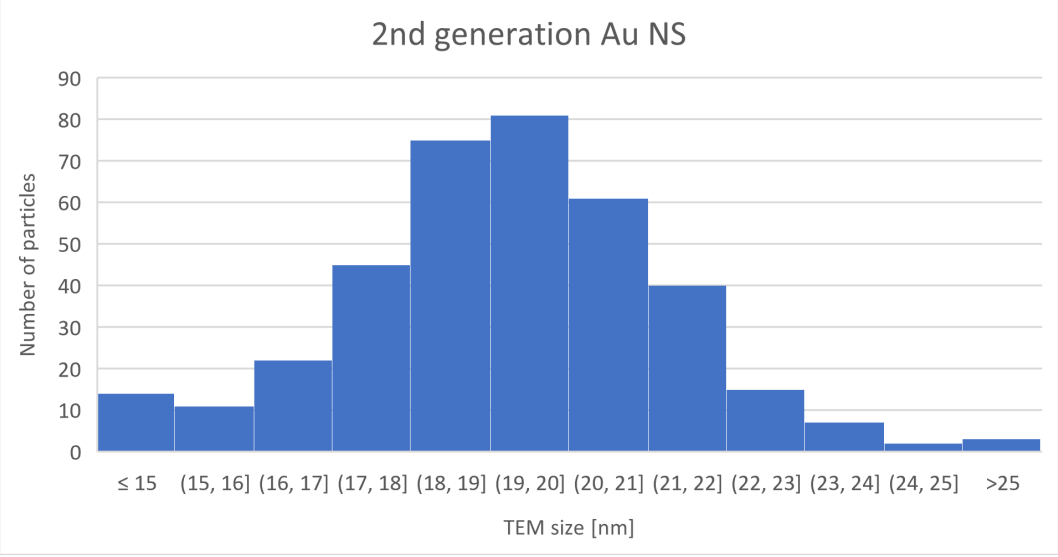

Size histograms of 3rd generation Au NSs

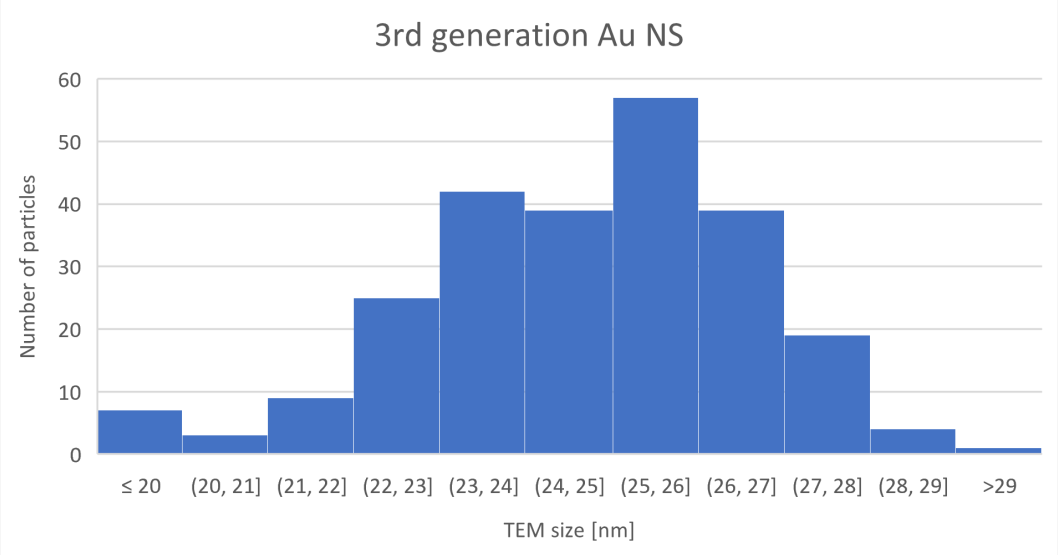

Size histograms of 4th generation Au NSs

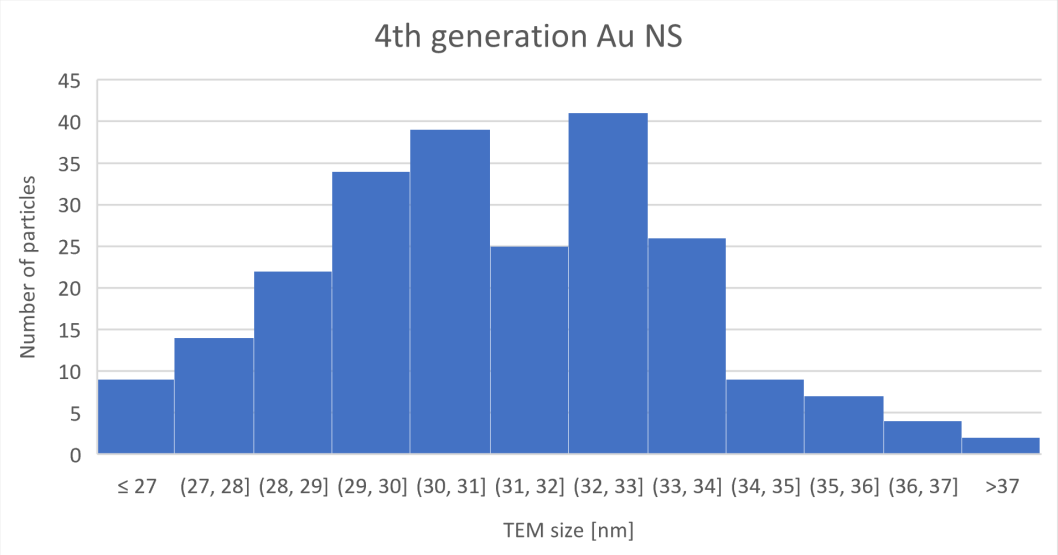

Size and aspect ratio histograms of Au NRs (250 µL silver nitrate)

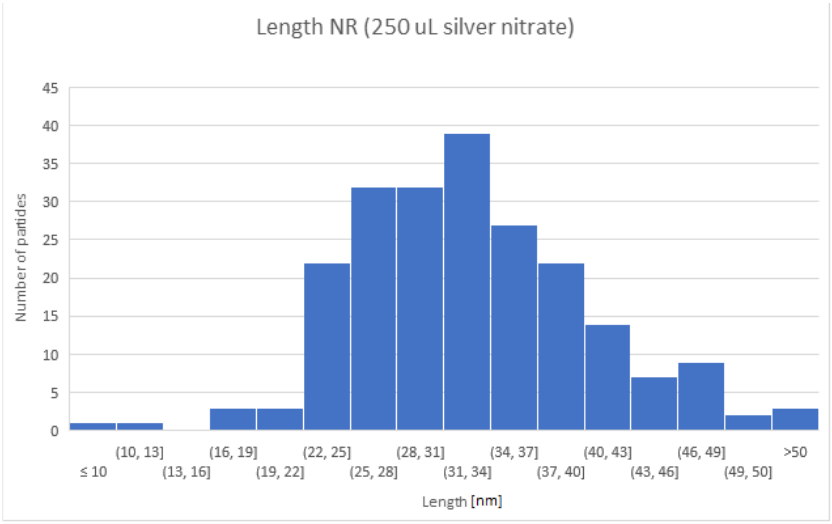

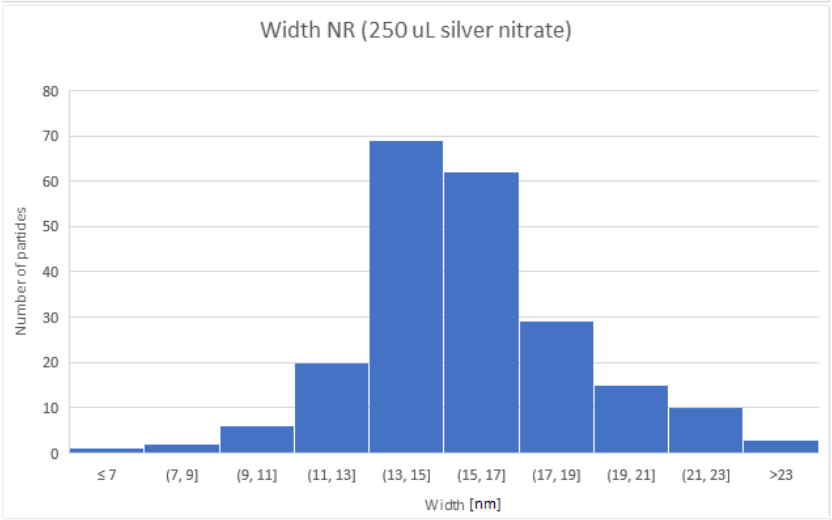

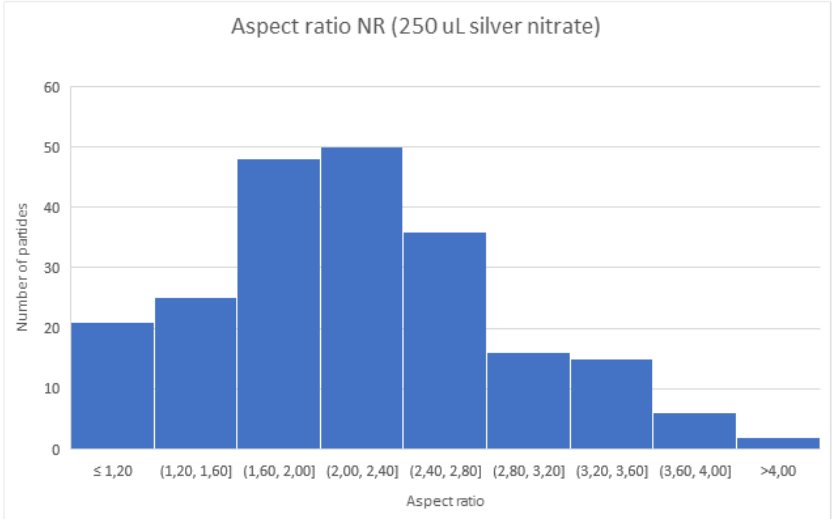

Size and aspect ratio histograms of Au NRs (500 µL silver nitrate)

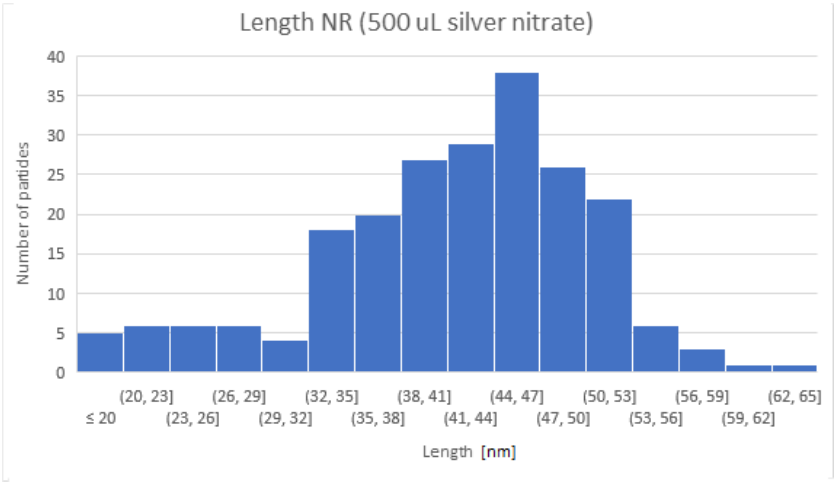

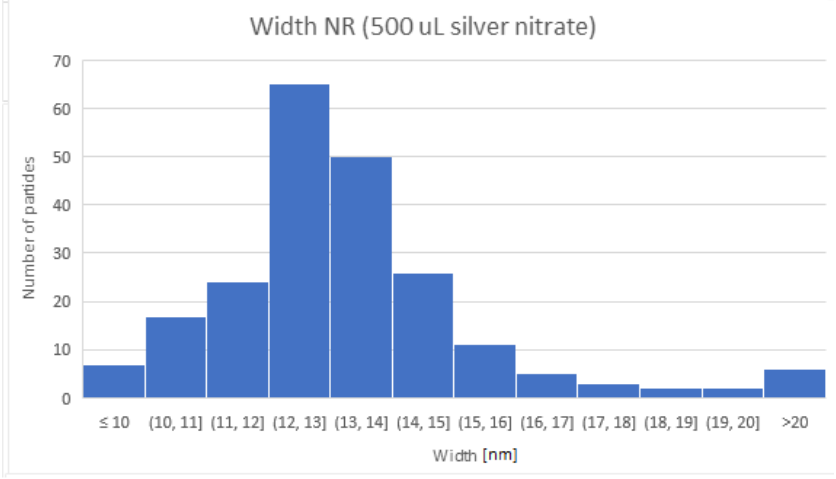

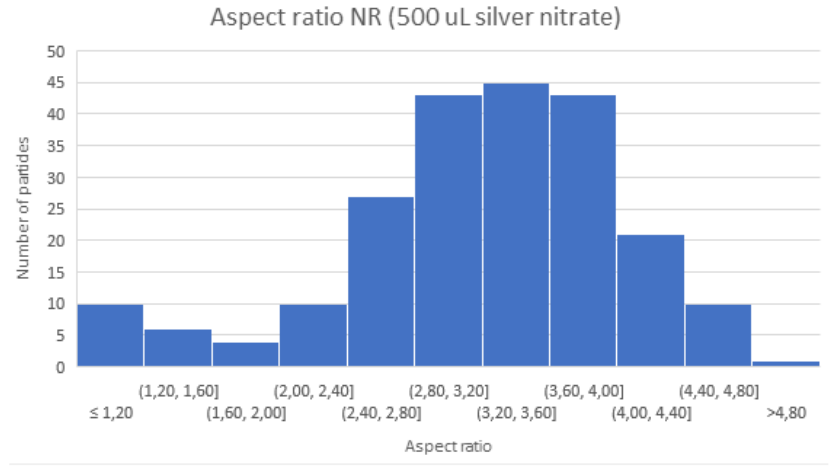

Size and aspect ratio histograms of Au NRs (750 µL silver nitrate)

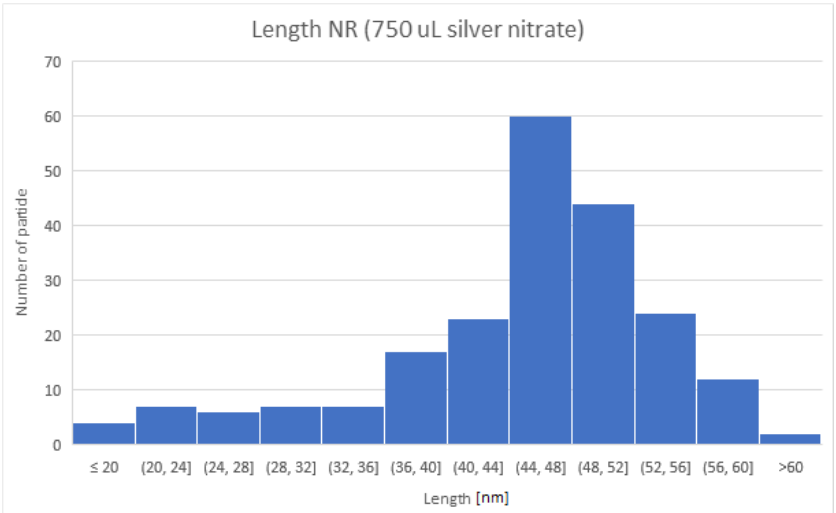

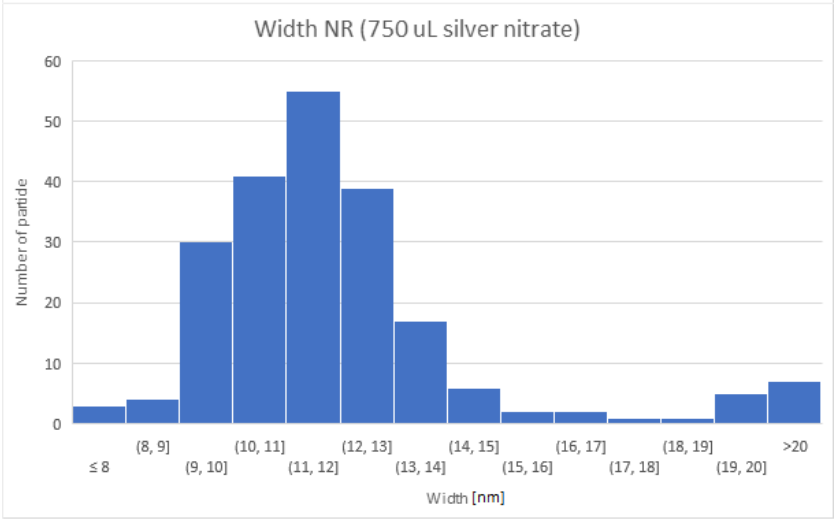

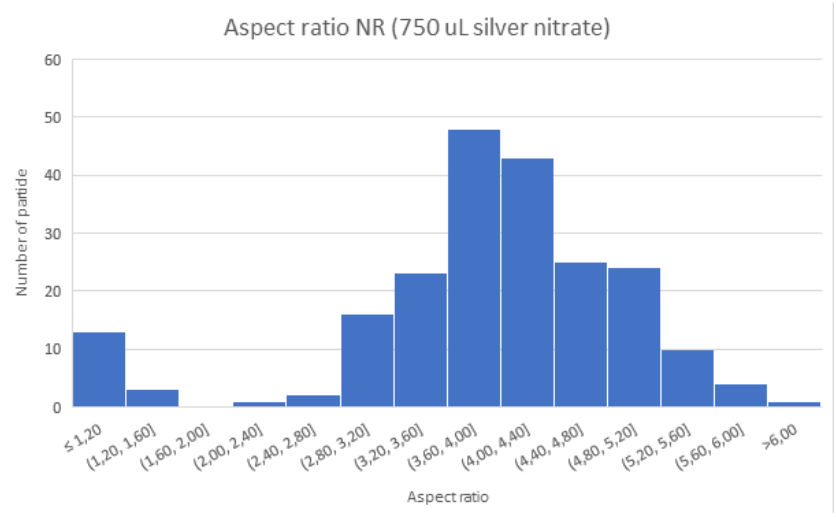

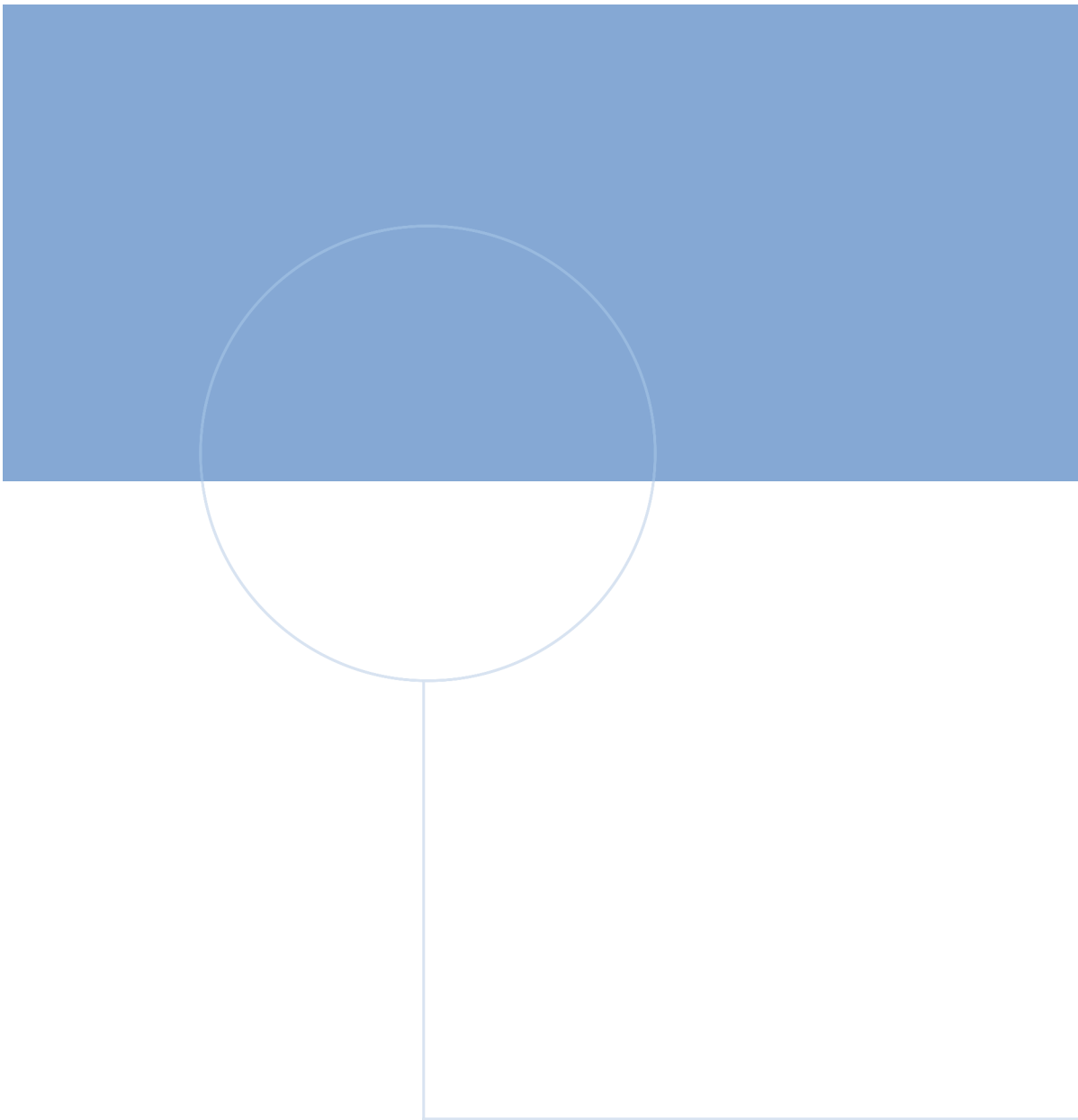

NTNU

Norwegian University of
Science and Technology